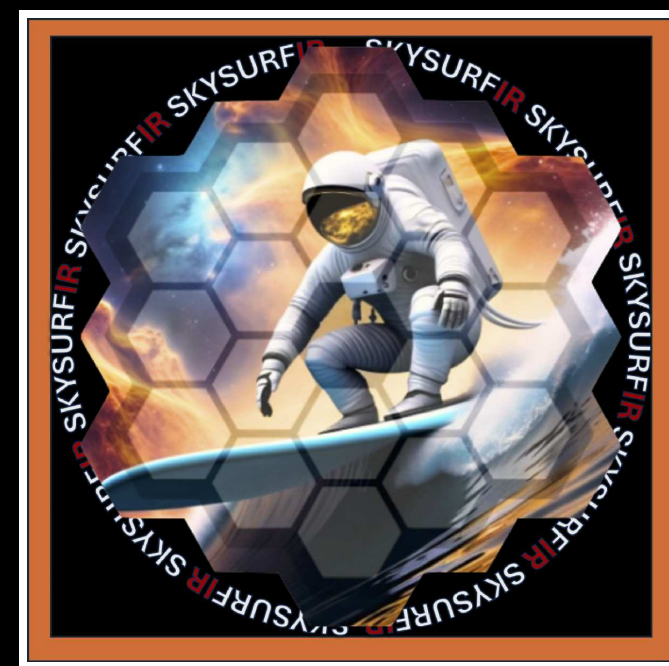
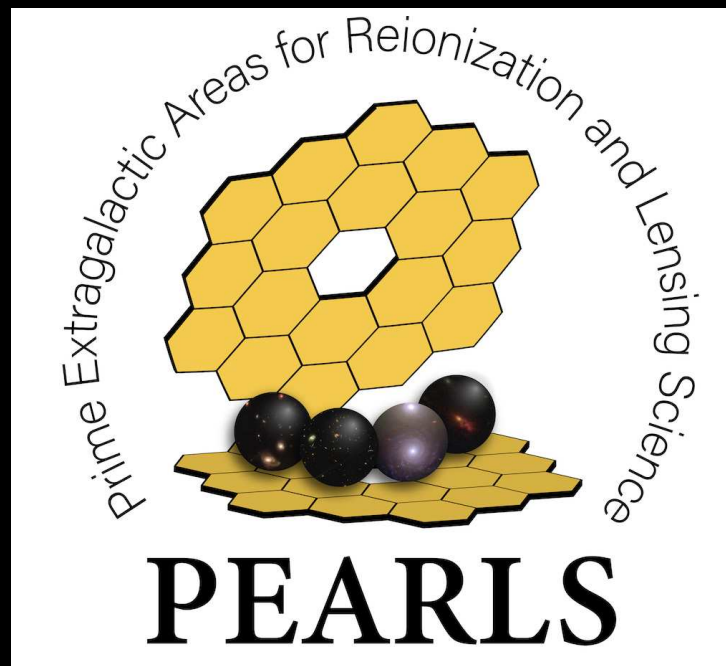


Projects SKYSURF & SKYSURFIR: How to constrain Diffuse Light from 30 years of Hubble and 2 years of Webb images

Rogier Windhorst (ASU) — JWST Interdisciplinary Scientist

+ HST SKYSURF and JWST PEARLS & SKYSURFIR teams: T. Carleton, S. Cohen, R. Jansen, R. O'Brien, T. Acharya, P. Bahtia, J. Berkheimer, D. Carter, L. Conrad, Z. Goisman, R. Honor, H. Ingram, D. Kramer, I. McIntyre, M. Miller, R. Ortiz, C. Redshaw, B. Smith, J. Summers, S. Tompkins, A. Koekemoer, N. Adams, H. Archer, R. Arendt, S. Caddy, D. Coe, C. Conselice, J. Diego, S. Driver, J. D'Silva, G. Fazio, N. Foo, B. Frye, N. Grogin, B. Holwerda, P. Kamieneski, A. Kashlinsky, W. Keel, S. Kenyon, J. MacKenty, M. Marshall, T. McCabe, N. Pirzkal, C. Robertson, A. Robotham, R. Ryan Jr., J. Trussler, C. Willmer, H. Yan, + 70 more scientists over 18 time-zones



Talk at AstroParticle Symposium 2024, Institut Pascal, Paris (France); Thursday Nov. 14, 2024

PDF on: http://www.asu.edu/clas/hst/www/jwst/skysurfir_paris24_windhorst.pdf

Projects SKYSURF & SKYSURFIR: How to constrain Diffuse Light from 30 years of Hubble and 2 years of Webb images

Rogier Windhorst (ASU) — JWST Interdisciplinary Scientist

+ HST SKYSURF and JWST PEARLS & SKYSURFIR teams: T. Carleton, S. Cohen, R. Jansen, R. O'Brien, T. Acharya, P. Bahtia, J. Berkheimer, D. Carter, L. Conrad, Z. Goisman, R. Honor, H. Ingram, D. Kramer, I. McIntyre, M. Miller, R. Ortiz, C. Redshaw, B. Smith, J. Summers, S. Tompkins, A. Koekemoer, N. Adams, H. Archer, R. Arendt, S. Caddy, D. Coe, C. Conselice, J. Diego, S. Driver, J. D'Silva, G. Fazio, N. Foo, B. Frye, N. Grogin, B. Holwerda, P. Kamieneski, A. Kashlinsky, W. Keel, S. Kenyon, J. MacKenty, M. Marshall, T. McCabe, N. Pirzkal, C. Robertson, A. Robotham, R. Ryan Jr., J. Trussler, C. Willmer, H. Yan, + 70 more scientists over 18 time-zones



Conclusions: NIR Diffuse Light $\sim 20 \text{ nW/m}^2/\text{sr}$ (dim Zodi!); Visible diffuse IGL (tidal tails) $\lesssim 10\text{--}20\%$ of total IGL.

SKYSURF-ers and HST+Webb researchers in ASU group (not all shown):



Hangy Andras-Letanovszky



Haylee Archer



Jessica Berkheimer



Alex Blanche



Sarah Caddy



Timothy Carleton



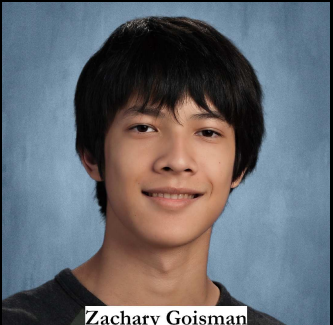
Delondrae Carter



Seth Cohen



Tzvetelina Dimitrova



Zachary Goisman



Daniel Henningsen



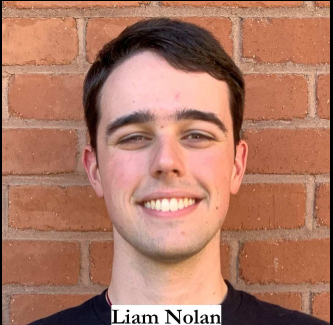
Megan Householder



Rolf Jansen



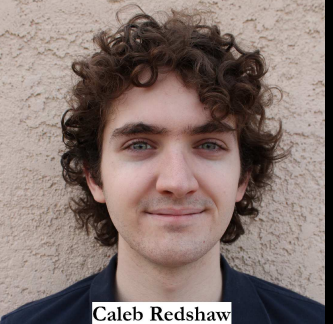
Darby Kramer



Liam Nolan



Rosalia O'Brien



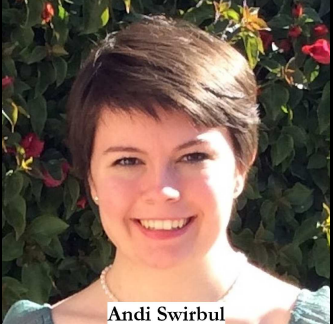
Caleb Redshaw



Sydney Scheller



Jake Summers



Andi Swirbul

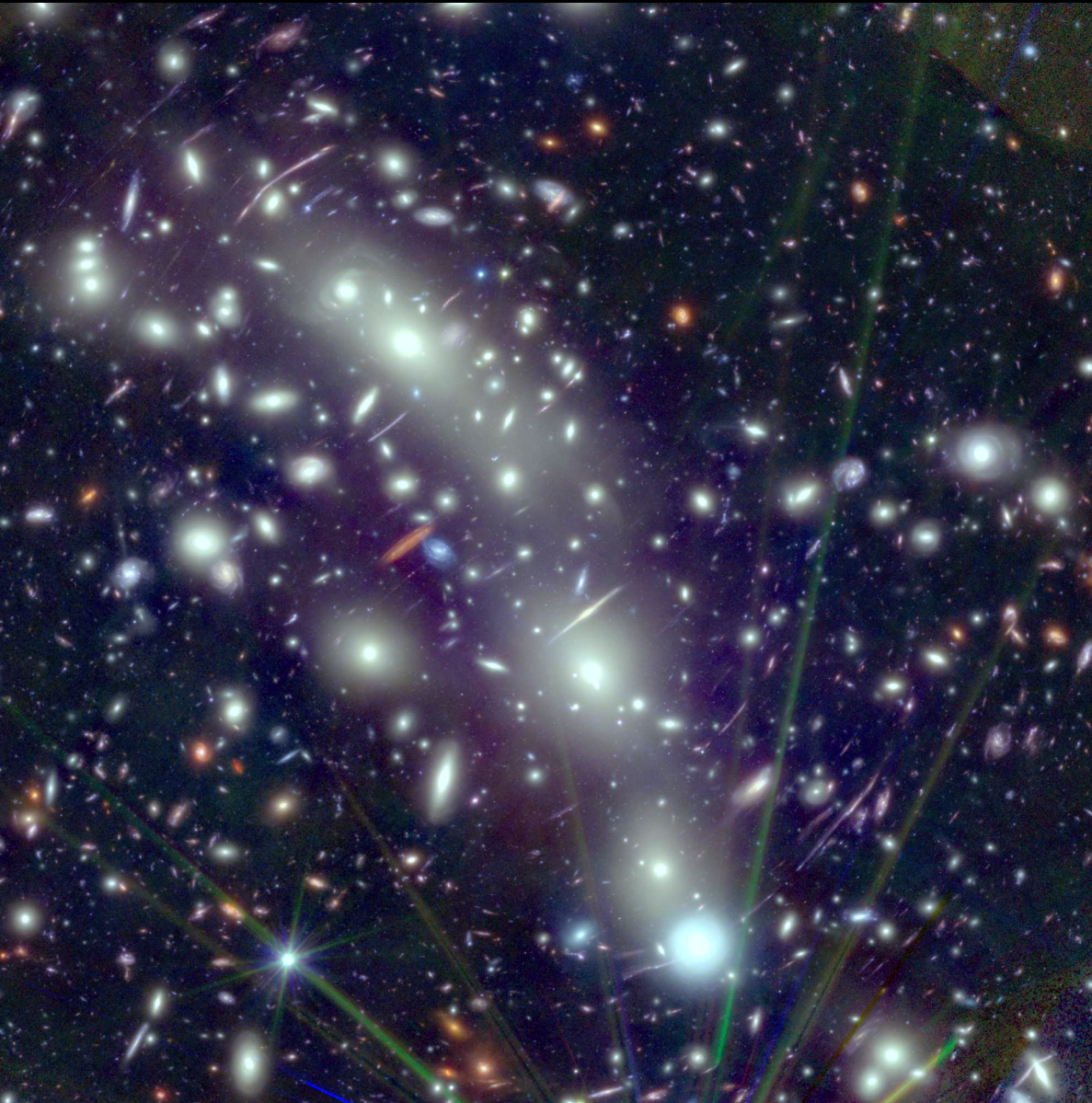
Outline and Conclusions

- (0) Plea from 414–500 hr combined HST+JWST images: keep HST alive!
- (1) Summary of the HST SKYSURF project and Diffuse Light
 - (1a) Discrete object catalogs and counts from SKYSURF
 - (1b) Diffuse Light studies from SKYSURF: sky-SB and straylight
 - (1c) Can undetected (low-SB) galaxies cause 0.3 dex Diffuse Light? No!!
- (2) Summary of JWST PEARLS & SKYSURFIR limits and Diffuse Light
- (3) Conclusions: Combined HST+JWST Diffuse Light limits

Some remarkable results from PEARLS and SKYSURFIR projects:

- Abundance of red (dusty) spirals, $\sim 30\%$ more than seen by HST.
- Accurate 0.9–5 μm galaxy counts to $\text{AB} \lesssim 28.5\text{--}29$ mag.
- (Old) tidal tails everywhere: $\lesssim 10\text{--}20\%$ of Integrated Galaxy Light (IGL).
- Webb 0.9–5 μm Diffuse Light limits are $\lesssim 10\%$ of Zodiacial.
- HST 1.25–1.6 μm Diffuse Light: $\sim 20 \text{ nW/m}^2/\text{sr}$ (6% of Zodi).

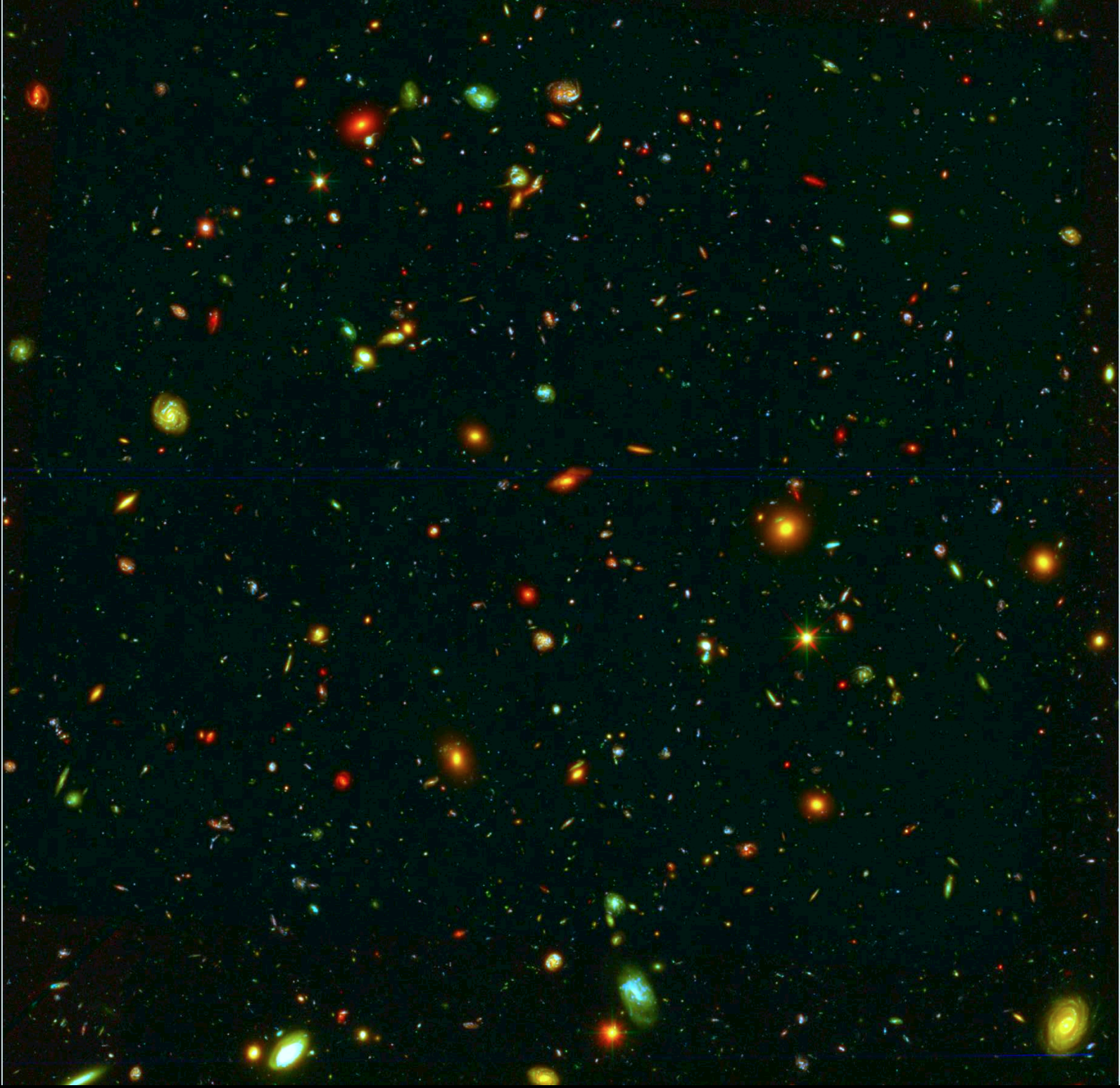
(0) Plea from 414–500 hr combined HST+JWST images: keep HST alive!



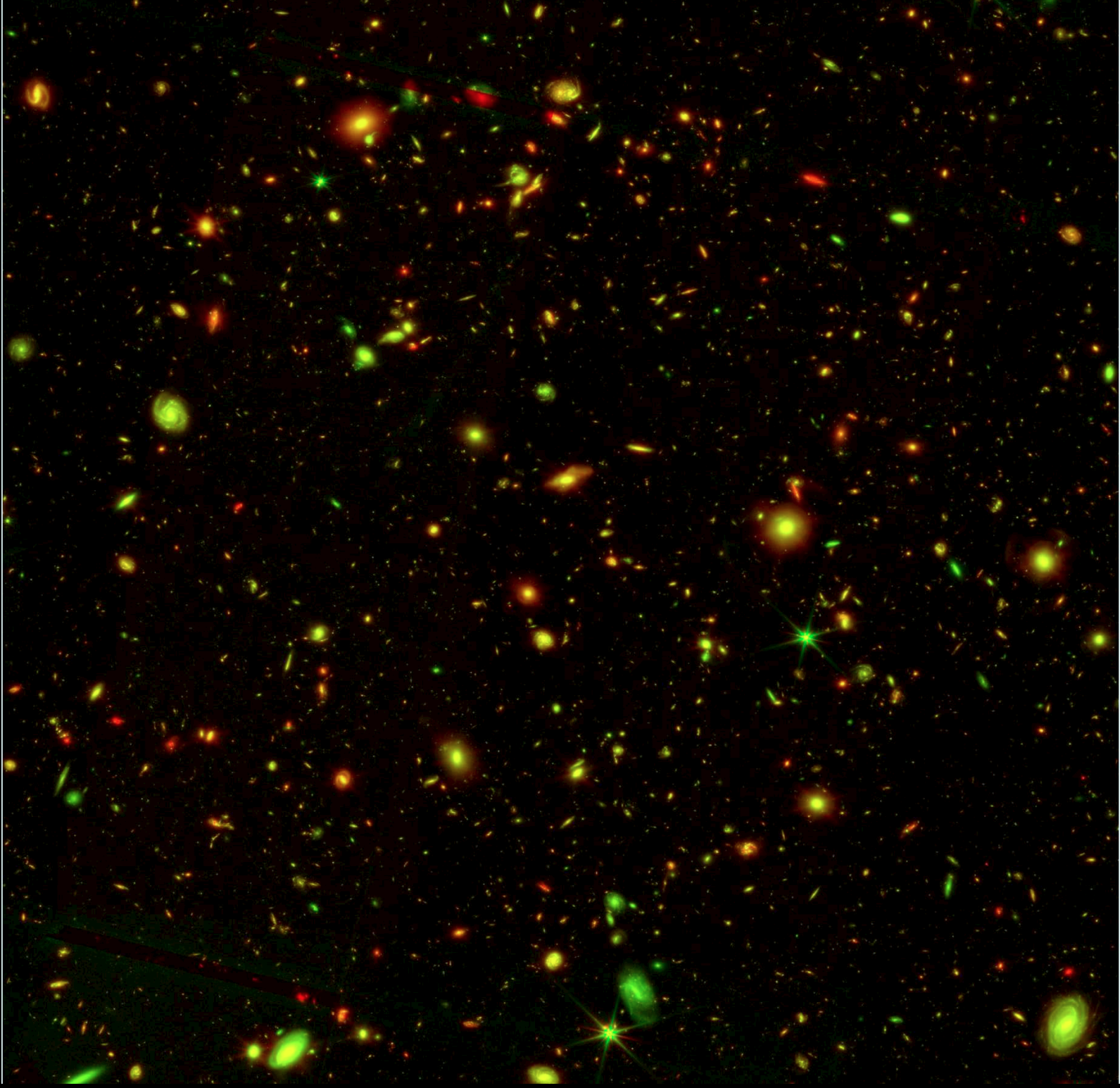
Combined 500 hr HST+JWST image in 45 filters (0.2–5.0 μ m) on lensing cluster MACS0416:

- HST darkest skies ($10\text{--}10^3 \times$ darker) + JWST's dark skies ($10^3\text{--}10^5 \times$ darker than ground based):
- Together with ZPs stable to 1–3% over decades, this helps a lot with Diffuse Light studies!

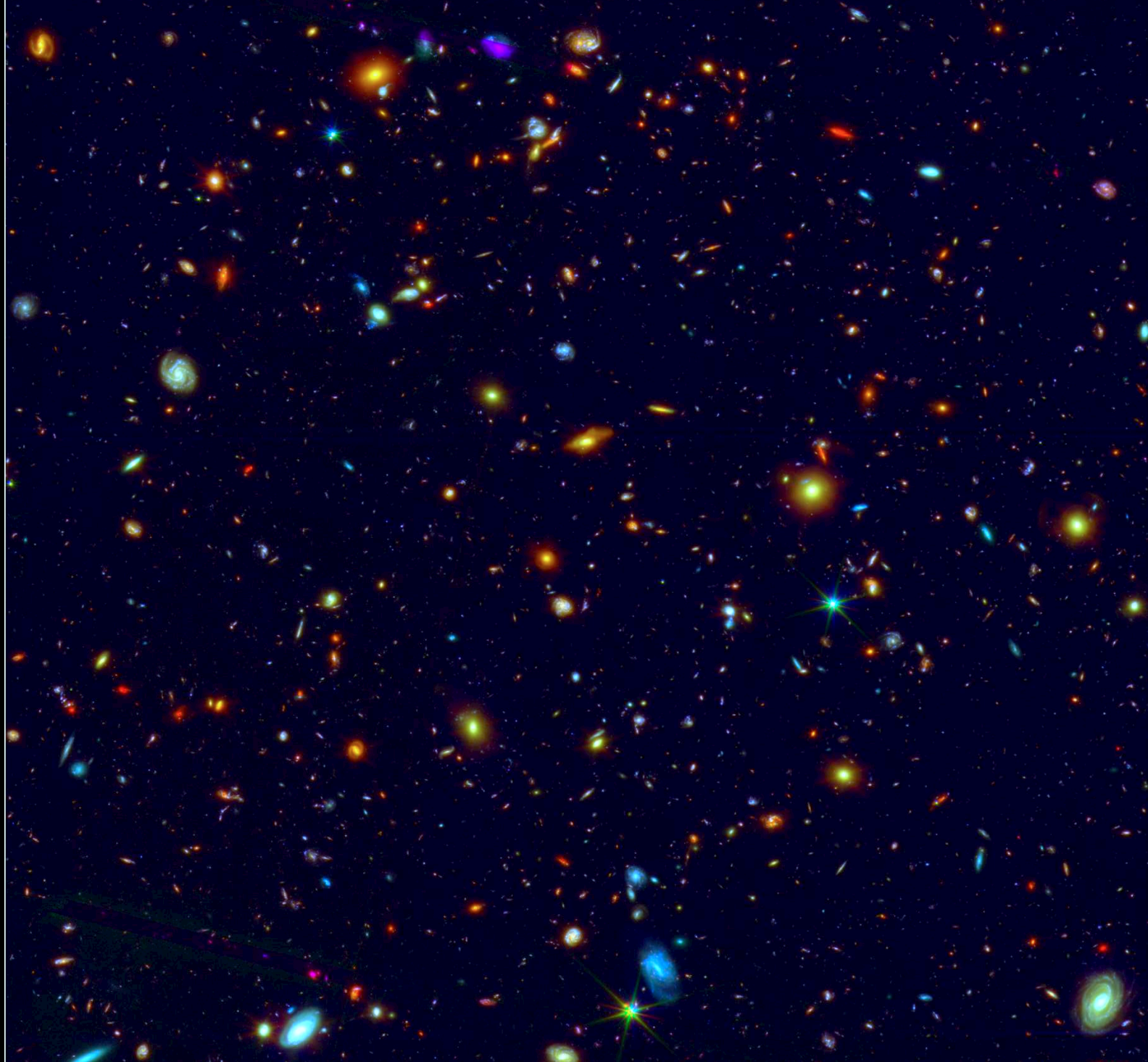
(Diego, J. M. et al. 2023, A&A, 679, A31; Yan, H. et al. 2023, ApJS, 269, 43; image by A. Koekemoer, R. Honor).



556 hr HST Hubble UltraDeep Field: 12 filters at 0.2–1.6 μ m (AB \lesssim 31 mag; $F_{\nu}\gtrsim$ 2 nJy; full BGR).



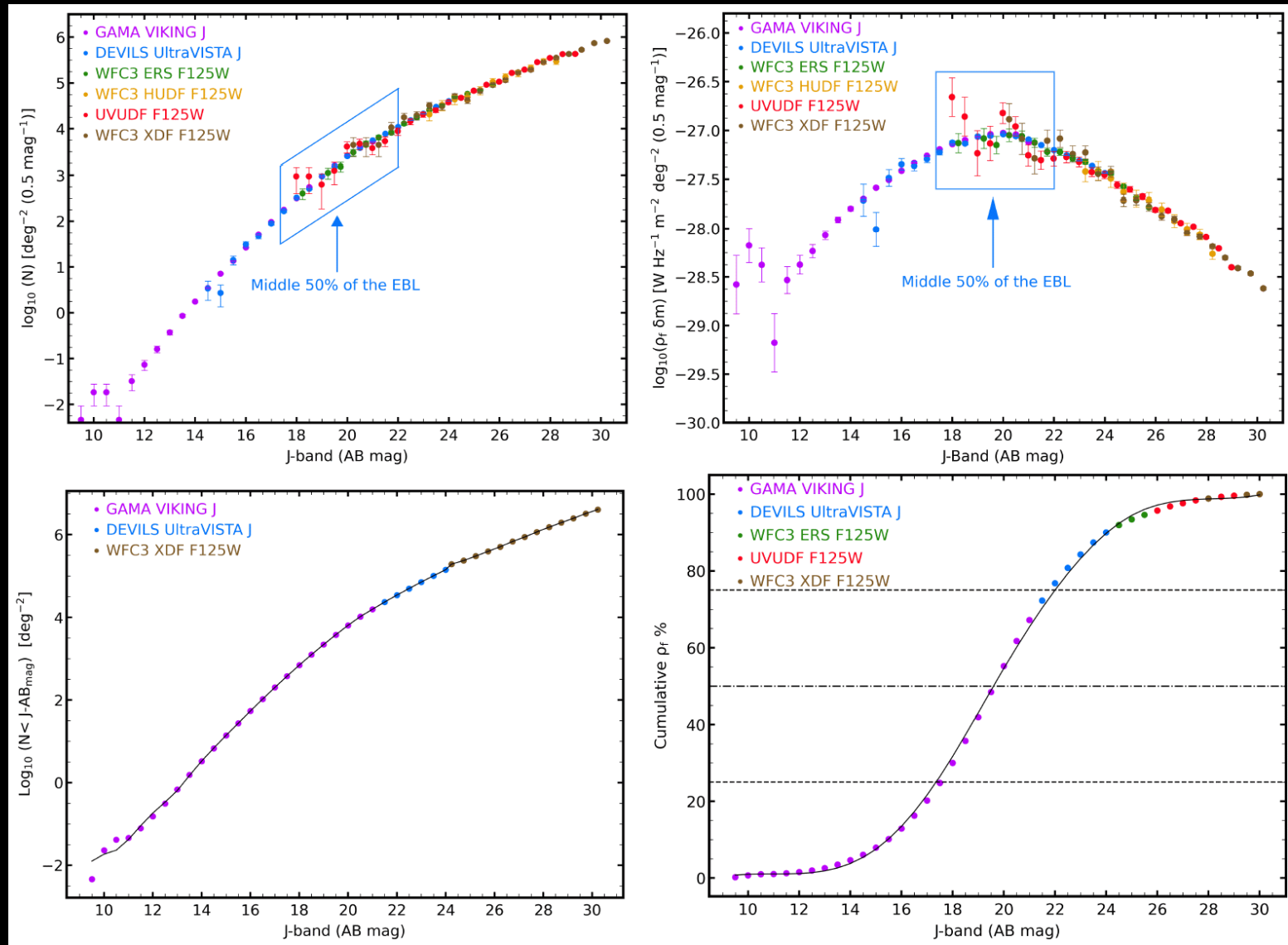
53 hr JWST/NIRCam Hubble UltraDeep Field: 12 filters at 0.9–5.0 μm ($\text{AB} \lesssim 31$ mag; in green + red).



414 hr HST+JWST Hubble UltraDeep Field: 20 filters at 0.2–5.0 μ m (AB \lesssim 31.5 mag; full BGR).

(1) Summary of the HST SKYSURF project and Diffuse Light

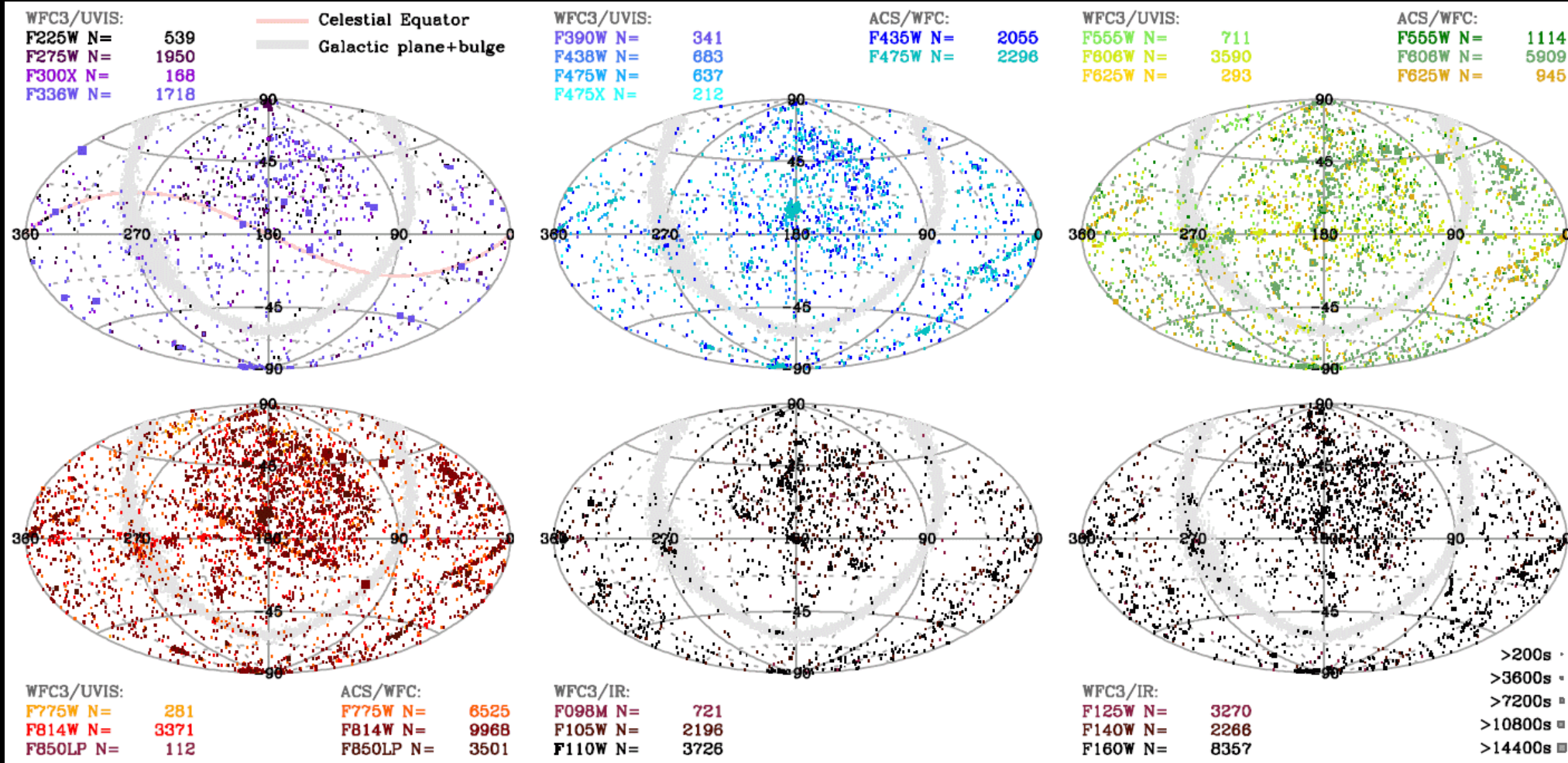
(1a) Discrete object catalogs and counts from SKYSURF



SKYSURF number counts: nearby galaxies → HUDF (Tompkins).

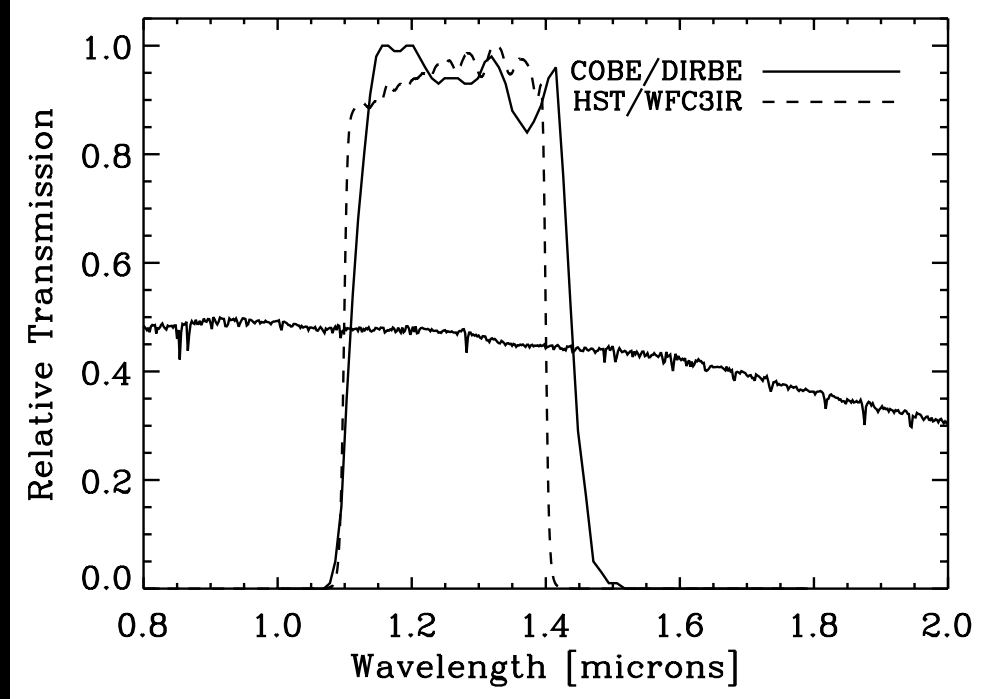
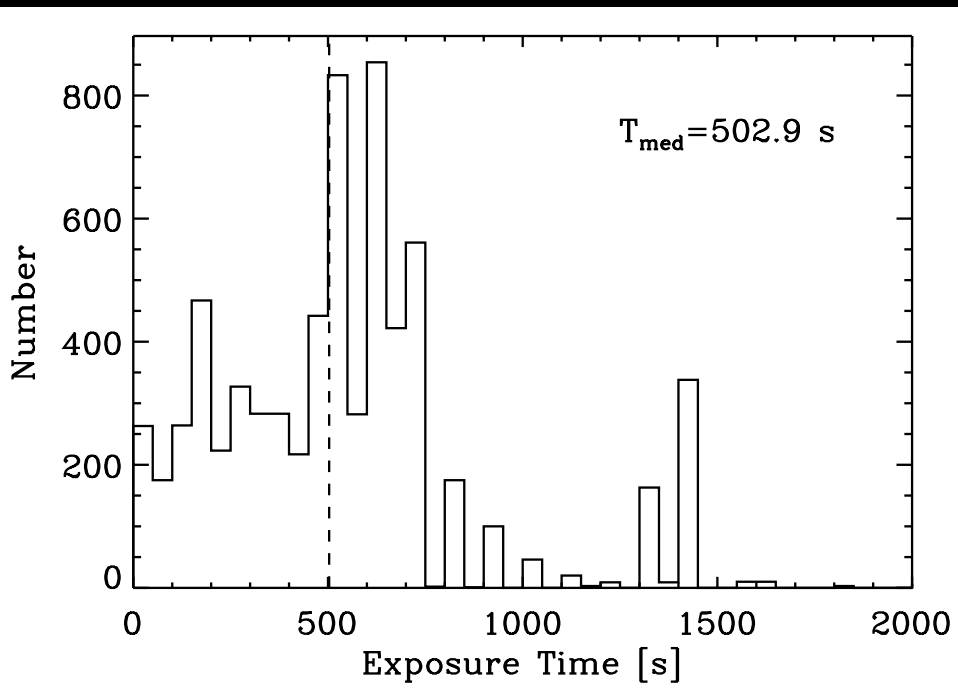
Top: counts, Bottom: integrals; Left: Number-, Right: Energy-counts.

⇒ Box: Middle 50% of IGL from brighter galaxies ($17 \lesssim \text{AB} \lesssim 22$)!



- SKYSURF's database: 249,861 exposures (878,000 readouts) in 16,822 HST field-of-views (FOVs) taken over 28 years.
- 28 filters from 0.2-1.6 μm ; with 12 main broad-band filters in \sim 1400 independent HST fields. (Note the denser SDSS footprint!)

(Tim Carleton, Rosalia O'Brien: SKYSURF database lead. UGs built database in 2020).

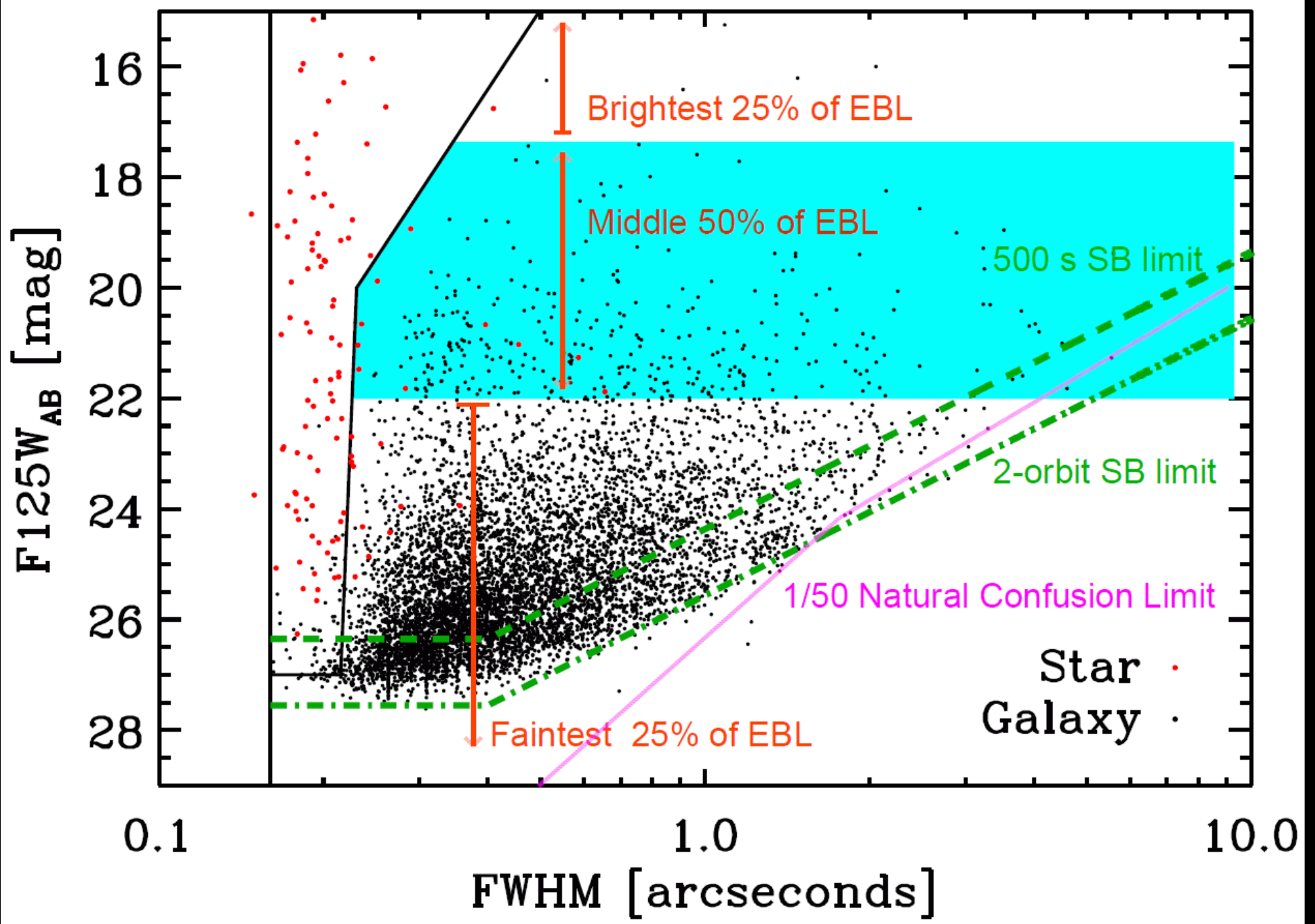


[Left]: Exposure time distribution with median $t_{\text{exp}} \simeq 500$ sec (Goisman).

- Typical HST exposure depth reaches AB ~ 26 mag, *i.e.*, already detects $\gtrsim 95\%$ of the discrete EBL (IGL)!

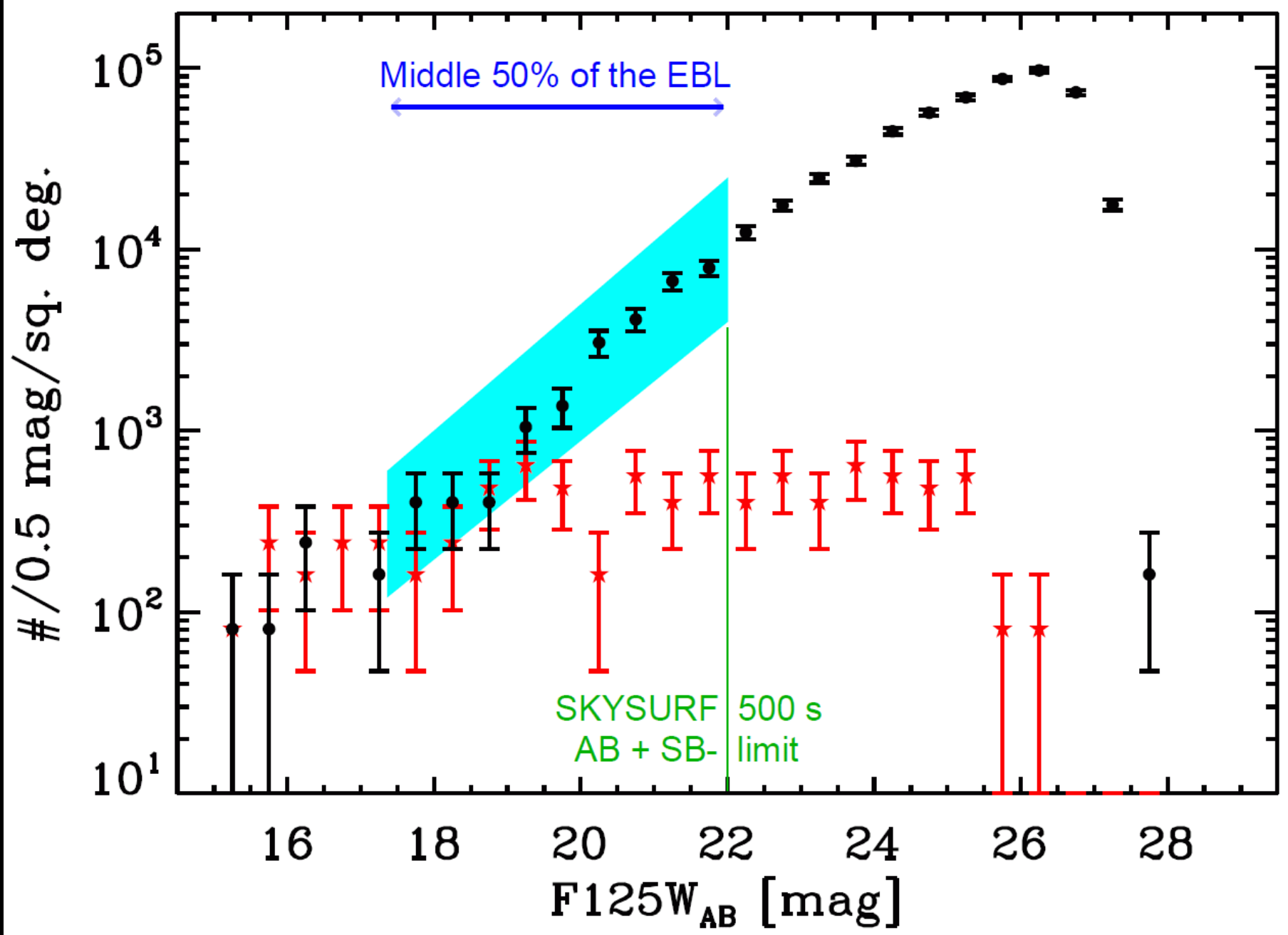
[Right]: Two main filters used for SKYSURF HST–COBE comparison: needed for precision differences in sky-SB (Seth Cohen).

- For the Zodiacal spectrum shown, 1.25 μm filter difference is only 0.56%.



SKYSURF star-galaxy separation, with SB- and natural confusion limits.

- Subset of deeper exposures yield accurate completeness corrections.



Star+Galaxy counts 100% complete to AB $\lesssim 22$ [where 75% of IGL is seen], and 74% complete to AB $\lesssim 26$ mag [where 95% of discrete IGL is seen].

(1b) Diffuse Light studies
from HST SKYSURF

Galactic plane and the
Zodiacal disk at night:
They are inclined by 60° .

SKYSURF aims to map
both their diffuse light
across the sky.

JWST is now doing the
same, but in much darker
 $0.9\text{-}5 \mu\text{m}$ L2 skies.

More than 95% of photons in STScI Archive
(outside the Galactic plane; $|b^{II}| \gtrsim 25^\circ$) come
from distances $D \lesssim 5$ AU.



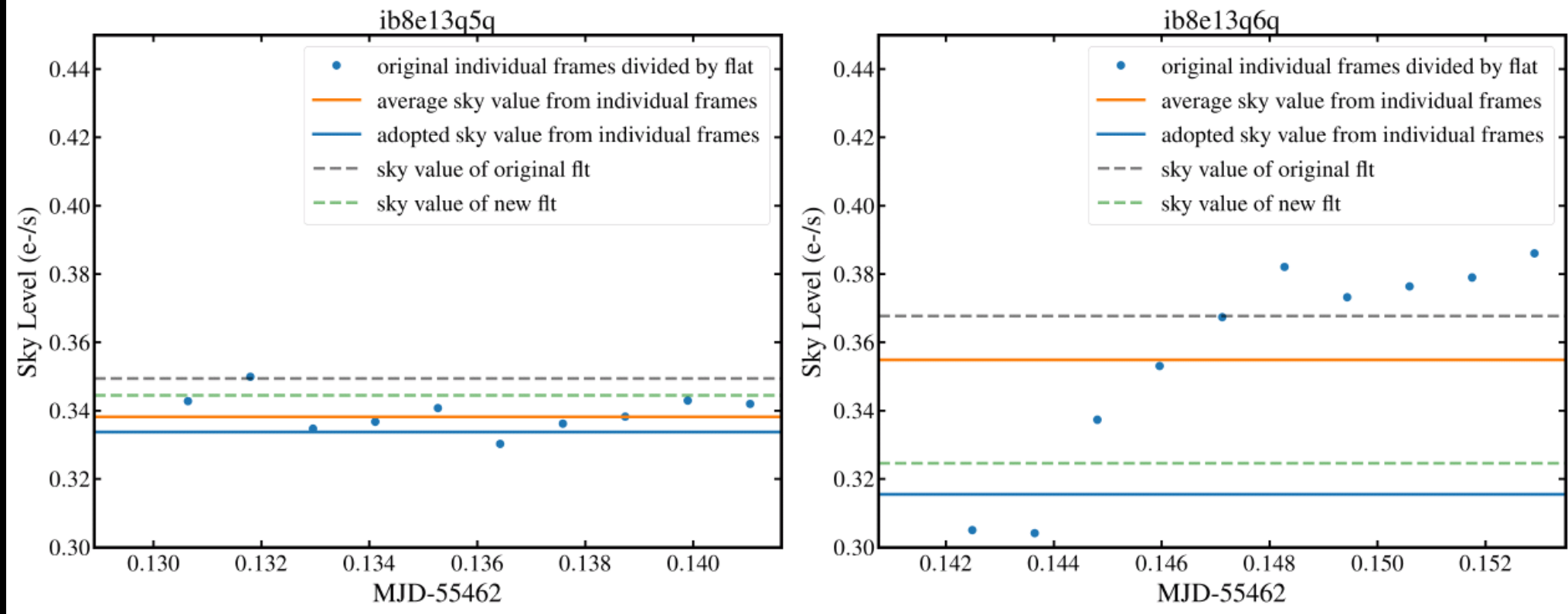
(1b) Diffuse Light studies from SKYSURF: sky-SB and straylight



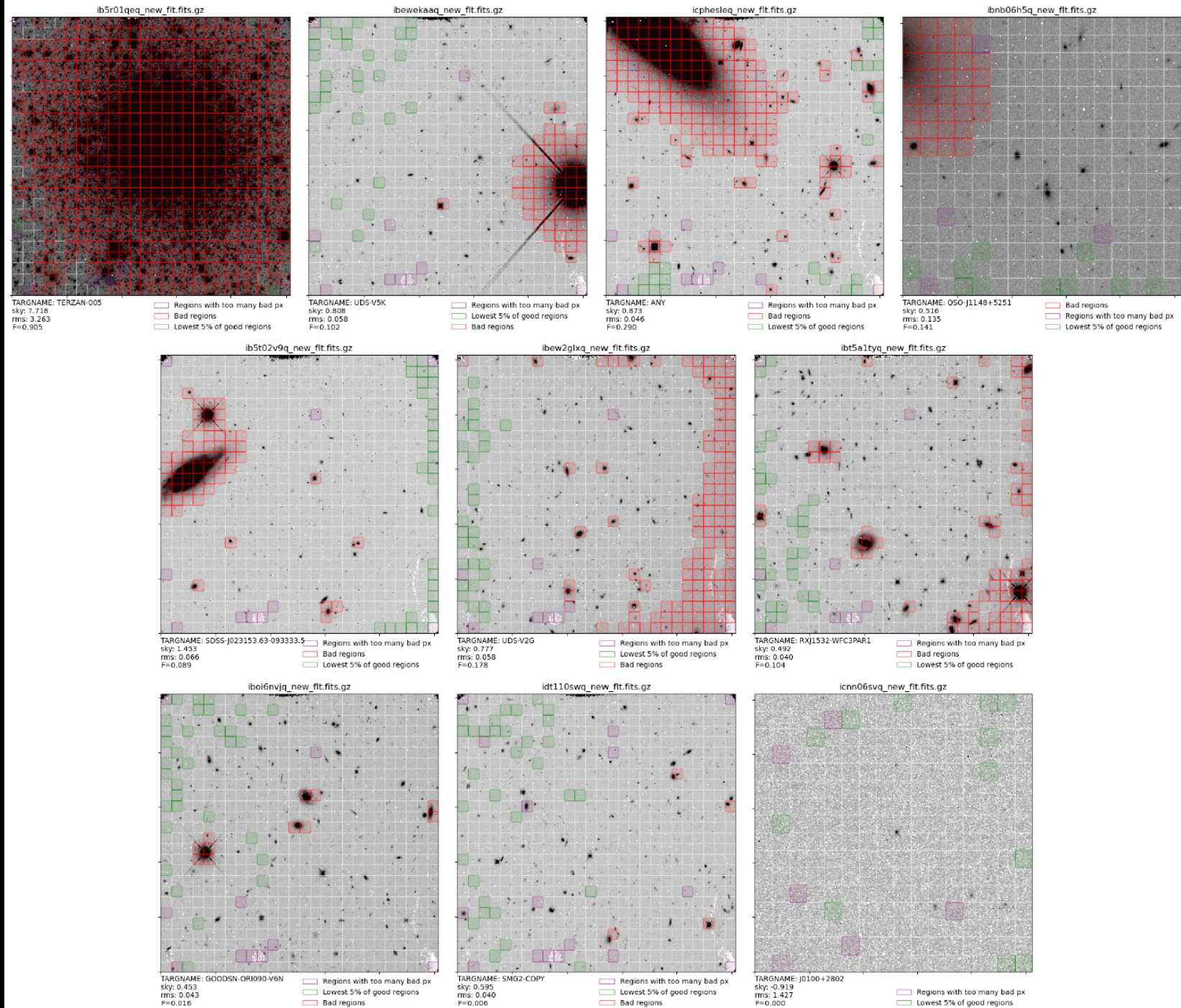
In all SKYSURF images we need to identify straylight from:

- 1) Earthshine [Limb Angle]; 2) Sunlight [Sun Angle and Sun Altitude above Earth]; 3) Moonlight [Moon Angle] (Sarah Caddy).

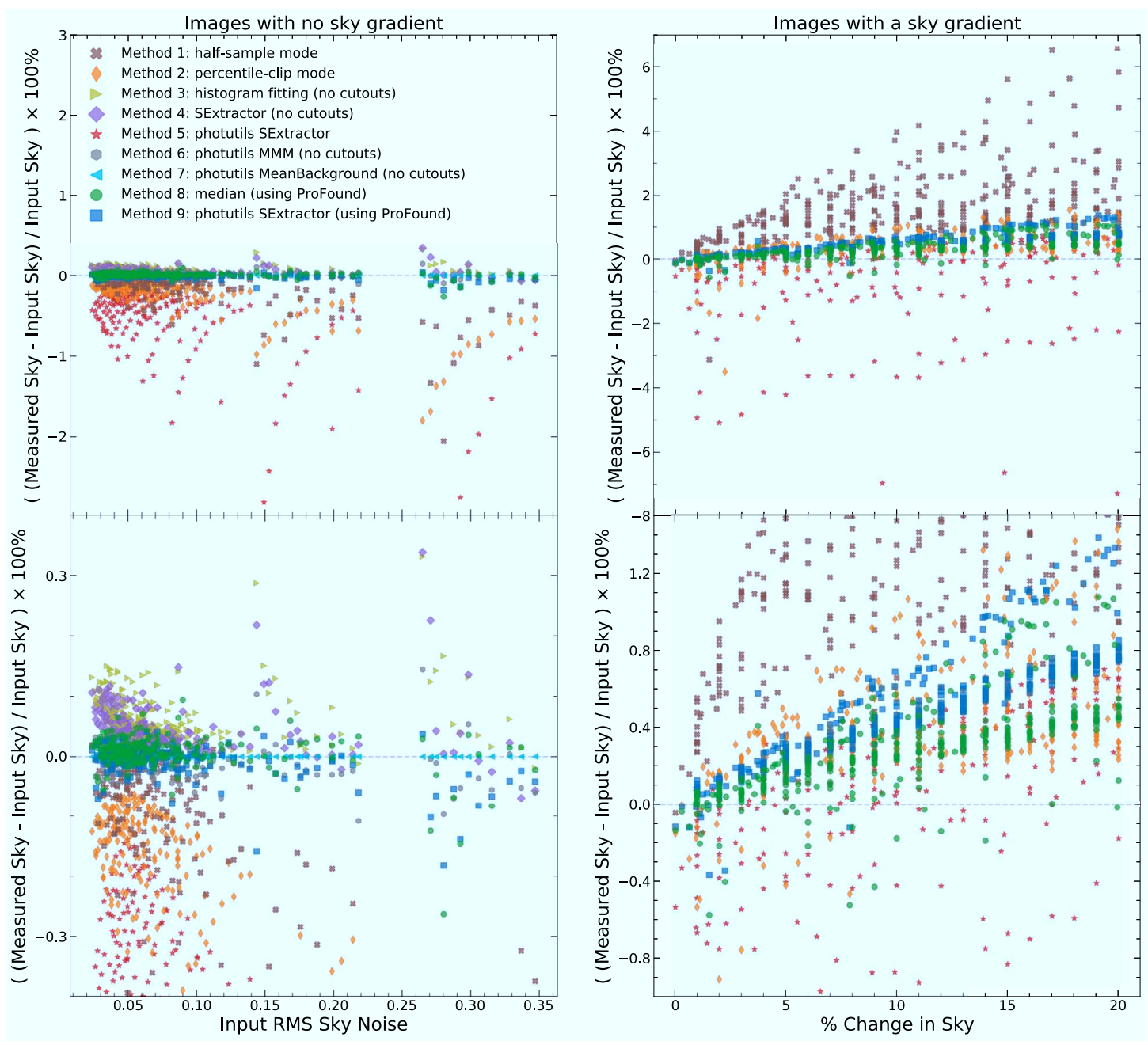
(Earth's Limb is down 24° from LEO orbital vector due to Earth curvature).



- SKYSURF's 50,073 WFC3/IR exposures are split into $\gtrsim 400,000$ on-the-ramp sub-exposures (Carleton et al.) — we are not lacking statistics.
- These (+all 210,000 sub-orbital CCD exposures) allow us to monitor sky-SB vs. HST's orbital phase [Left: Start; Right: End of orbit].
- Critical for flagging & removing SKYSURF exposures with straylight.



First, identify all sub-grid regions with objects or defects (R. O'Brien).
 5% of object-free boxes give best match with simulated sky-SB (D. Carter).



[Top]: Relative error in Measured / Simulated sky-SB in %;

[Bottom]: same but enlarged;

[Left]: simulated without gradients;

[Right]: images with 5–20% (straylight) gradients.

(Real Zodiacal gradients are always less across HST FOVs).

- W/O gradients: Best 3 out of 9 algorithms recover sky-SB $\lesssim 0.1\text{--}0.2\%$.
- With 5–10% gradients: recover sky-SB $\lesssim 0.4\%$ (Carter, O'Brien).

Table 5. Error Estimates^a in Calibration, Zeropoints, Sky-SB Measurements, and Thermal Dark Signals

Source of Error	WFPC2	ACS/WFC	WFC3/UVIS	— WFC3/IR —			(§§)	
	(1)	(2)	(3)	(4)	F125W	F140W	F160W	(8)
Bias/Darkframe subtraction	~1.0%	~1.5%	~1.5%	~1.0%	~1.0%	~1.0%	4.1	
Dark glow subtraction	~2%	—	—	—	—	—	4.1.1	
Postflash subtraction	—	~1%	~1%	—	—	—	4.1	
Global flat-field quality ^b	~1–3%	0.6–2.2%	~2–3%	~0.5–2%	~0.5–2%	~0.5–2%	4.1	
Numerical accuracy of LES ^c	≤0.1–0.4%	≤0.1–0.4%	≤0.1–0.4%	≤0.1–0.4%	≤0.1–0.4%	≤0.1–0.4%	4.2.3	
Photometric zeropoints ^d	~2%	0.5–1%	0.5–1%	~1.5%	~1.5%	~1.5%	4.1.5	
Thermal Dark signal ^e	—	—	—	~1%	~1%	~3%	4.1.4, 5.2	
Total Error ^f	~4.3%	~3.0%	~3.7%	~2.9%	~2.9%	~4.1%		

^a All relative errors in this table are expressed as a percentage of the typical Zodiacal sky-SB in the F125W, F140W, and F160W filters, which are ~331, ~282, ~240 nW m⁻² sr⁻¹, respectively (e.g., Fig. 1).

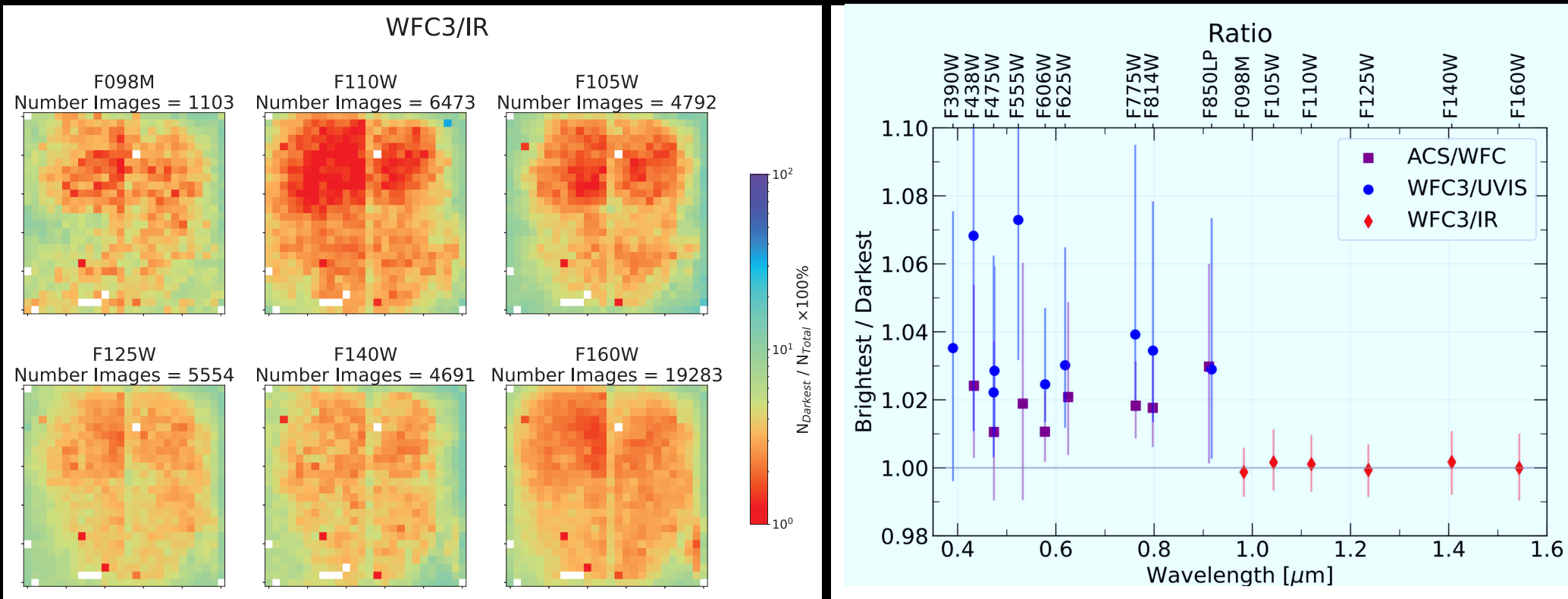
^b For WFPC2, the large-scale flat-field errors in the filters F439W and redwards are ≤1%, but the upper bound includes the 1% error in the contamination correction and the ~3% error in the residual CTE correction. For the less frequently used WFPC2 UV filters, these errors can be larger.

^c Numerical accuracy of Lowest Estimated Sky values away from detected objects (§ 4.2). The LES algorithms also avoid areas of significant persistence or cross-talk when estimating the sky-SB, so these effects are not included as an extra term in the error budget.

^d For WFC3/IR, this includes the ~0.5% uncertainty in the applied detector count-rate non-linearity correction (§ 4.1.4).

^e The errors in the estimated Thermal Dark signal values are given for the F125W and F140W filters as a percentage of the typical Zodiacal sky-SB, and are larger for the F160W filter (§ 5.2).

- Absolute HST sky-SB photometry errors ≤3–4% (as fraction of Zodi).



[Left]: Relative use of 676 WFC3/IR sky-boxes due residuals in delta-flats:

- Residual flat-field errors prefer some boxes over many thousands of fields.

[Right]: Residual FF errors: ACS: $\lesssim 2\%$; WFC3/UVIS: $\lesssim 4\%$; WFC3/IR: $\lesssim 1\%$.

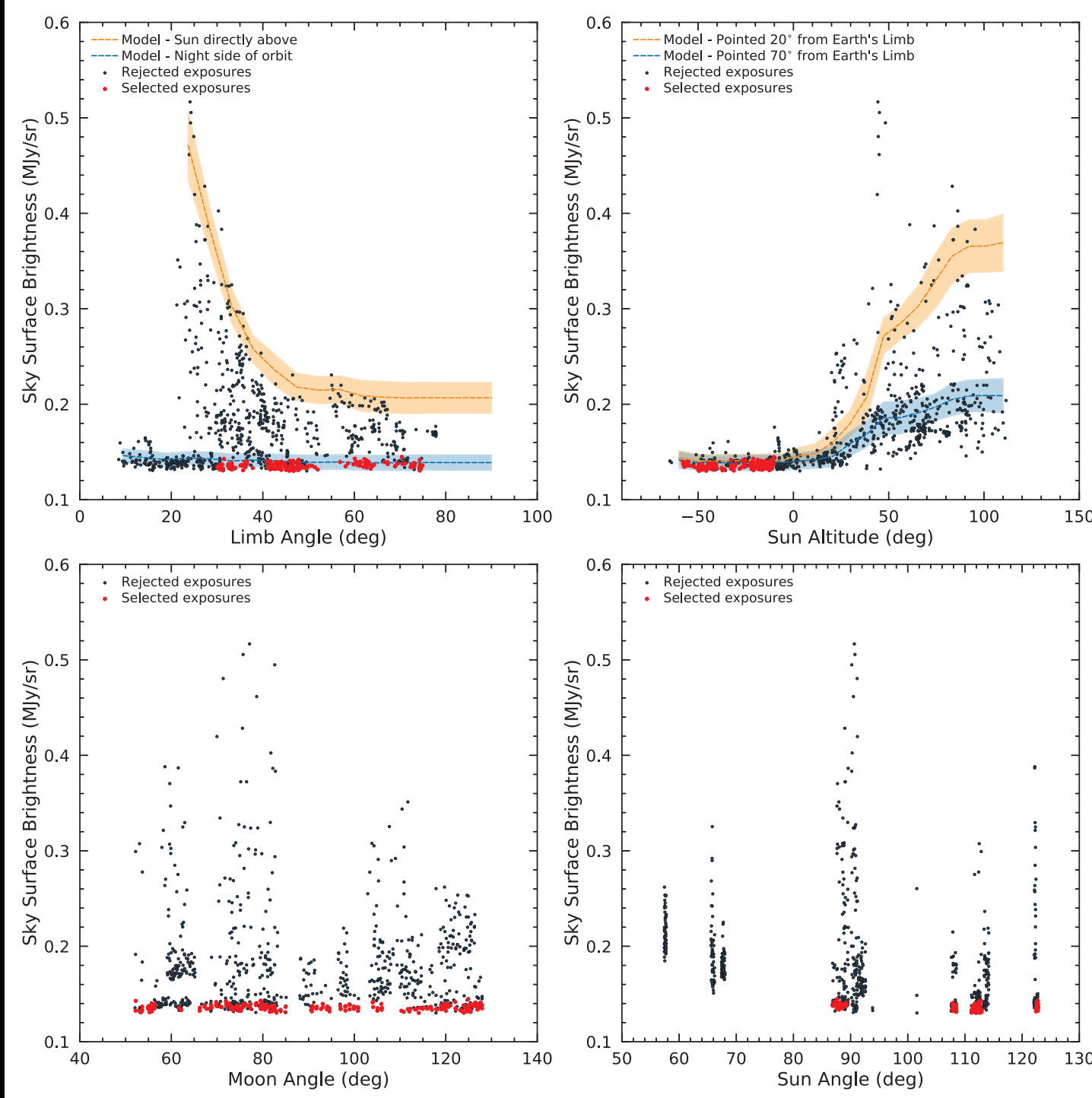
(O'Brien et al. 2023, AJ, 165, 237; astro-ph/2210.08010).

- Also, WFC3 ZPs stable to $\lesssim 1\text{--}2\%$ over 13 years ($\lesssim 0.1\%/\text{yr}$).

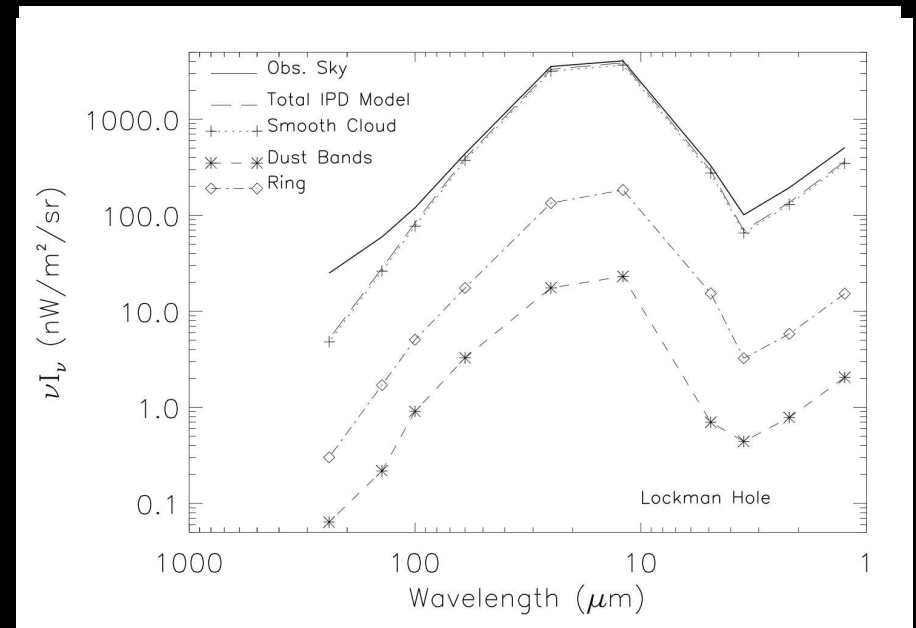
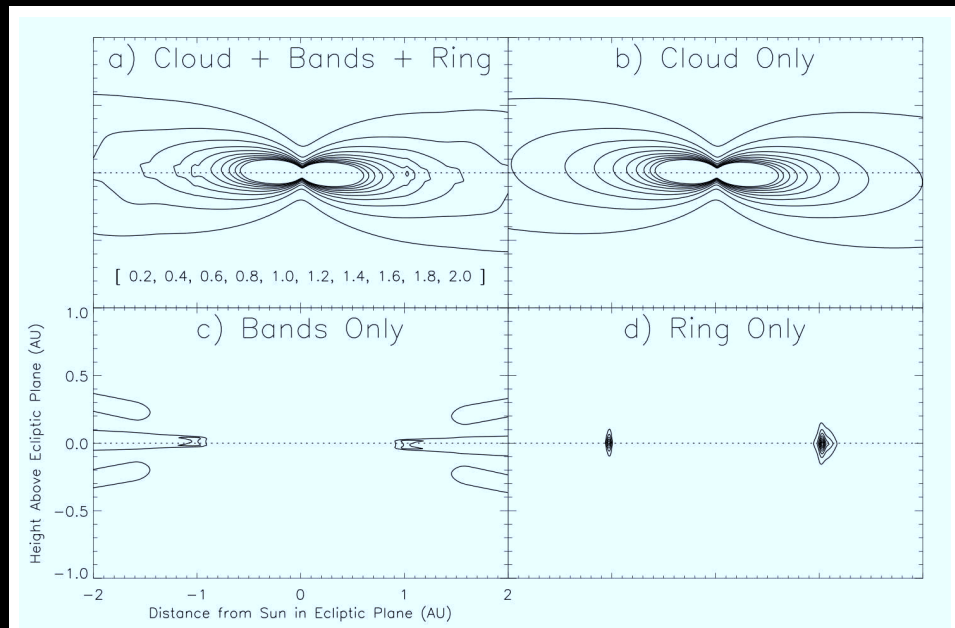
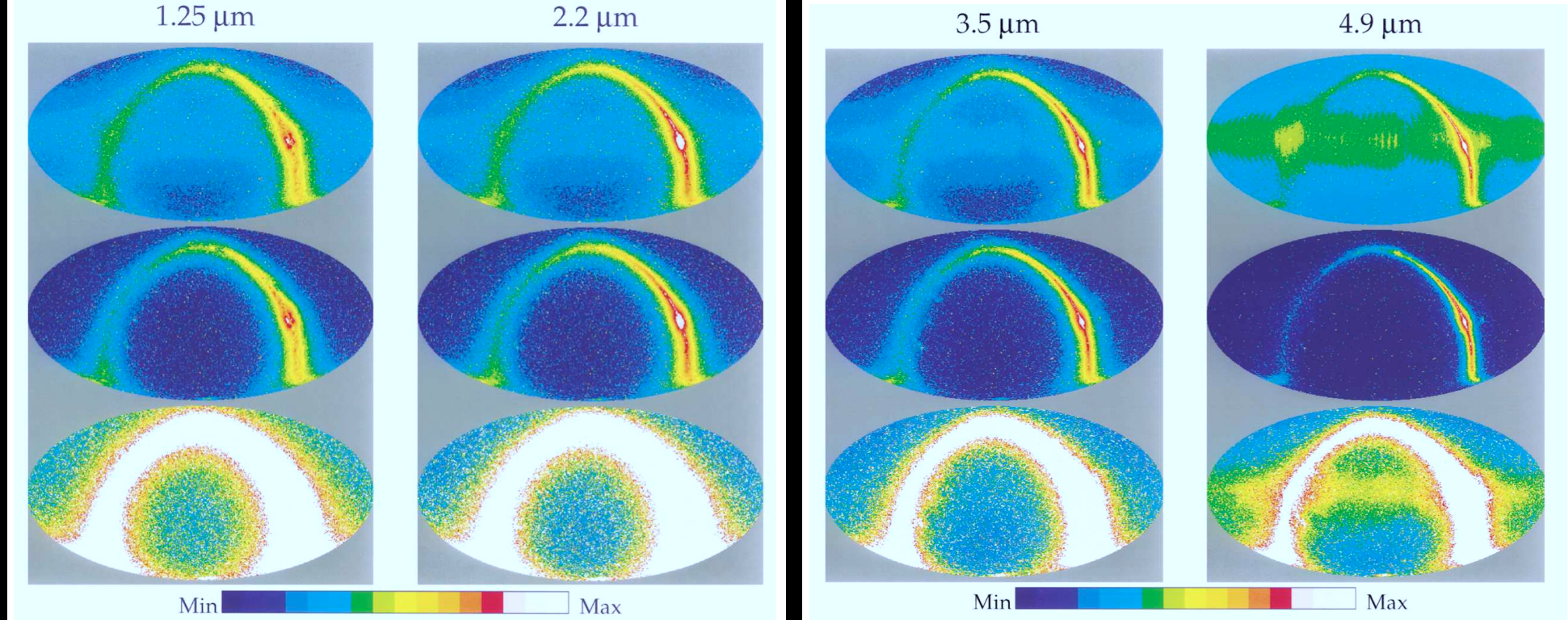
(Calamida, A. et al. 2022, AJ, 164, 32).

Sarah Caddy's study to minimize straylight:

- (a) Earth Limb Angle $LA \gtrsim 30\text{--}40^\circ$ to avoid Earthshine; and
- (b) Sun Altitude above Earth $\alpha_\odot \lesssim -10^\circ$ (orbital night side) minimizes Sunlight scattered off the bright Earth; and
- (c) The Moon Angle $MA \gtrsim 50^\circ$; and
- (d) Sun Ang. SA $\gtrsim 80^\circ$ avoids straylight into the HST optics.



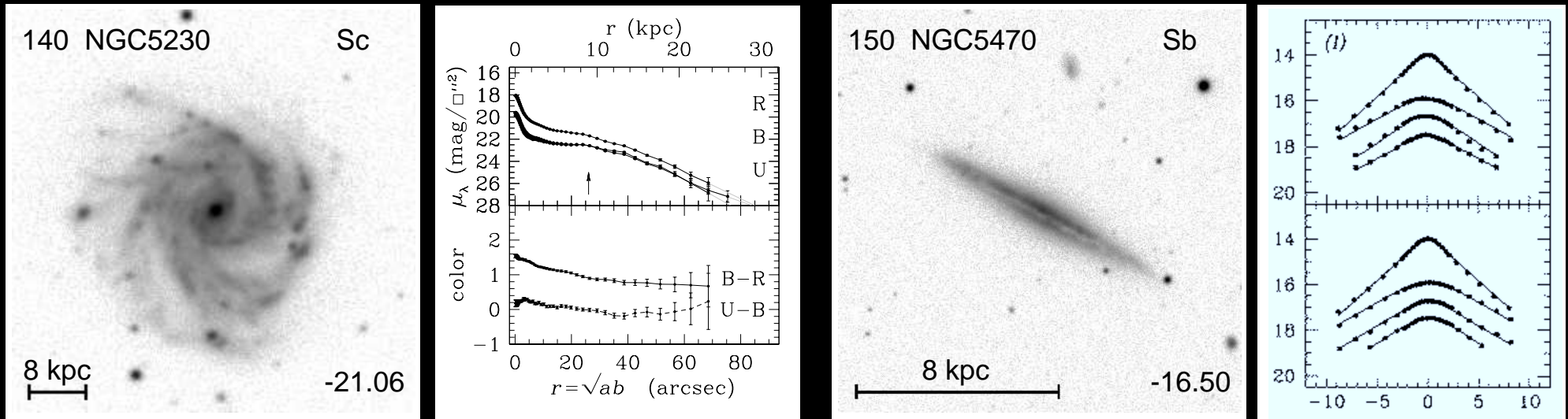
- SKYSURF's high-fidelity sample applies all these constraints (R. O'Brien).



Kelsall (1998) Zodi model based on Cosmic Background Explorer data.

We'll show that compared to HST, Kelsall misses significant 1-2 μm sky-SB.

(1b) How SKYSURF measures residual sky compared to Zodiacal models



[Left]: Face-on disks: *exponential radial* light-profiles (Jansen⁺ 2000).

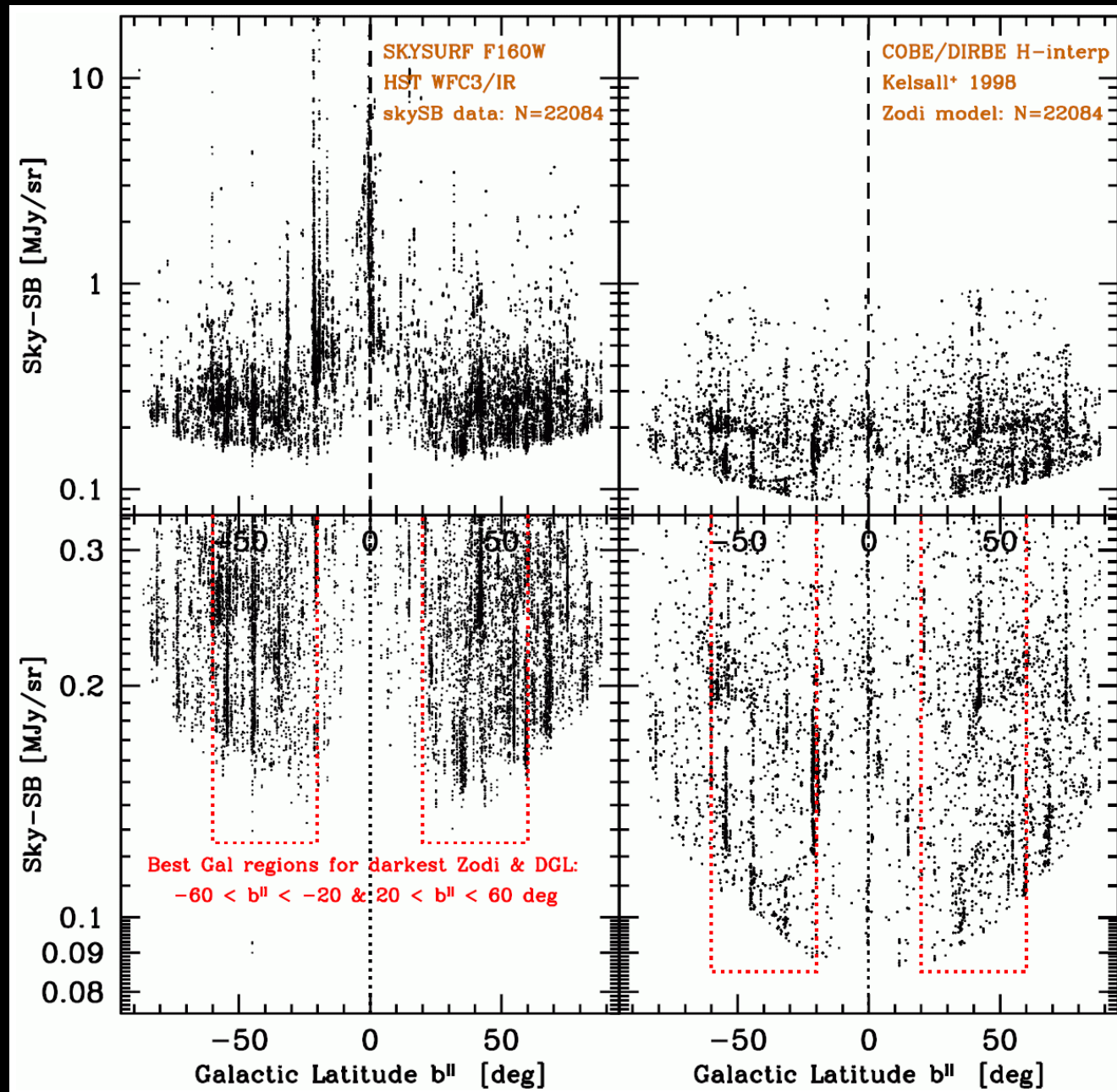
[Right]: Edge-on disks: *vertical sech* light-profiles (de Grijs⁺ 1997).

For Zodiacal disk-SB we use: $\text{sech}(z) = [\exp(z) + \exp(-z)] / 2$, which provide remarkable good fits to both dimmest HST data and Zodi models!

The (observed-model) sky-SB lets SKYSURF identify diffuse light sources:

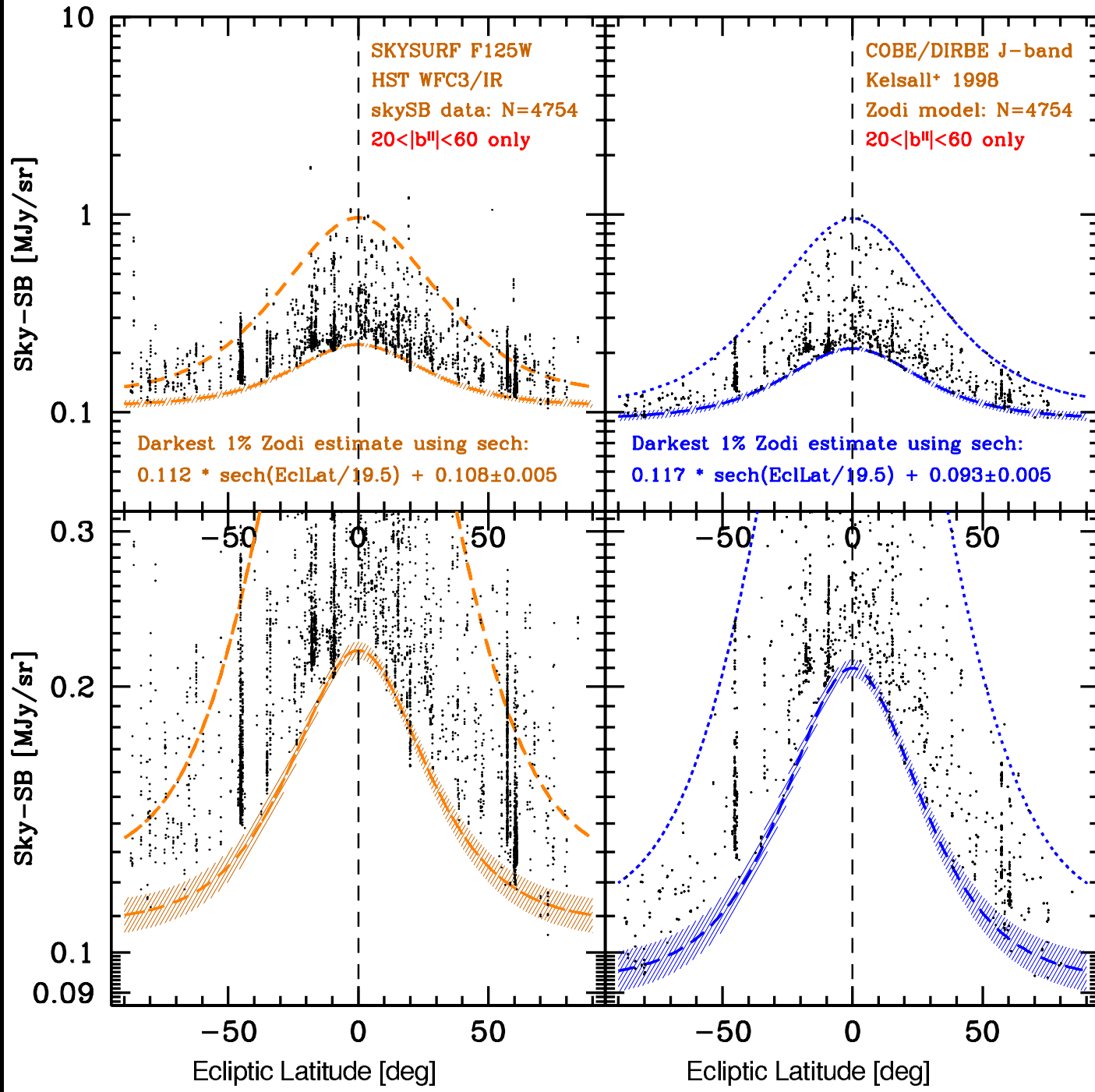
- 1) Residual instrumental effects; 2) Diffuse ZL component not in the model;
- 3) Diffuse Galactic Light (DGL); 4) Diffuse EBL between discrete galaxies.

(1b) SKYSURF's results and estimates of diffuse 1.25-1.6 μm light

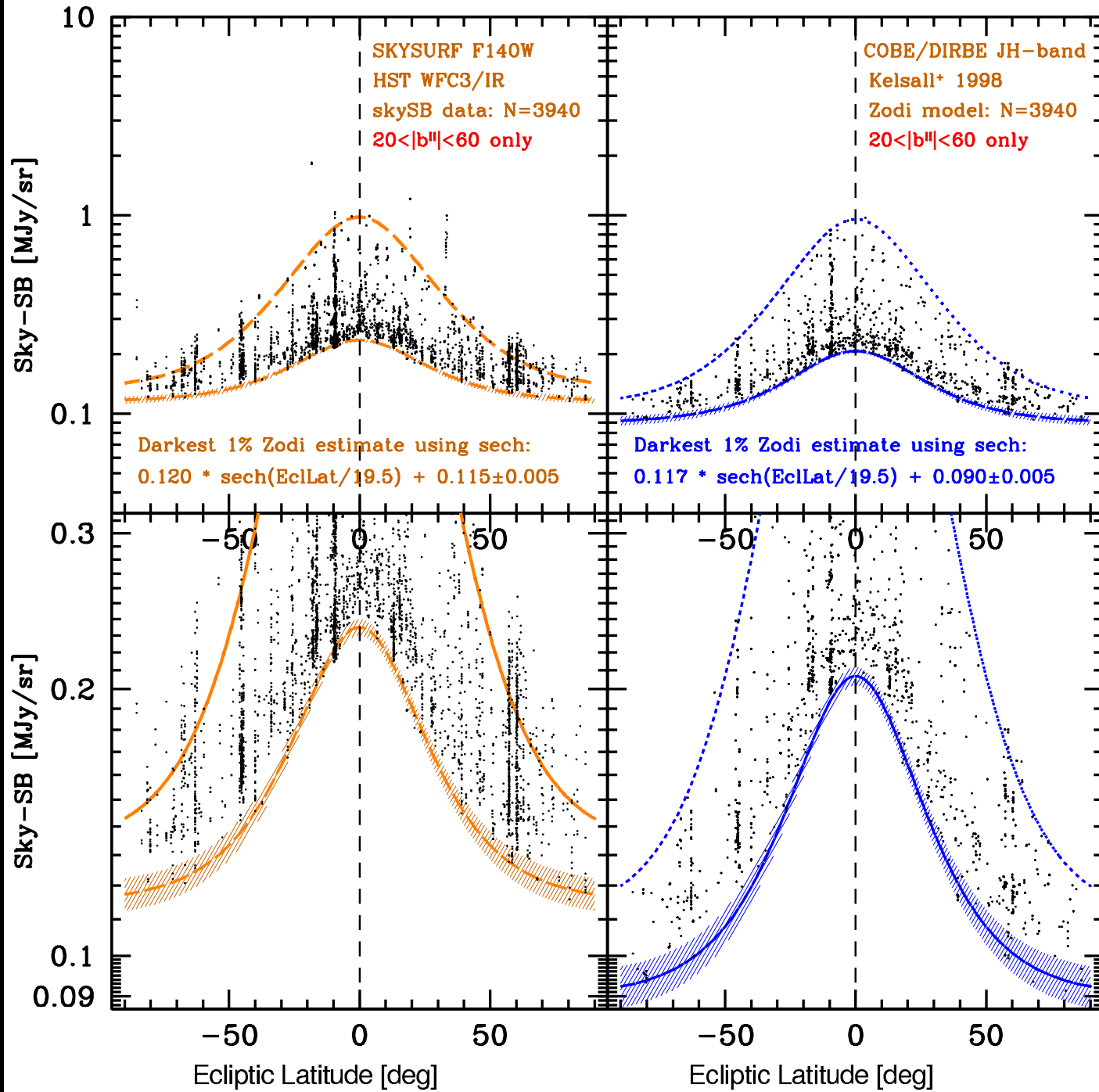


[Left]: 1.60 μm HST sky-SB; [Right]: Kelsall model for *same* (RA, Dec, t).

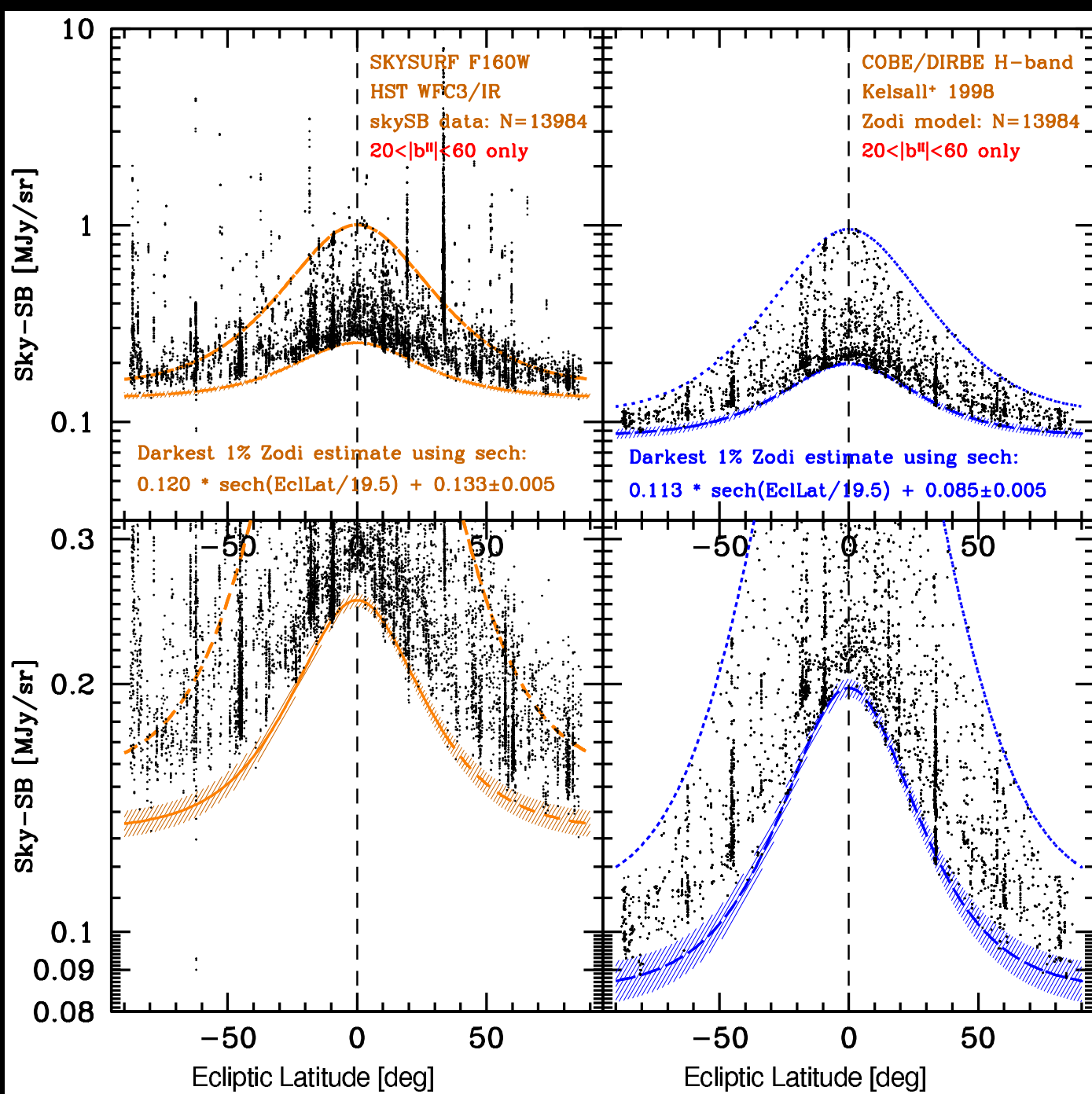
First, identify *darkest* regions in Galactic coordinates ($20^\circ \lesssim |b''| \lesssim 60^\circ$).



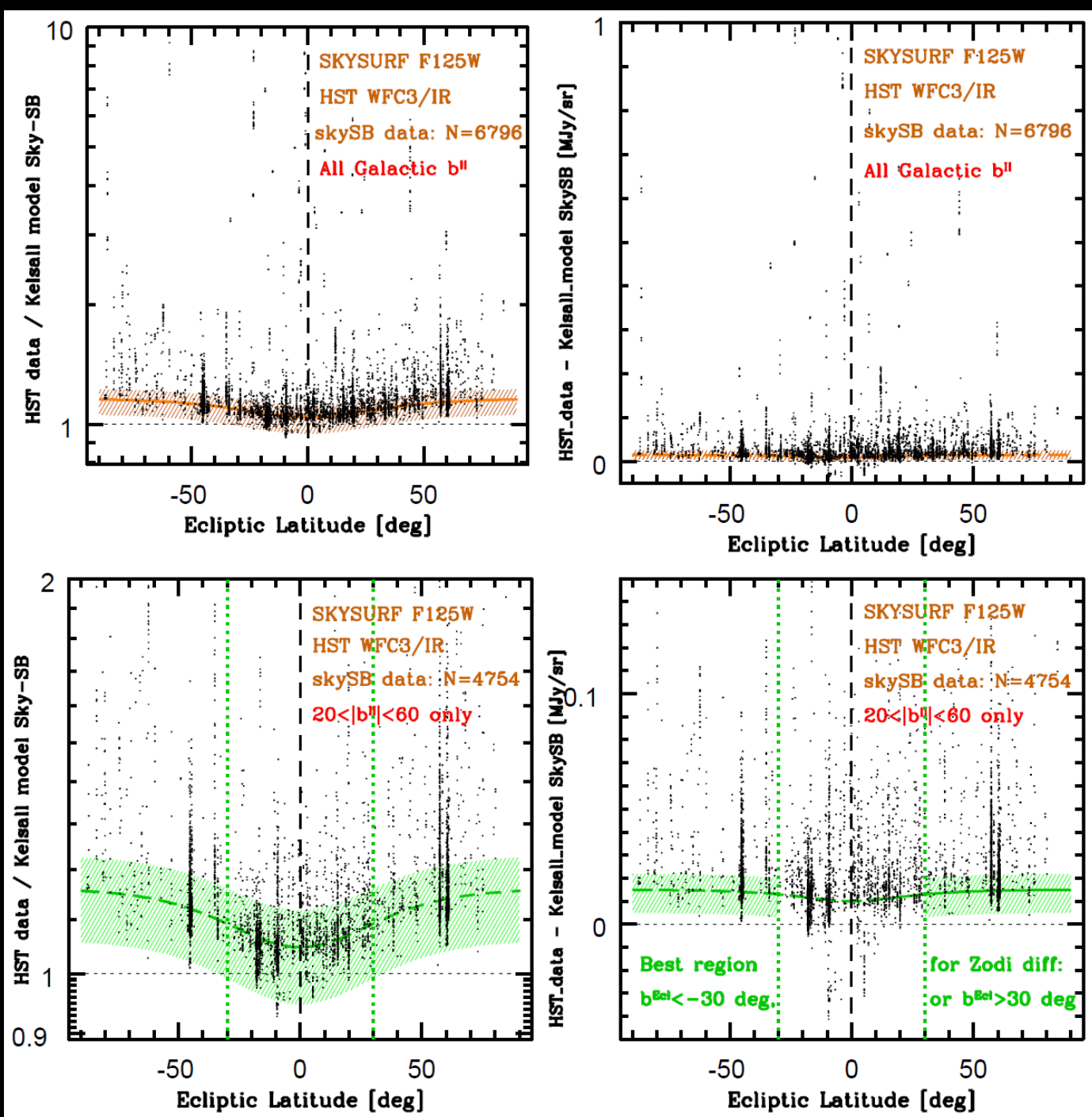
1.25 μm HST+Kelsall vs. b^{Ecl} : $\text{sech}+\text{error} = \text{lowest } 1\% \text{ of sky-SB.}$
 Lowest 1% $\Delta(\text{HST}-\text{Kelsall}) \simeq 0.015 \pm 0.008 \text{ MJy/sr}$ at darkest Galactic.



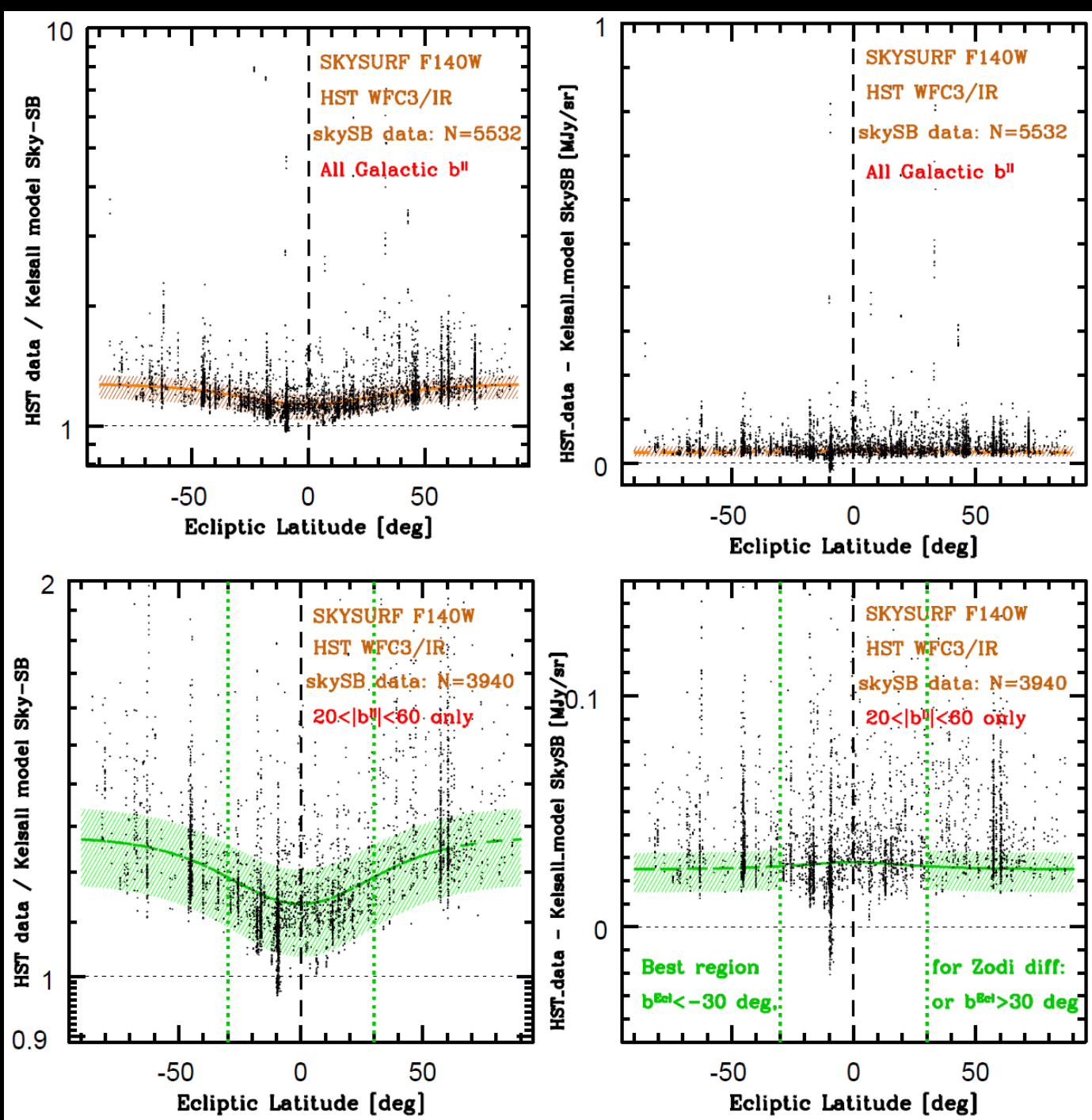
$1.40\ \mu\text{m}$ HST+Kelsall vs. b^{Ecl} : $\text{sech}+\text{error} = \text{lowest } 1\% \text{ of sky-SB.}$
 Lowest 1% $\Delta(\text{HST}-\text{Kelsall}) \simeq 0.025 \pm 0.009$ MJy/sr at darkest Galactic.



$1.60 \mu\text{m}$ HST+Kelsall vs. b^{Ecl} : $\text{sech}+\text{error} = \text{lowest } 1\% \text{ of sky-SB.}$
 Lowest 1% $\Delta(\text{HST}-\text{Kelsall}) \simeq 0.048 \pm 0.009 \text{ MJy/sr}$ at darkest Galactic.

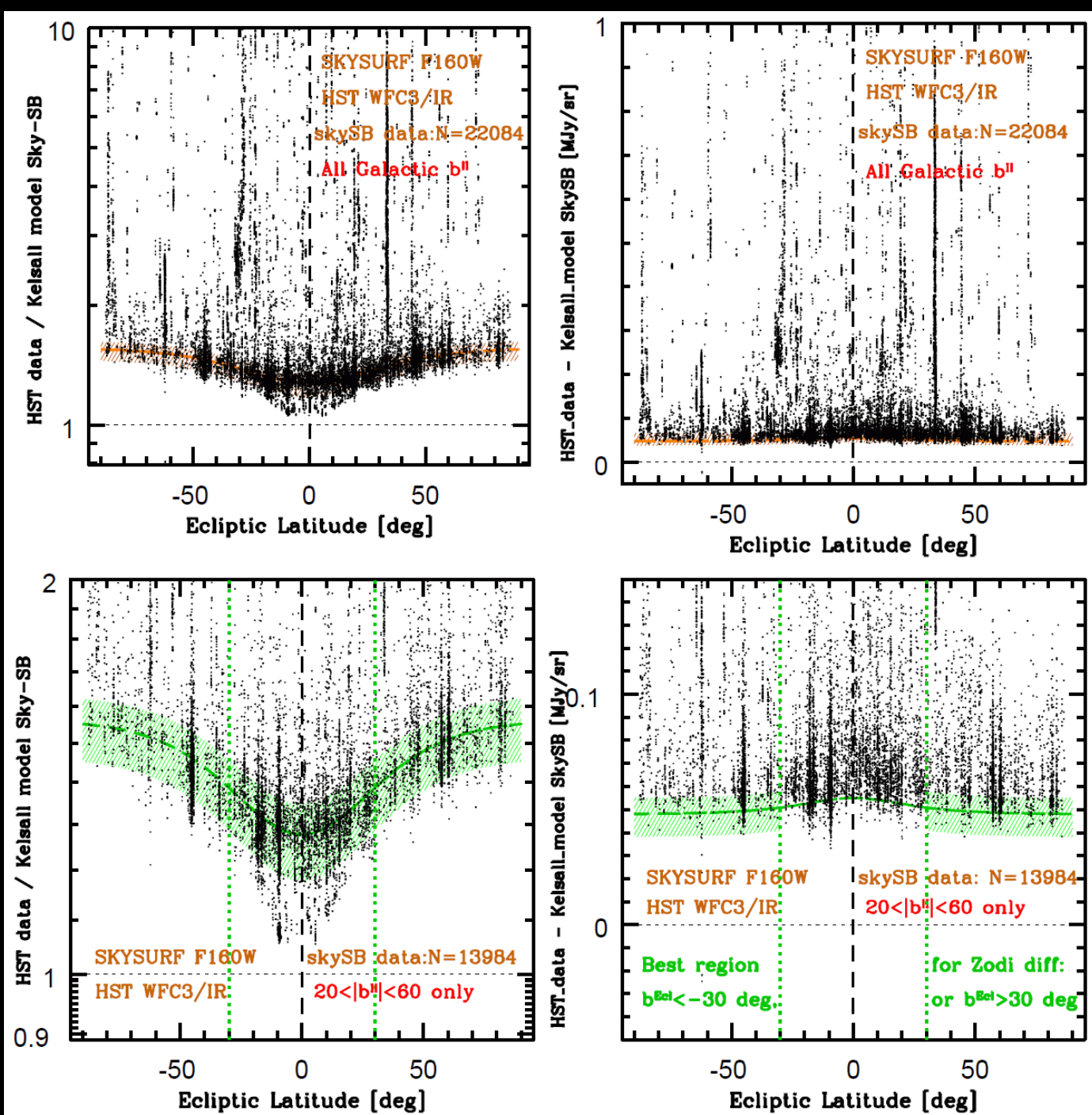


$1.25 \mu\text{m}$ [Left]: $HST/\text{Kelsall}$ ratio vs. b^{Ecl} ; [Right]: $HST-\text{Kelsall}$ difference.
 Linear offset $\Delta(HST-\text{Kelsall}) \simeq 0.015 \pm 0.008 \text{ MJy/sr}$ remains best fit.



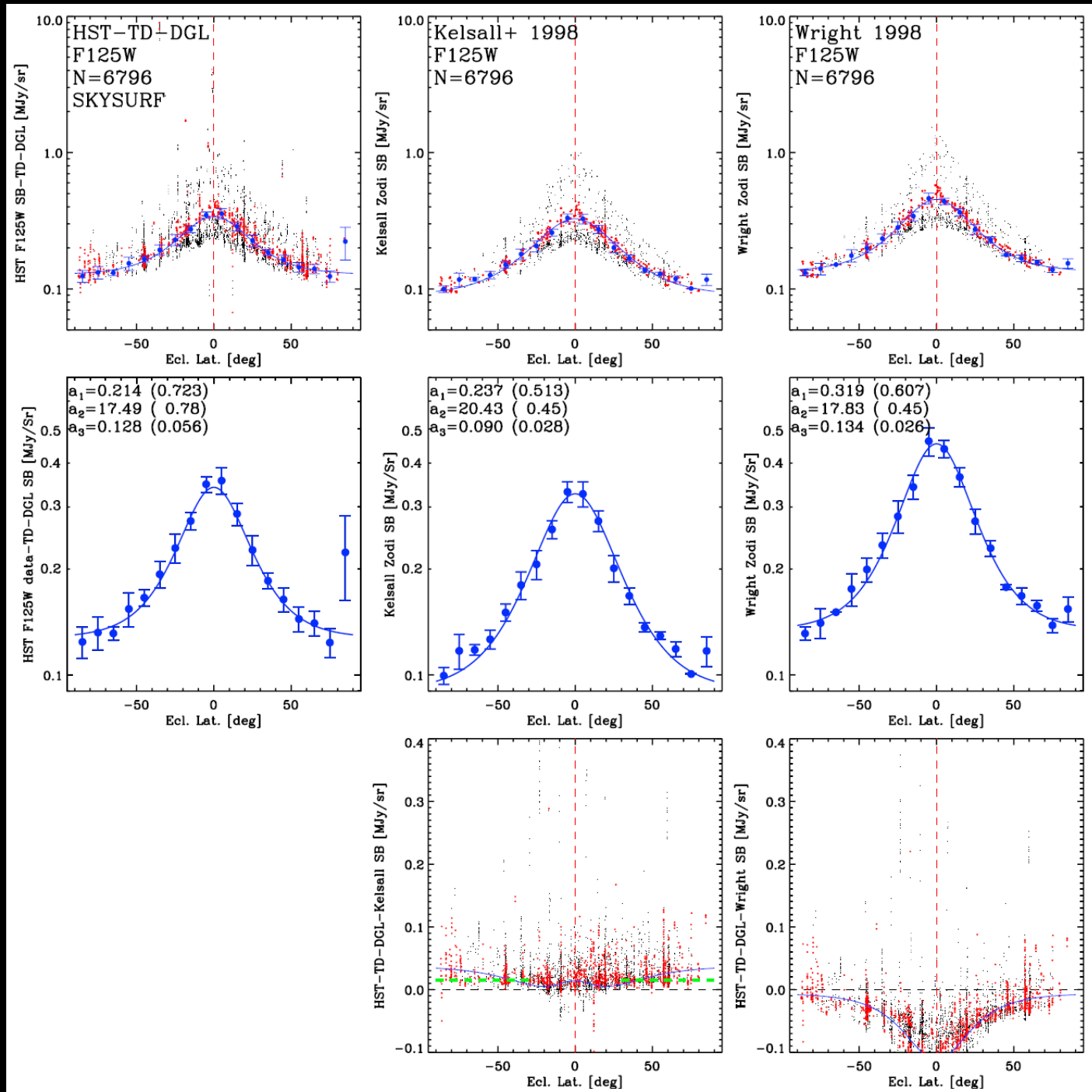
$1.40 \mu\text{m}$ [Left]: HST/Kelsall ratio vs. b^{Ecl} ; [Right]: HST–Kelsall difference.

Linear offset $\Delta(\text{HST} - \text{Kelsall}) \simeq 0.025 \pm 0.009 \text{ MJy/sr}$ remains best fit.

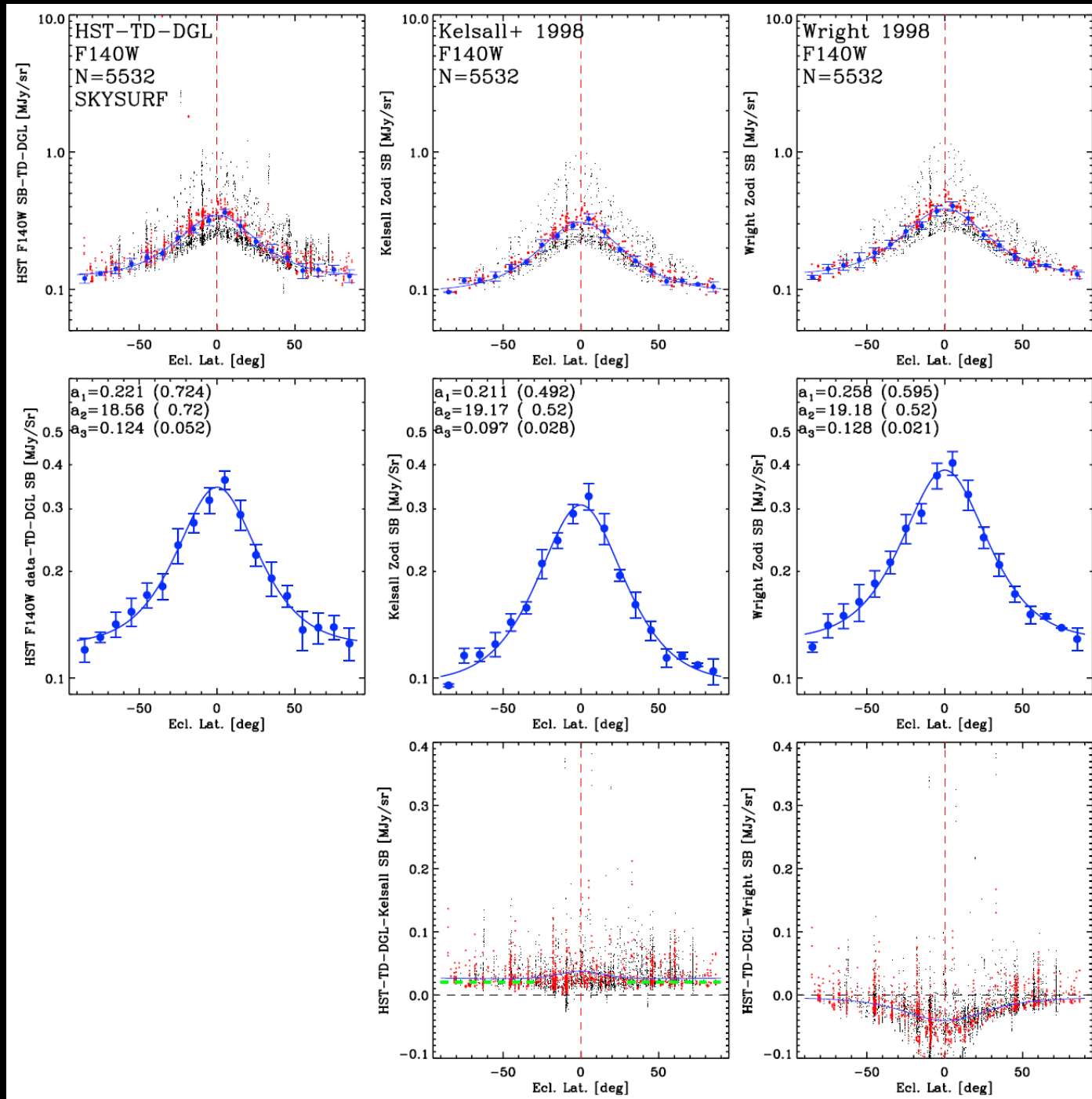


$1.60 \mu\text{m}$ [Left]: $\text{HST}/\text{Kelsall}$ ratio vs. b^{Ecl} ; [Right]: $\text{HST}-\text{Kelsall}$ difference.

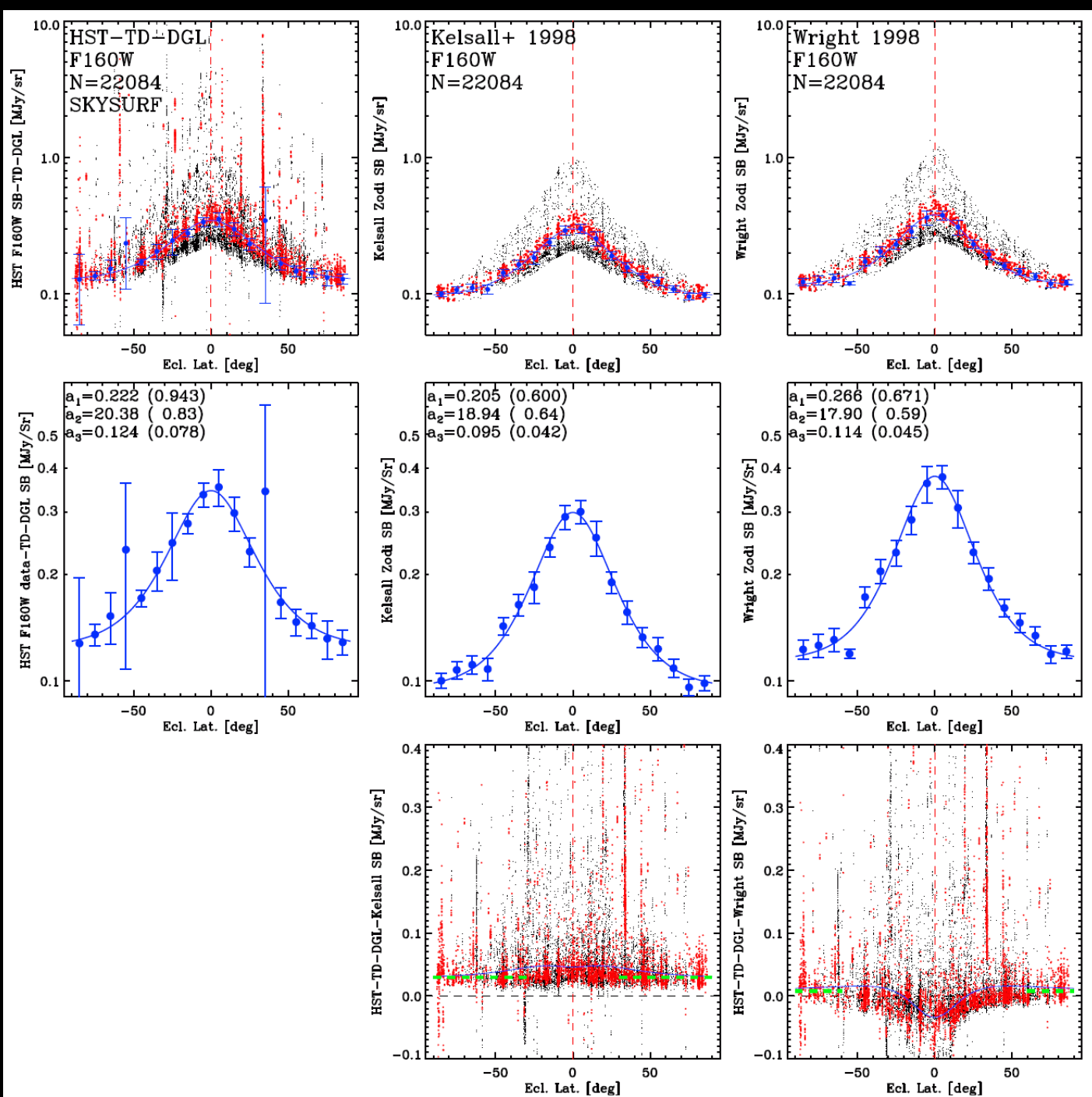
Linear offset $\Delta(\text{HST}-\text{Kelsall}) \simeq 0.048 \pm 0.009 \text{ MJy/sr}$ remains best fit.



$1.25 \mu\text{m}$ [Left]: HST; [Middle] Kelsall; [Right] Wright model vs. b^{Ecl} .
 HST(TD+DGL-subtracted): Kelsall linear offset stays; Wright shows none.

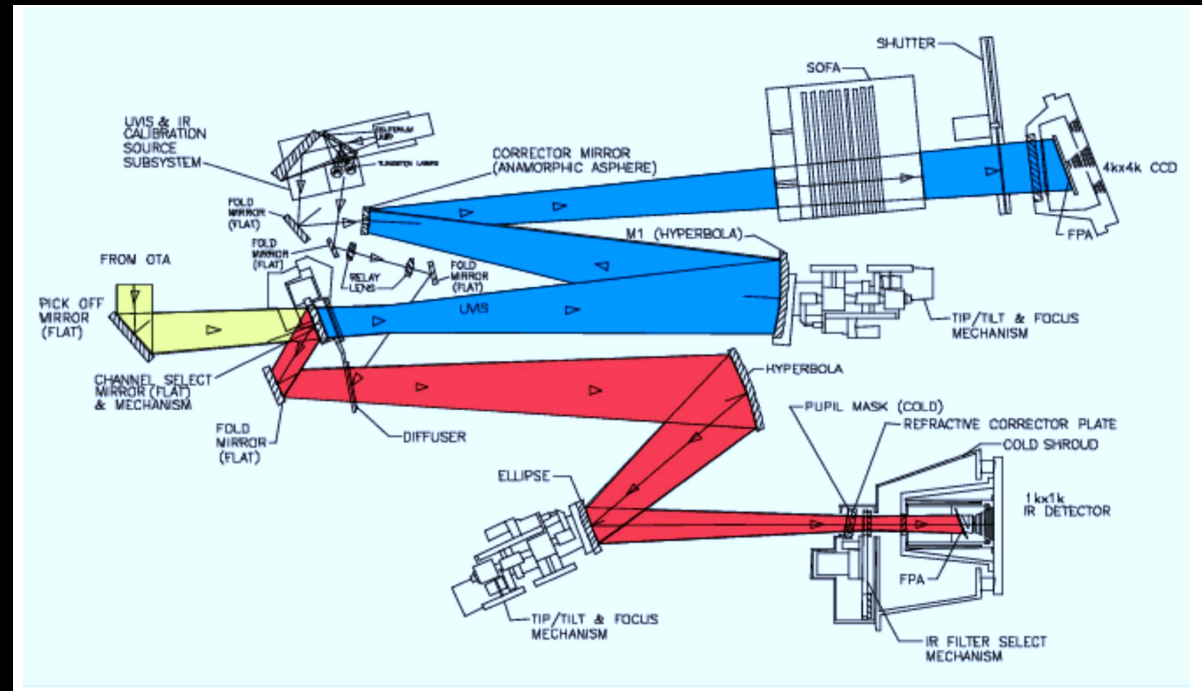
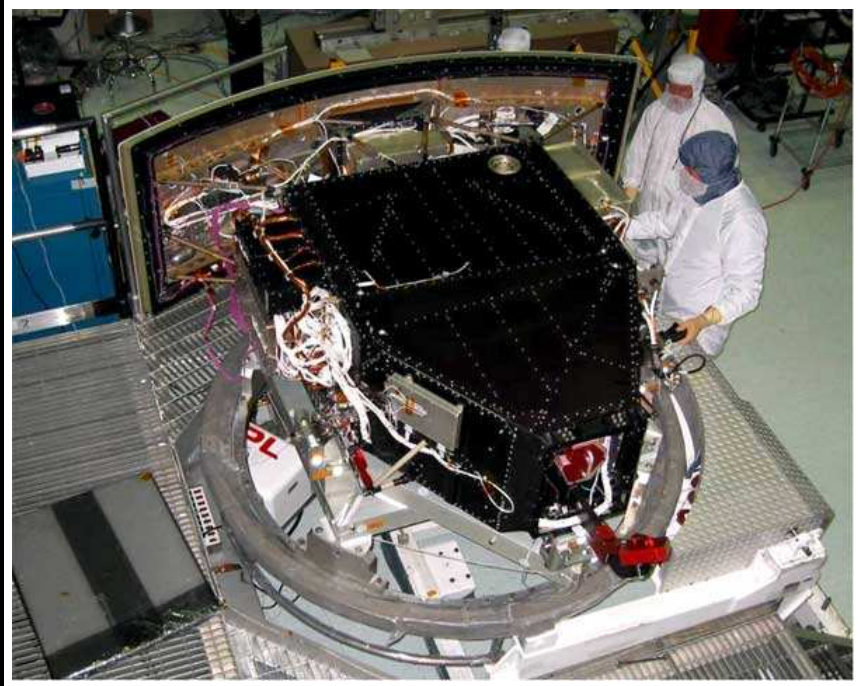


1.40 μm [Left]: HST; [Middle] Kelsall; [Right] Wright model vs. $b^{\text{Ecl.}}$.
 HST(TD+DGL-subtracted): Kelsall linear offset stays; Wright shows none.



1.60 μm [Left]: HST; [Middle] Kelsall; [Right] Wright model vs. b^{Ecl} .
 HST(TD+DGL-subtracted): Kelsall linear offset stays; Wright has marginal.

(1b) We must also subtract the HST WFC3/IR Thermal Dark signal:

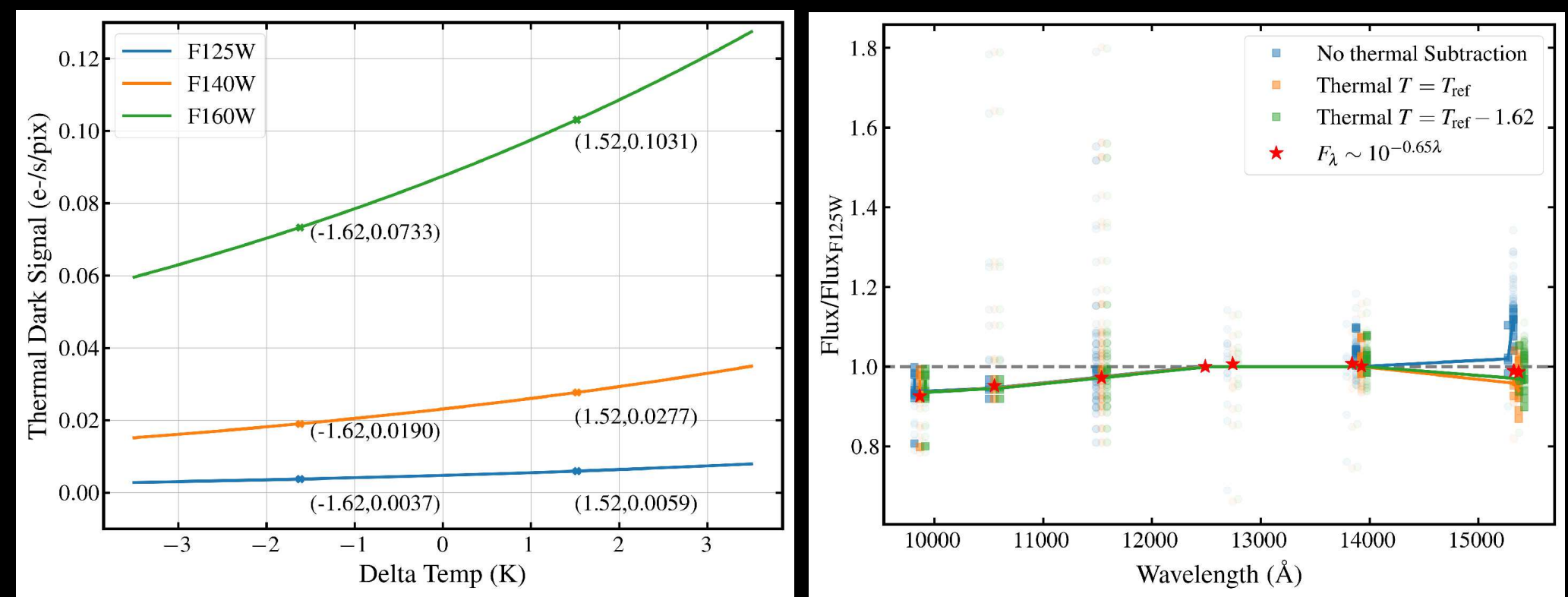


[Left]: WFC3 at NASA GSFC before May 2009 Shuttle launch.

[Right]: WFC3 model: optical train Temp ranges from $T=287-173$ K.

- Several dozen temperature sensors monitor temperature T across orbit within 1–2 K, enabling predictions of Thermal Dark (TD) signal vs. T .
- The *synphot* package predicts Planck-BB/solid-angle contribution from each optical component vs. T as seen by the WFC3/IR-detector.

(Details in Carleton, T. et al. 2022, AJ, 164, 170; & McIntyre et al. 2024; astro-ph/2407.12290v2).

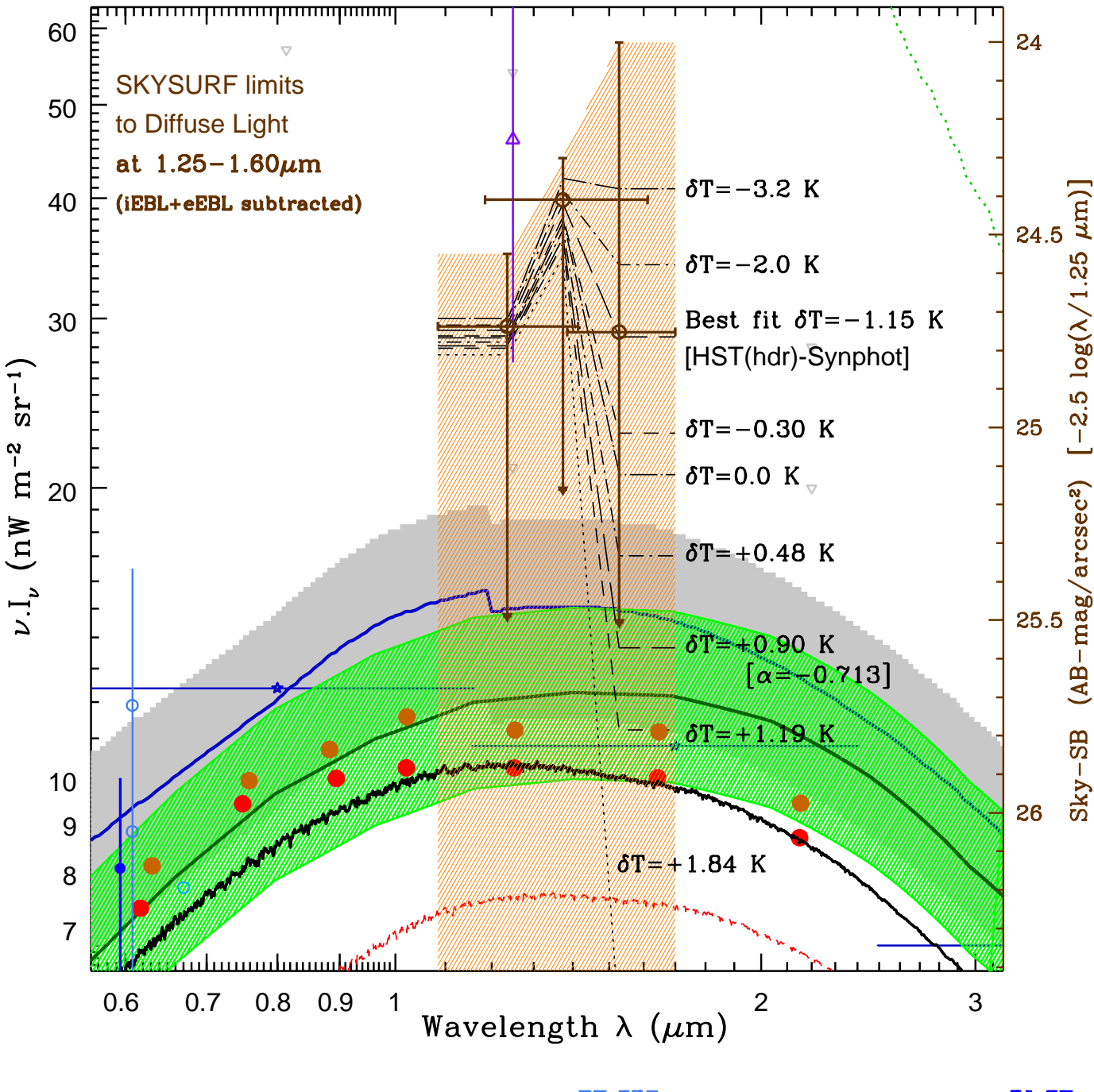


[Left]: *synphot* WFC3/IR Thermal Dark (TD) signal modeling.

[Right]: TD for $\langle \Delta T(\text{HST}) \rangle \simeq -1.62 \text{ K}$ (compared to nominal T).

- Thermal Dark signal largest at $1.6 \mu\text{m}$, but well determined and small at $1.25\text{--}1.40 \mu\text{m}$.

(Carleton, T. et al. 2022, AJ, 164, 170; & McIntyre et al. 2024; astro-ph/2407.12290v2).

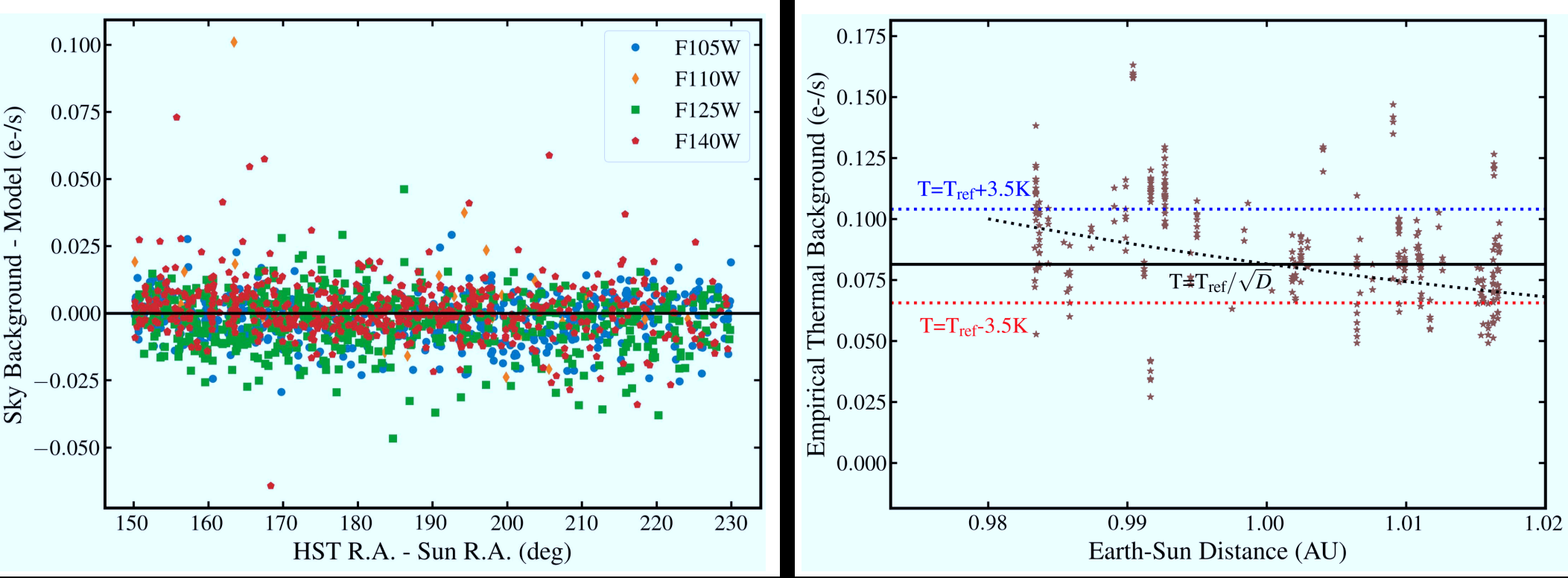


HST showed $\lesssim 29\text{--}40 \text{ nW/m}^2/\text{sr}$ of diffuse light at 1.25–1.6 μm compared to Kelsall's Zodiacal model (Carleton⁺, 2022, AJ, 164, 170).

- HST sees no significant signal compared to the Wright model.
- HST diffuse light at 1 AU larger than New Horizon's 8–10 $\text{nW/m}^2/\text{sr}$ at 43–51 AU (Lauer⁺ 20, 21).

Next step: Refine Zodiacal models to explain (most/all?) of the diffuse light.

- May need to include higher-albedo Oort Cloud Comet dust at $D \sim 1\text{--}3 \text{ AU}$.



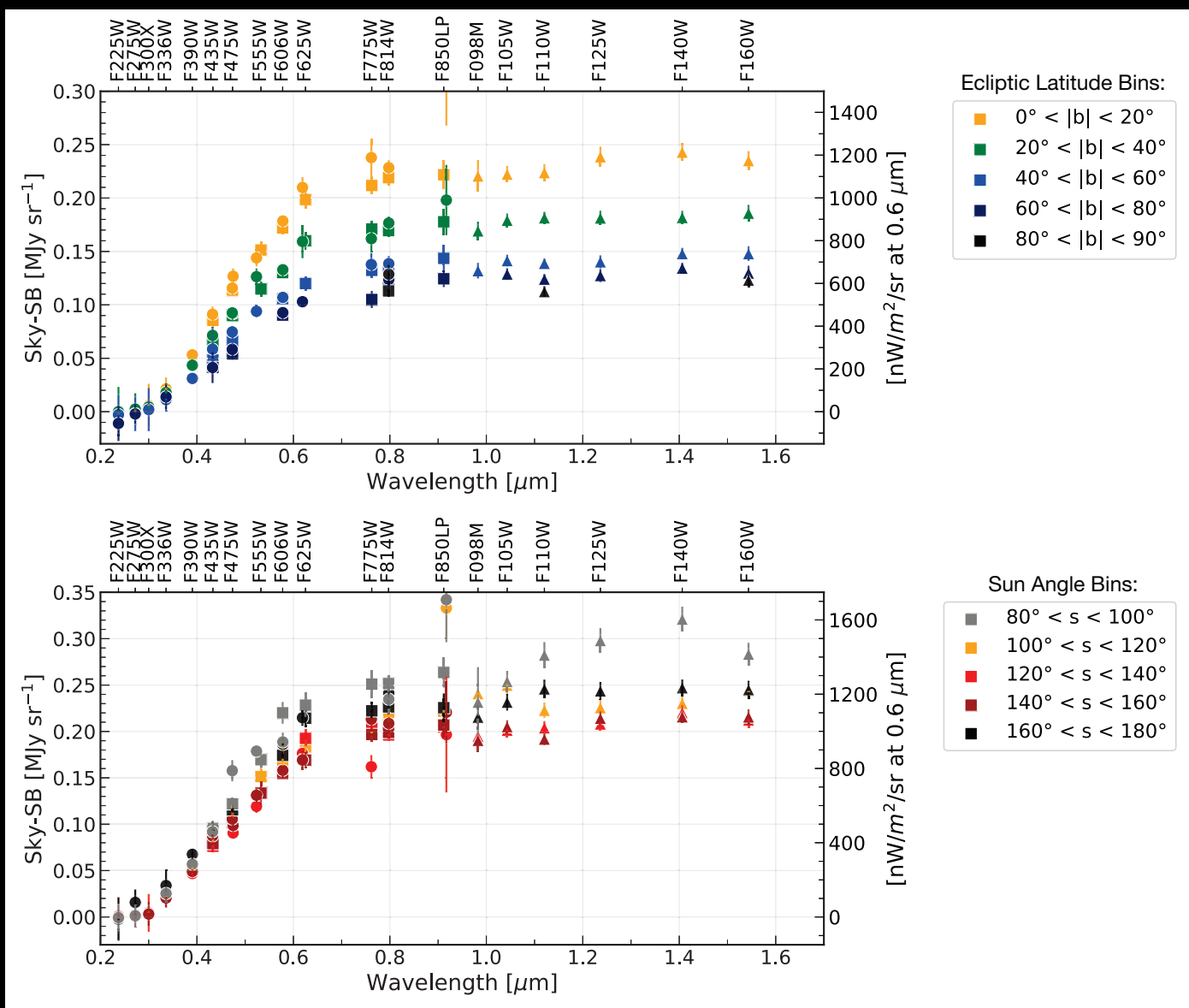
[Left]: HST Sky-SB – (best model and Thermal Dark signal) for the four bluest WFC3/IR filters.

[Right]: Thermal signal in WFC3/IR F160W vs. Earth-Sun distance.

⇒ Confidence in orbital-phase T-dependent Thermal Dark predictions:

- Well determined and small at 1.25–1.40 μm , but larger errors in F160W.

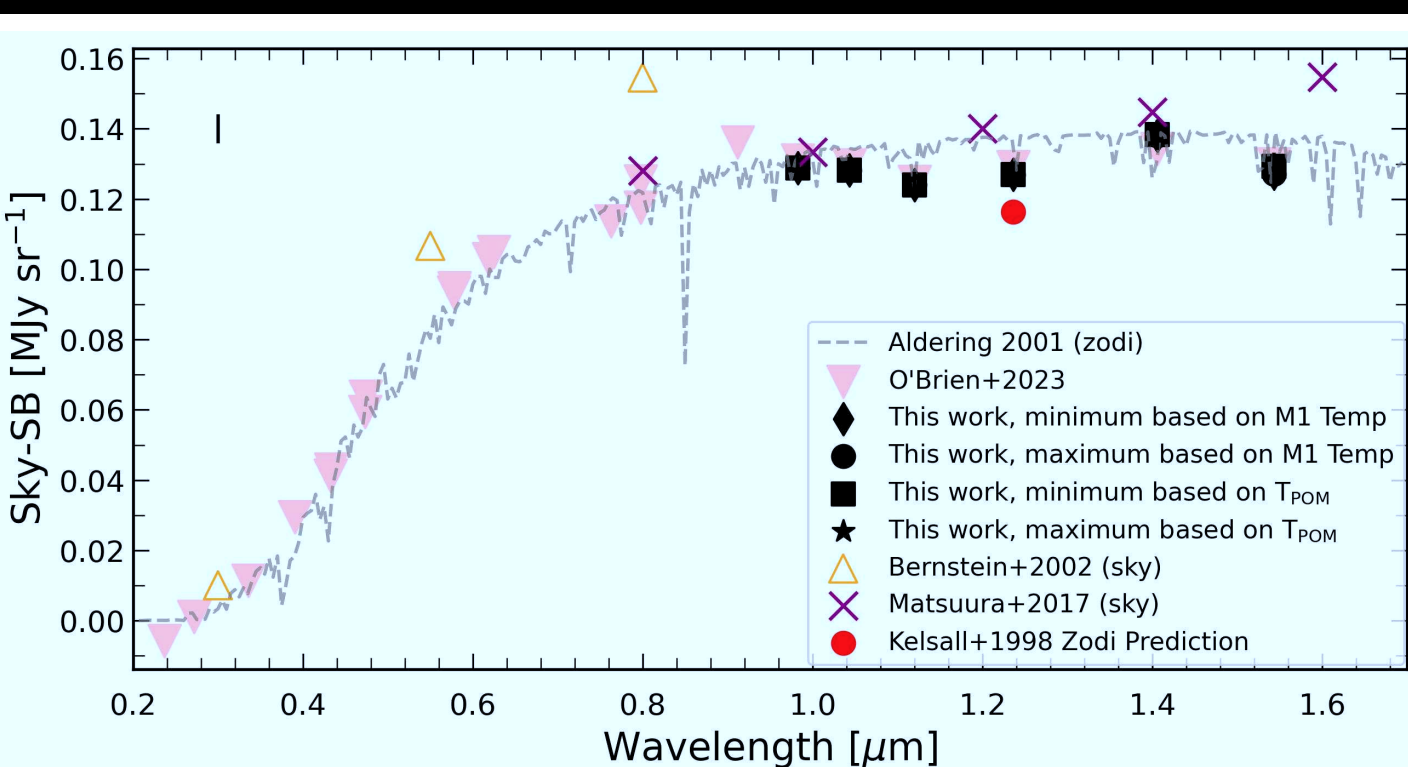
(Carleton, T. et al. 2022, AJ, 164, 170; & McIntyre et al. 2024; astro-ph/2407.12290v2).



Top: Ecliptic Latitude dependence of panchromatic HST sky-SB.

Bottom: Sun Angle dependence of panchromatic HST sky-SB.

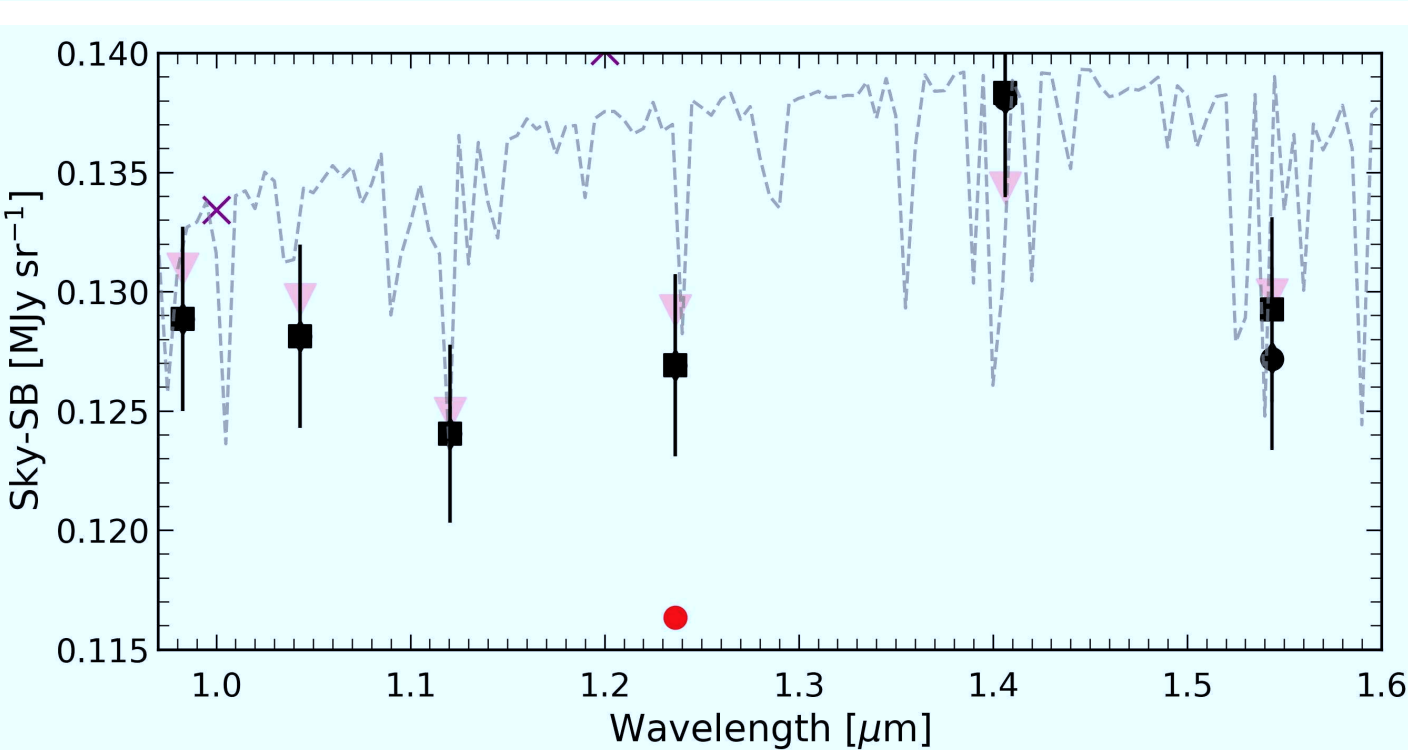
- Both show expected trends of higher sky-SB at lower $l^{\text{Ecl}}/\text{Sun-angles}$.

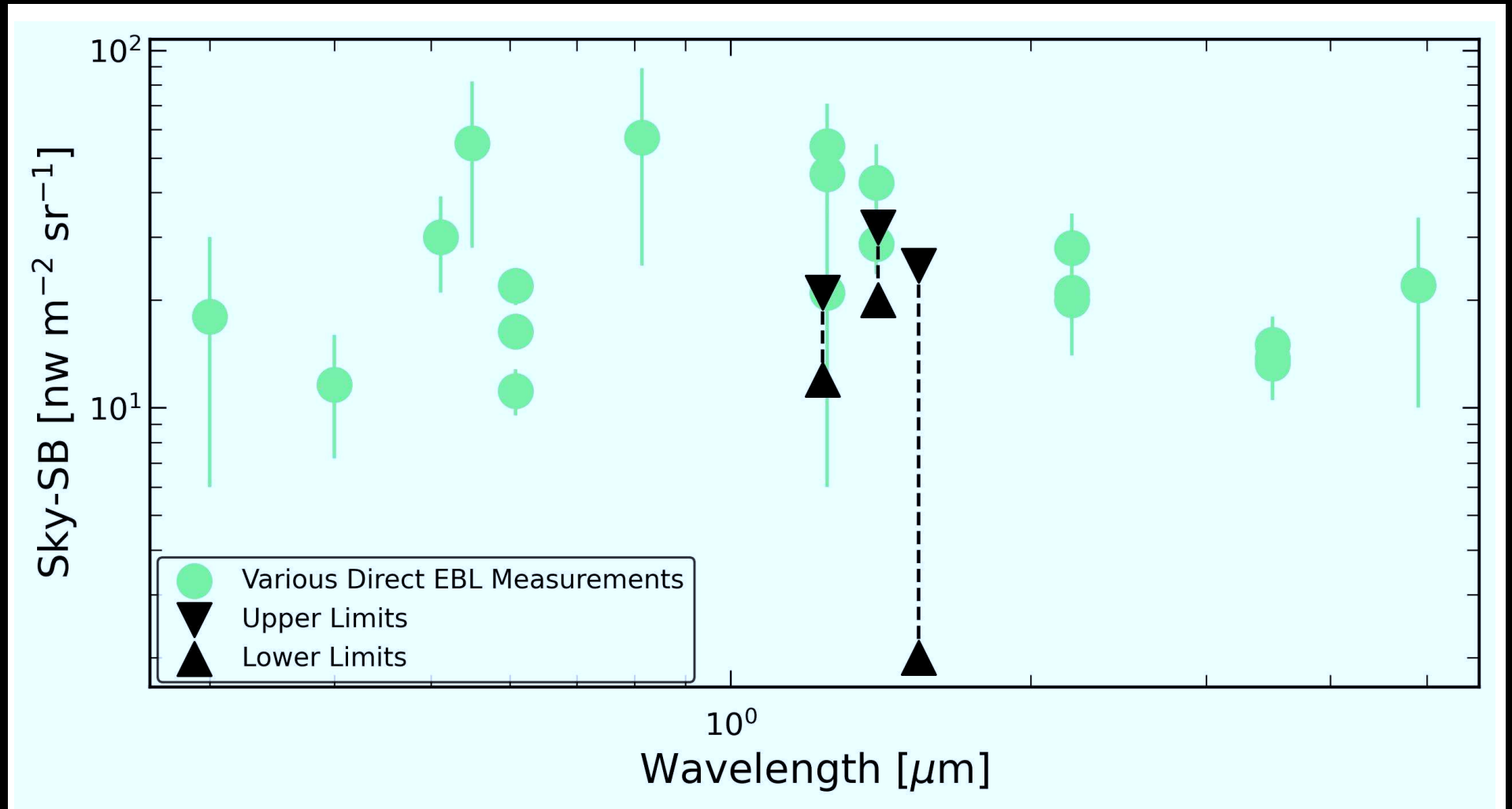


Top: Best SKYSURF sky-SB compared to earlier work.
Bottom: enlargement compared to (reddened) Aldering Zodiacal spectrum and Kelsall+ (1998) model.

- The best SKYSURF Zodiacal NIR spectrum is a bit bluer than reddened Aldering, but at 1.25 μm higher than Kelsall+ (1998), which needs updating.

(O'Brien et al. 2023, AJ, 165, 237;
McIntyre et al. 2024, AJ, in press,
[astro-ph/2407.12290v2](https://arxiv.org/abs/2407.12290v2)).

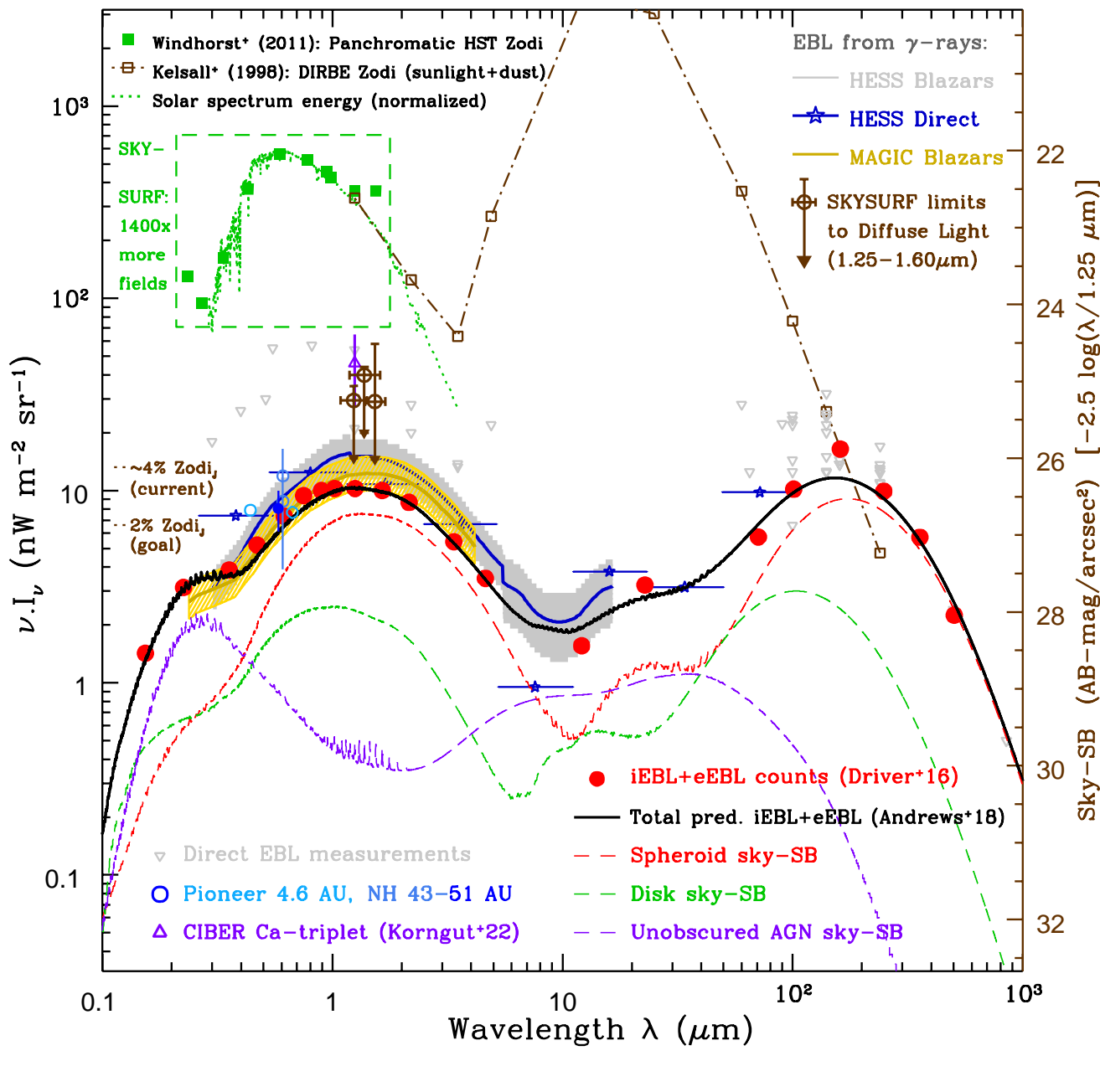




Residual SKYSURF 1.25–1.6 μm Diffuse Light compared to earlier work:

- Assuming the Diffuse Light near-IR spectrum is flat, the common 1.25–1.6 μm SKYSURF Diffuse Light levels are about $\sim 20 \text{ nW/m}^2/\text{sr}$.

(McIntyre et al. 2024, AJ, in press; astro-ph/2407.12290v2; see also Tim Carleton's talk here).



- At 1 AU, SKYSURF sees $\sim 20 \text{ nW/m}^2/\text{sr}$ of diffuse 1.25–1.6 μm light!

(Carleton⁺ 2022, AJ, 164, 170; O'Brien⁺ 2023, AJ, 165, 237; McIntyre⁺ astro-ph/2407.12290v2).

Total Energy vs. λ :

(Driver⁺ 16; Windhorst⁺ 18, 21):

Sunlight scattered off the
Zodiacal dust.

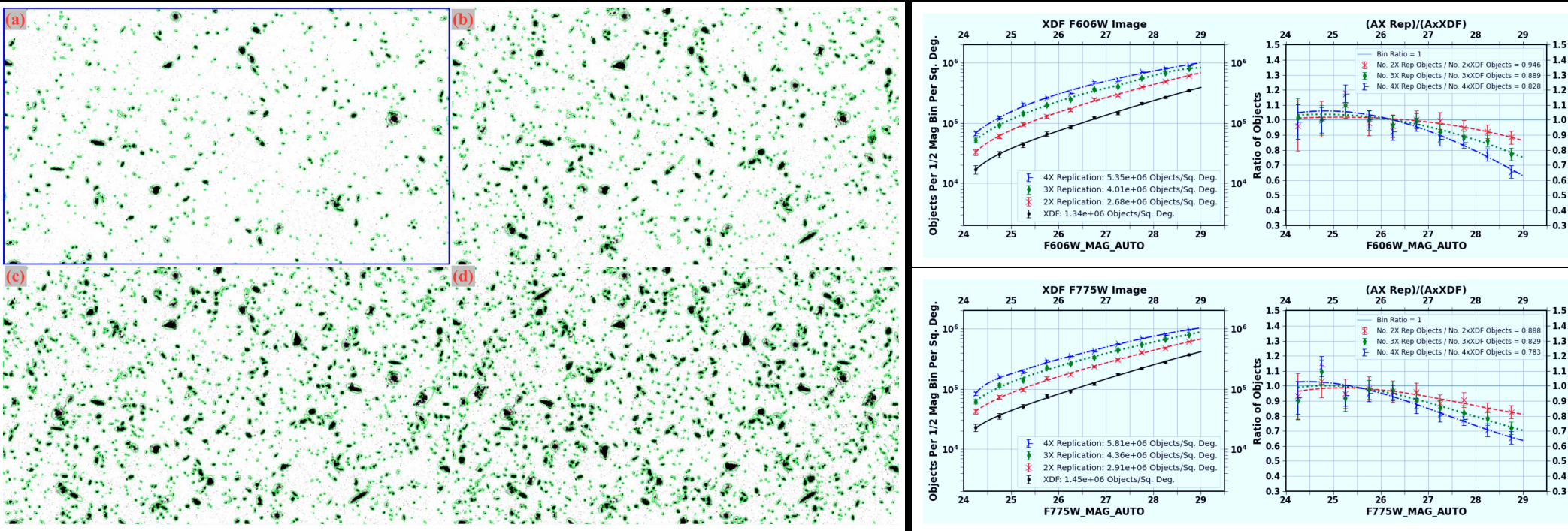
Thermal radiation from
 $\gtrsim 240 \text{ K}$ Zodiacal dust.

Grey dots: Diffuse EBL
from direct experiments.

Dots: Discrete EBL from
galaxy counts (+models).

Lauer (2021, 2022) NH
at 43–51 AU. SKYSURF
1.25–1.6 μm limits.

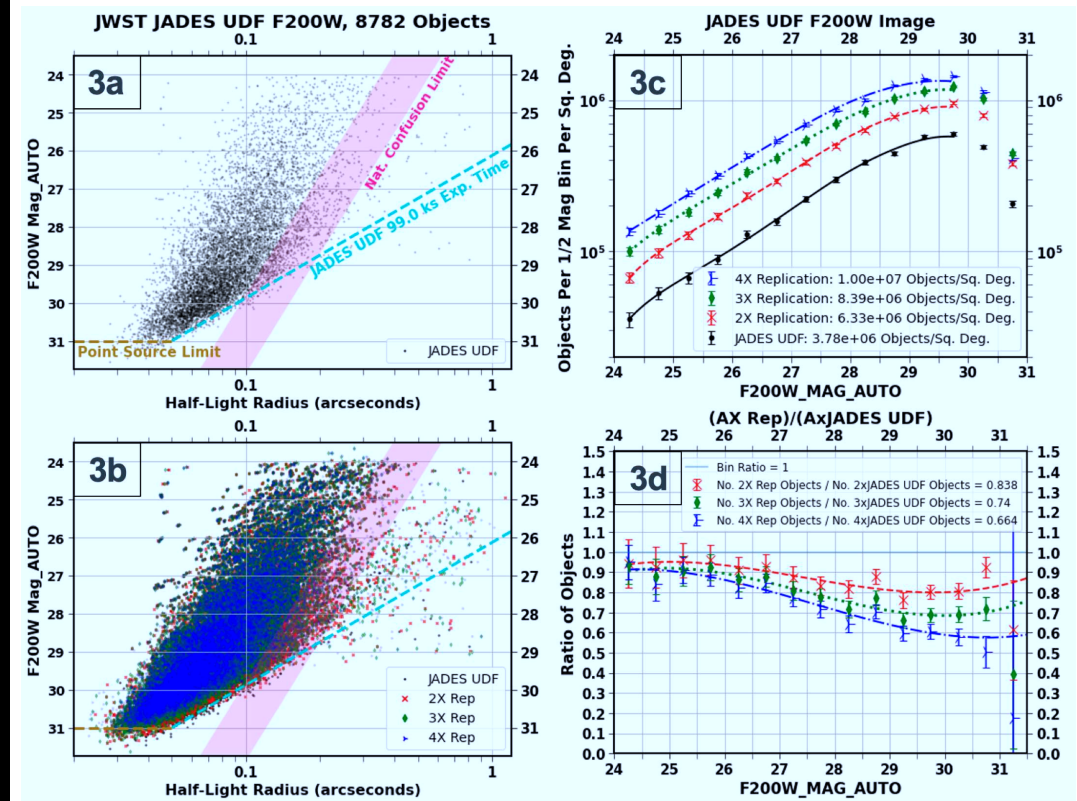
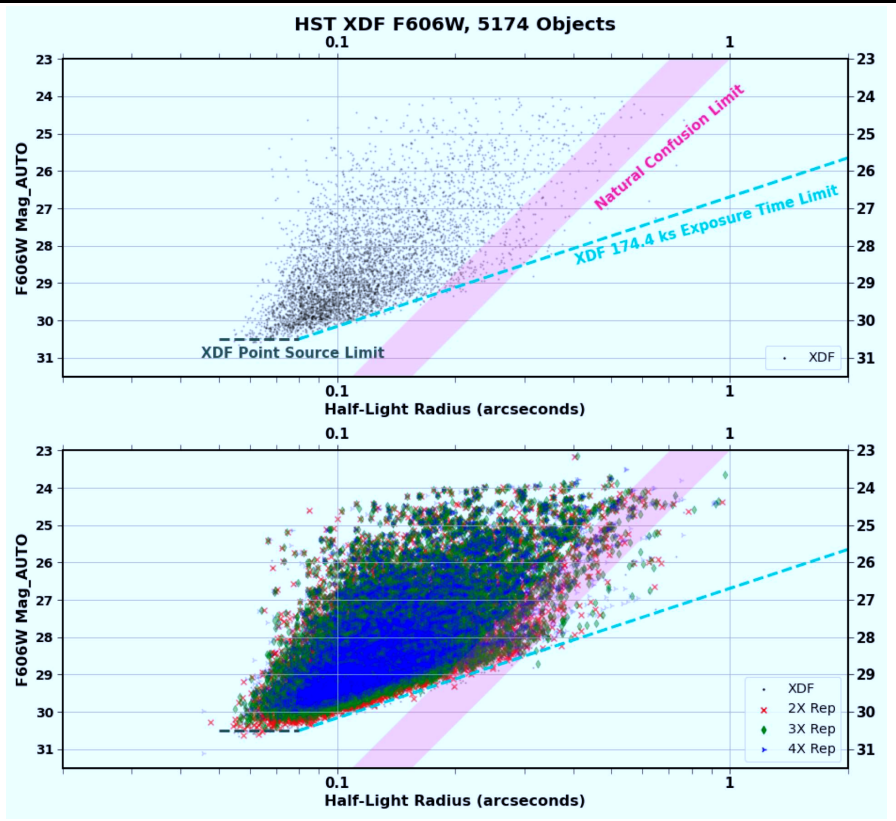
(1c) Can undetected (low-SB) galaxies cause 0.3 dex of Diffuse Light?



[Left]: Add HUDF image to itself $2\times$, $3\times$, $4\times$ after $n \times 90^\circ$ rotation:

[Right]: $4\times$ HUDF counts still $\gtrsim 65\%$ complete for $AB \gtrsim 28.5-29$ mag.

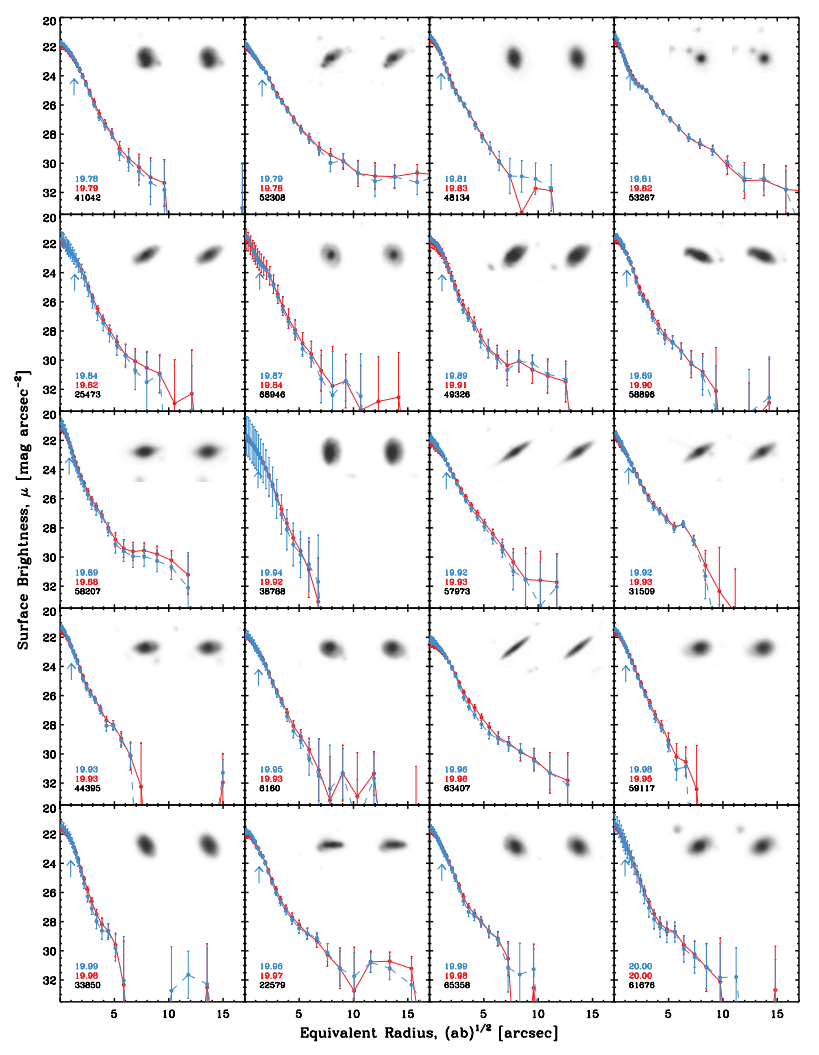
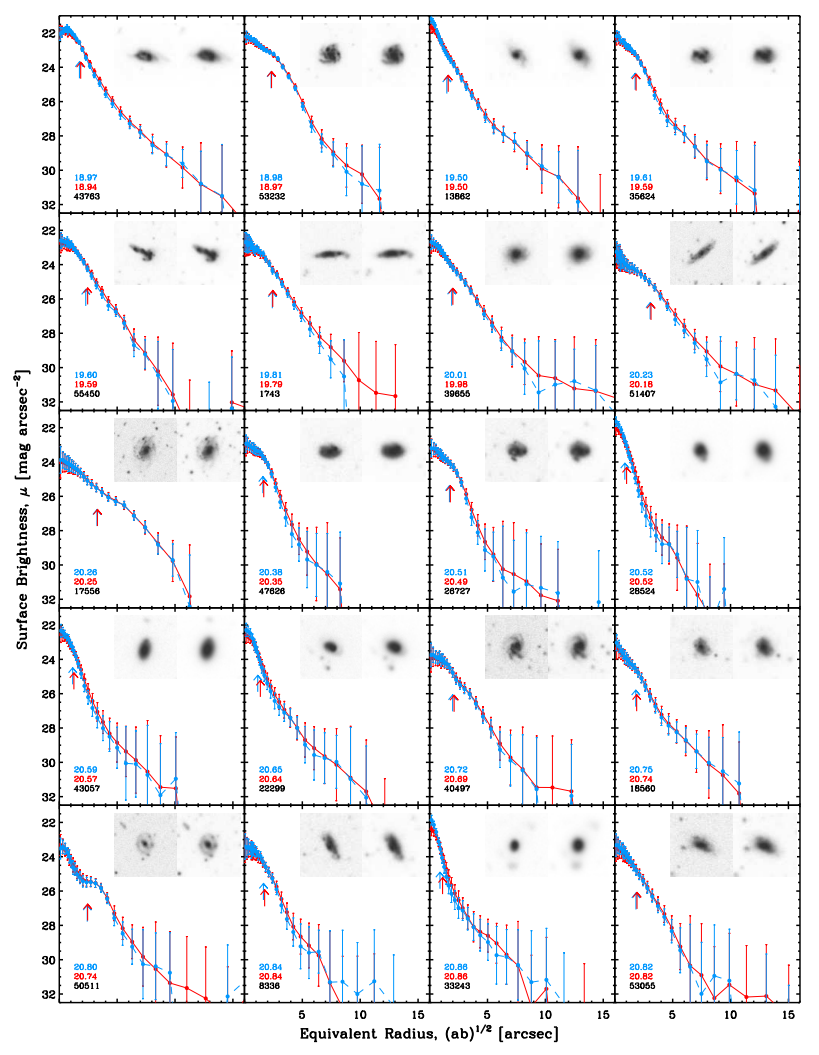
- Crowding not enough to explain factor ~ 2 diffuse flux at $AB \gtrsim 24$ mag.
- ⇒ Cannot explain diffuse light through missing ordinary galaxies!
- Missing diffuse light caused by other sources? (dim Zodi component!)



Top: mag vs r_e for 174 ksec XDF (left) & 99 ksec JADES (middle) galaxies.
 Bottom: Same for XDF & JADES rotated+replicated onto itself 2X, 3X, 4X.

Right: Counts and completeness functions for 2X, 3X, 4X rotated images.

- $\lesssim 35\%$ of faintest galaxies lost due to statistical object overlap.
- Factor of ~ 2 in Diffuse Light not explained by missing faint galaxy pops.
- Faint gals are $\lesssim 10\%$ of IGL \Rightarrow need factor $\gtrsim 10$ in missing objects!



[Left]: LBT U-band, [Right] r-band: 20 of ~ 300 galaxies with $17 \lesssim AB \lesssim 22$ (*i.e.*, comprising *middle* 50% of IGL; Ashcraft⁺ 2018, 2022).

- 27-hr LBT stack to $\lesssim 32$ mag/arcsec² shows on average $\lesssim 10\text{--}20\%$ extra flux in galaxy outskirts compared to 6-hr best-seeing LBT stack.

\implies Factor of ~ 2 diffuse light not likely hiding in dim galaxy outskirts!

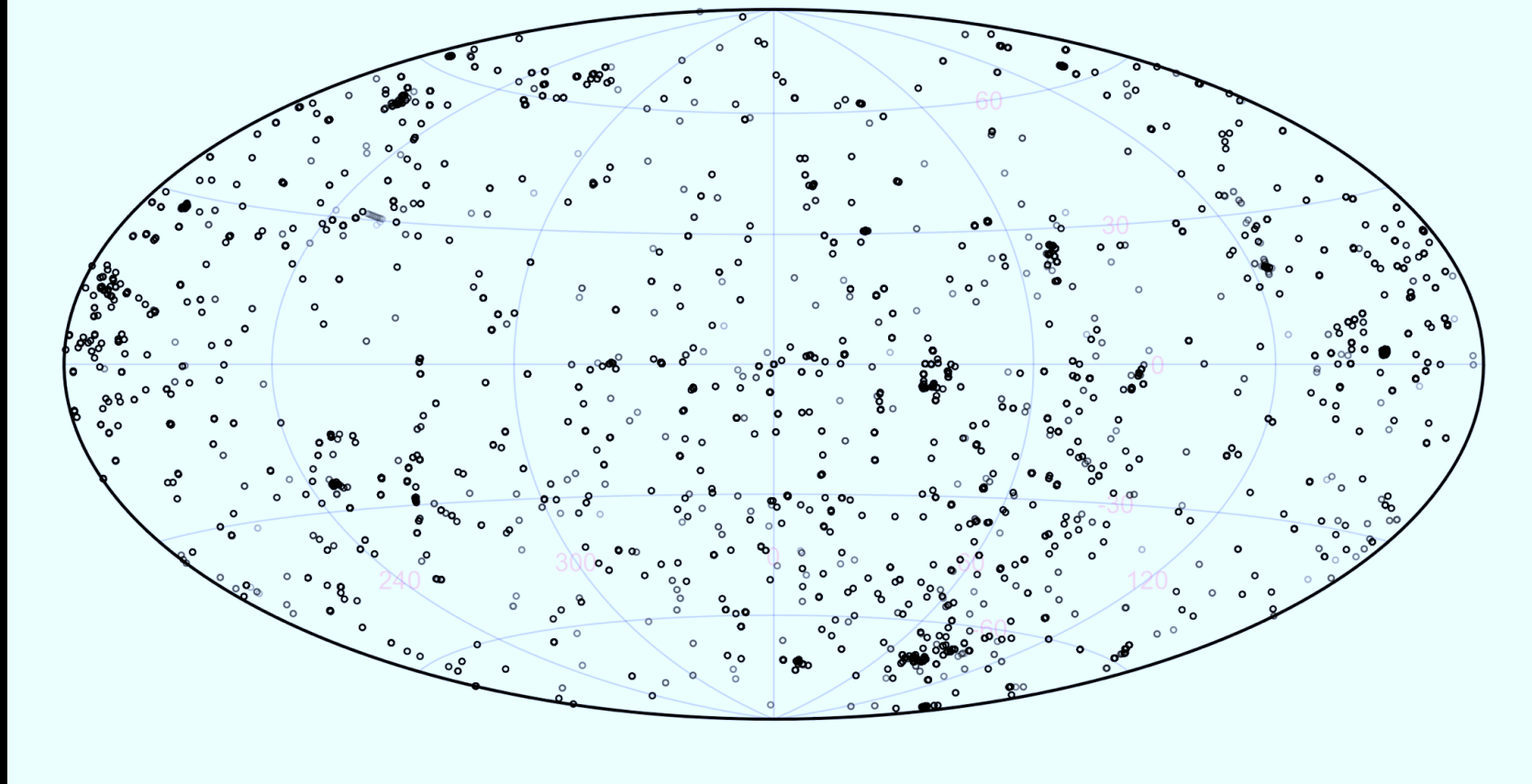
(2) Summary of JWST PEARLS & SKYSURFIR and its Diffuse Light limits



What Diffuse Light limits can JWST set from the ultradark L2 environment?

- HST has had 189,335 sunrises + sunsets since its April 1990 launch;
- JWST has had only 1 sunrise + 1 sunset since its Dec. 2021 launch!

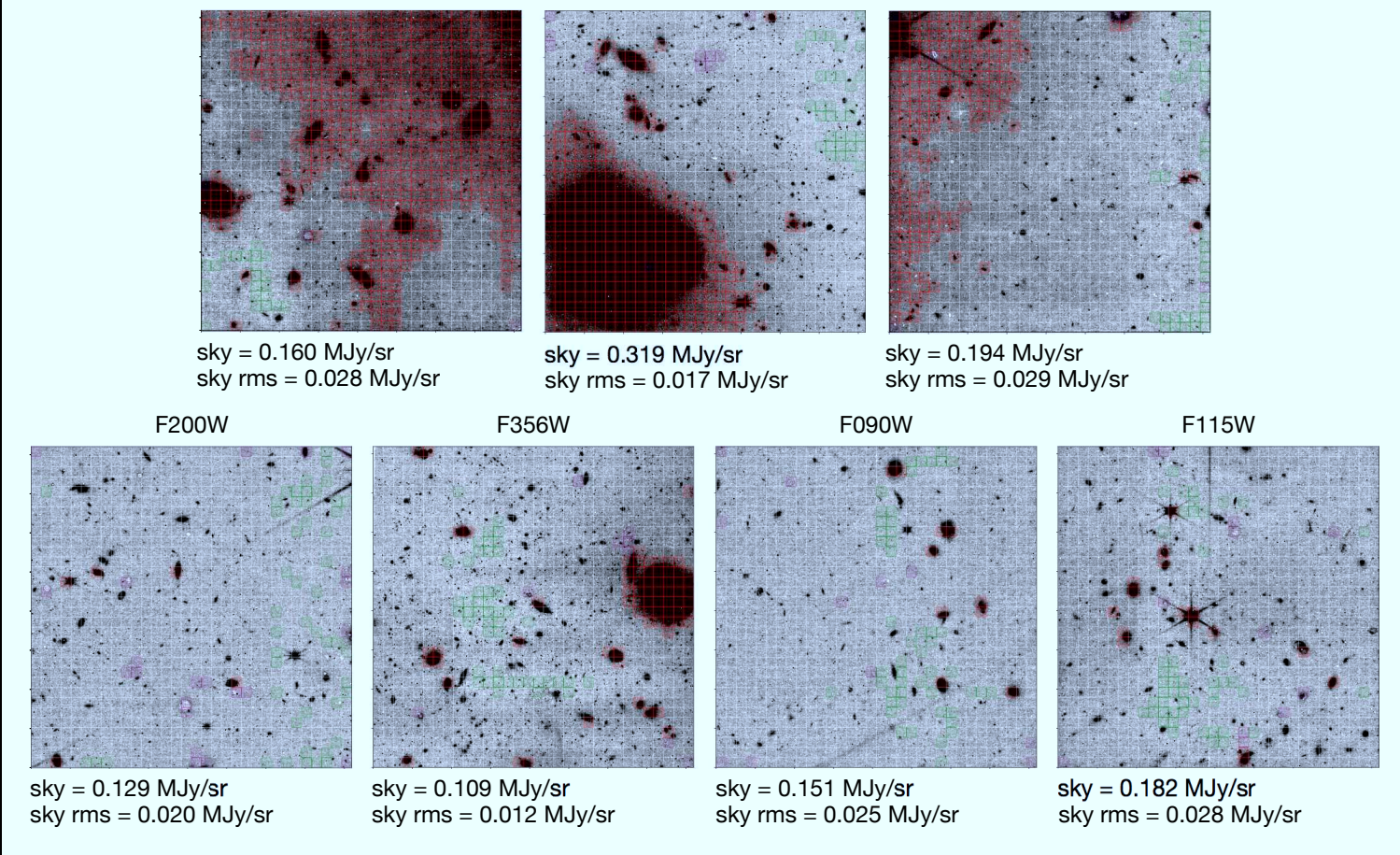
$\sim 1e5$ NIRCam+NIRISS Files



SKYSURFIR database: 62,706 exposures (564,000 ramp-reads) in $\gtrsim 130$ independent JWST NIRCam+NIRISS fields taken over 2 years.

- 20 filters from 0.9–5 μm , with 8 main broad-band filters.
- These cover $\gtrsim 0.51 \deg^{-2}$ across the sky, yielding $\gtrsim 1.5 \times 10^6$ galaxies to AB $\lesssim 29$ mag to reduce Cosmic Variance to $\lesssim 1\text{--}2\%$.

(Tim Carleton, Rachel Honor, Rafael Ortiz database lead. UGs built database in fall 2024).



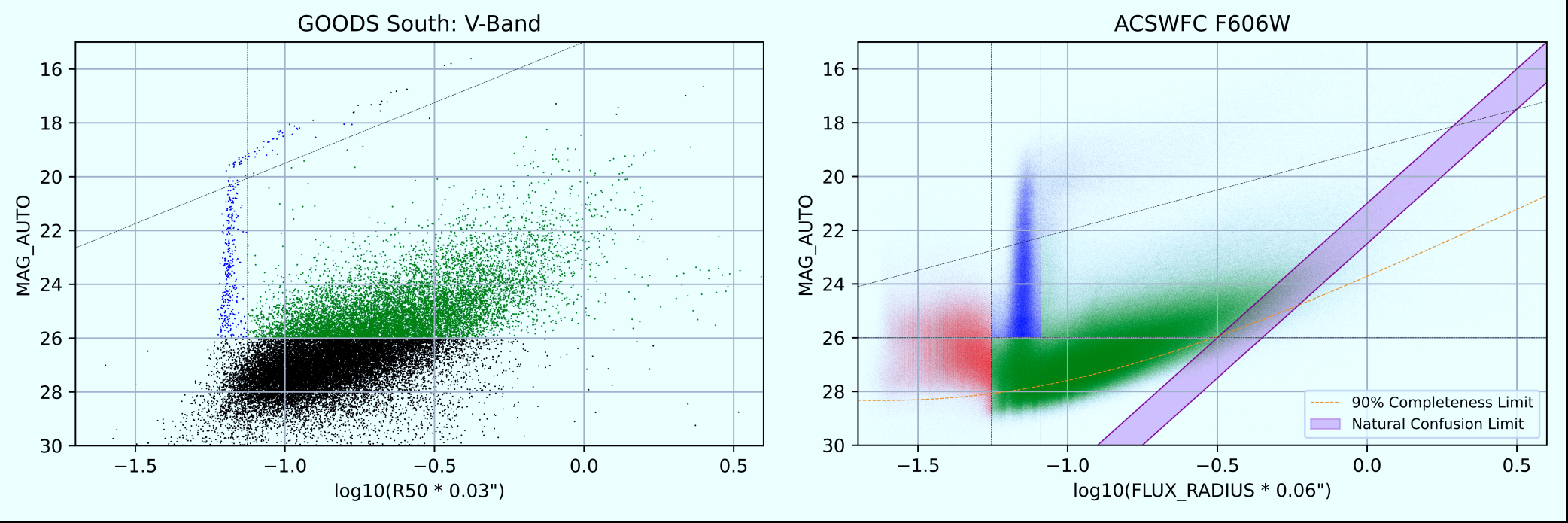
Example of sky-SB estimation algorithm on 7 JWST images:

[Top row]: Images discarded due to bright or large objects (red grid-boxes).

[Bottom row]: Images that *are* used for sky-SB measurements.

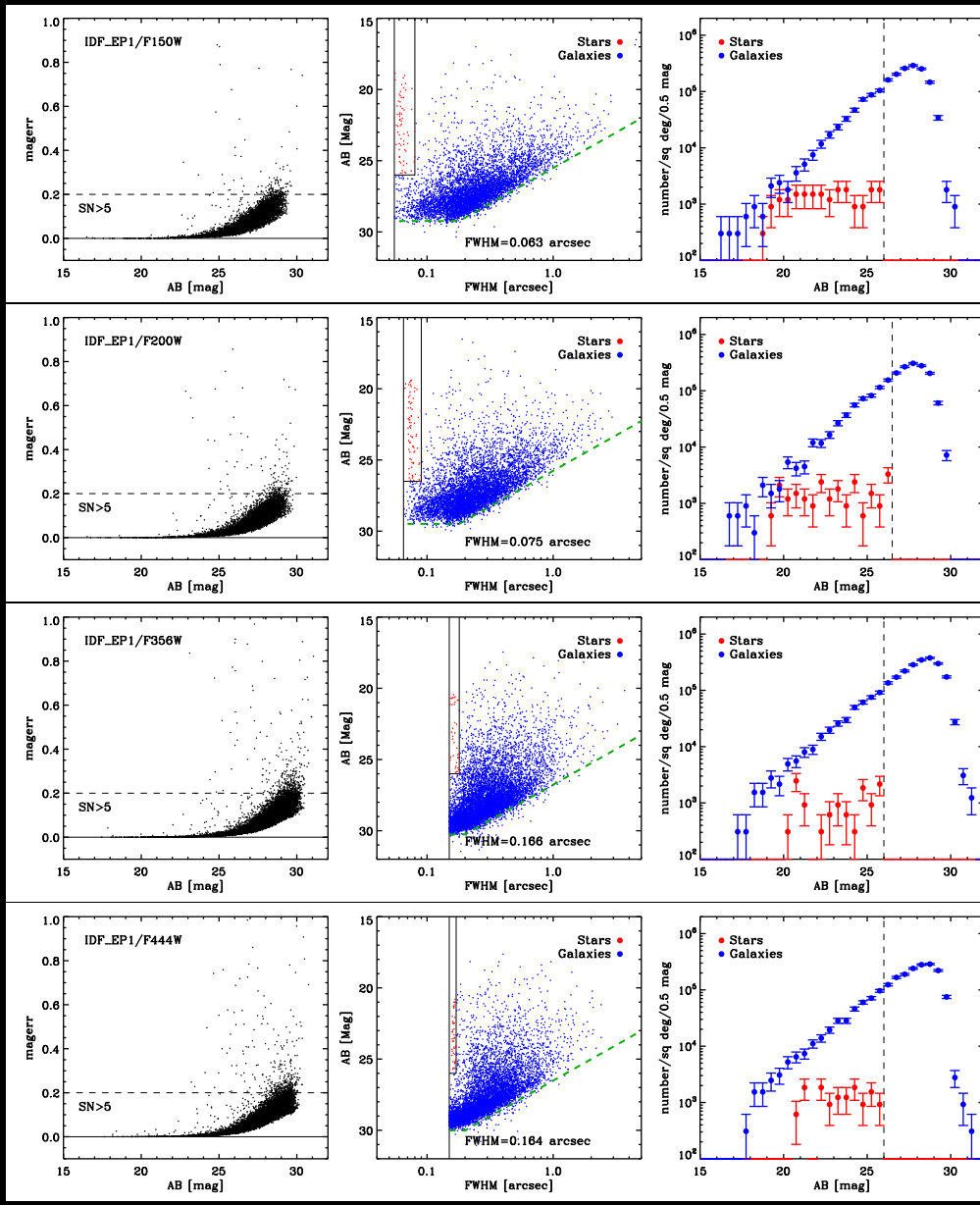
- Code selects non-contaminated **green grid-boxes**, which measure the sky-SB to within 0.2–0.4%, as calibrated with realistic simulations.

(O'Brien et al. 2023, AJ, 165, 237, astro-ph/2210.08010; Windhorst, R. et al. 2023, AJ, 165, 13).



- [LEFT]: SKYSURF star-galaxy separation in GOODS-S F606W mosaic.
- [RIGHT]: Same for all 11 million HST galaxies in 3000 SKYSURF fields.

- Total fluxes vs. r_{hl} with stars, galaxies, and artifacts indicated.
(D. Carter. 2024, S. Tompkins, 2024, inpreparation).
- SKYSURFIR: 1.5×10^6 galaxies to AB $\lesssim 29$ mag in ~ 130 JWST fields.
(J. Berkheimer, 2024, inpreparation).

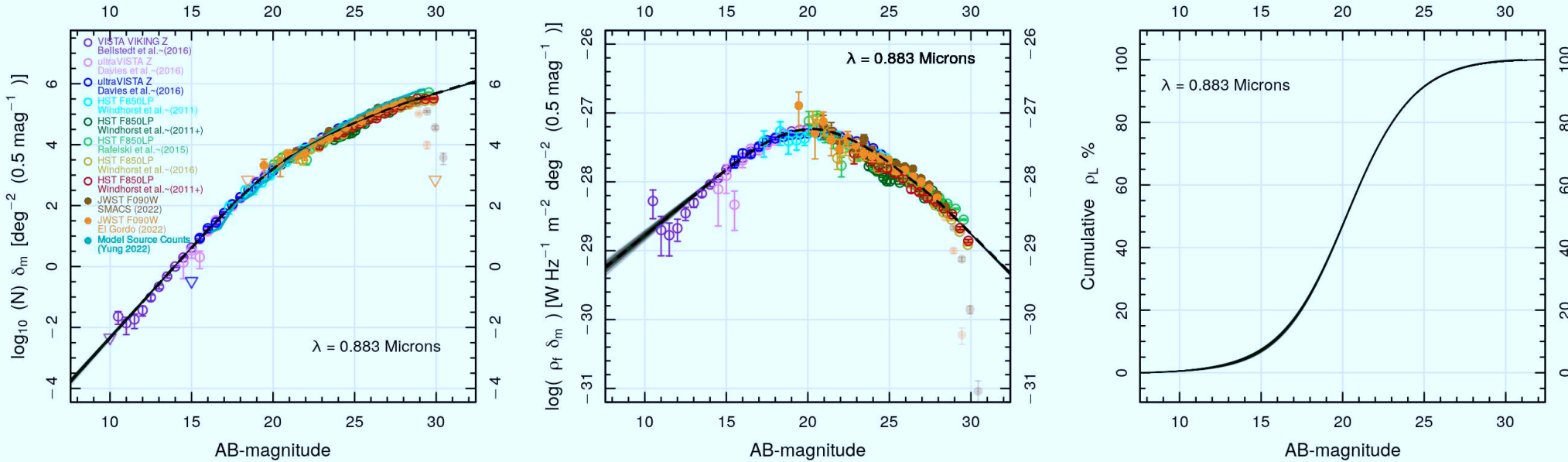


[Left]: Mag-error vs. AB: 5σ NIRCam completeness to $AB \lesssim 28.5\text{--}29$ mag.

[Middle]: AB vs. FWHM: accurate star-galaxy separation to $AB \lesssim 26\text{--}27$!

● Stellar sequence FWHM improves below $2.00\text{ }\mu\text{m}$ JWST diffraction limit!

[Right]: $0.9\text{--}4.5\mu\text{m}$ Galaxy counts complete to $AB \lesssim 28.5\text{--}29$ mag, resp.



[Left]: Normalized differential galaxy counts.

[Middle]: Galaxy energy counts (after dividing by 0.4 dex/mag slope).

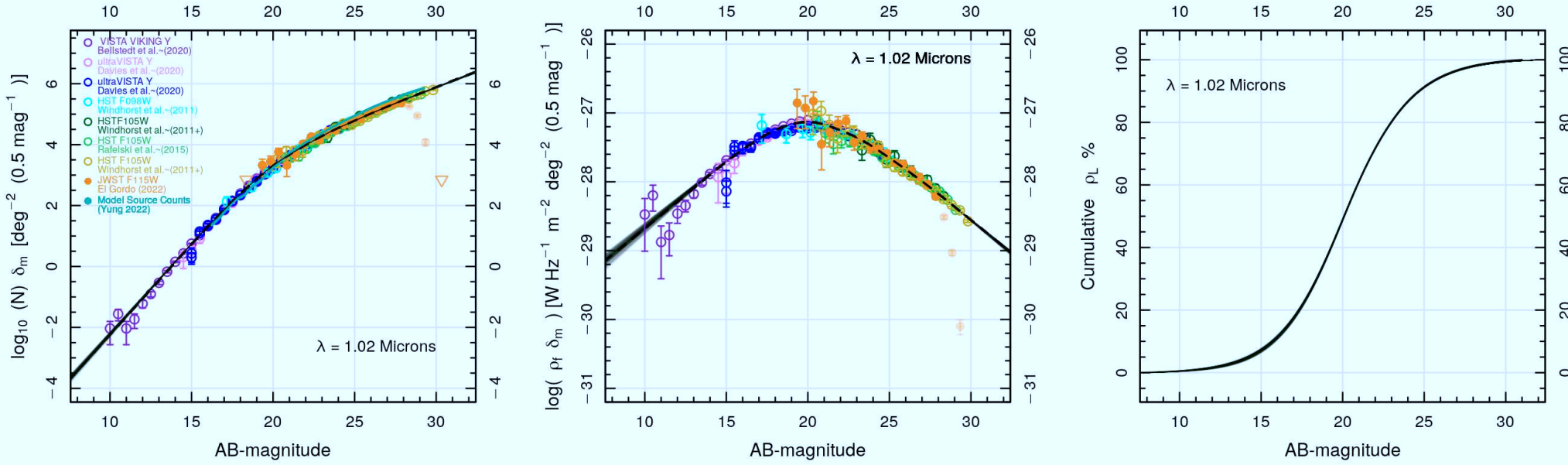
[Right]: Integrated Galaxy Light (IGL) from best fit spline.

$0.88 \mu\text{m}$ Ground-based+HST+JWST galaxy counts ($\text{AB} \simeq 10\text{--}30 \text{ mag}$).

- Energy counts narrow with increasing λ . Peak amplitude around $2 \mu\text{m}$.

(Windhorst, R. et al. 2023, AJ, 165, 13; astro-ph/2209.04119).

- SKYSURFIR detects/removes $\gtrsim 97\%$ of the IGL to $\text{AB} \lesssim 29 \text{ mag}$.



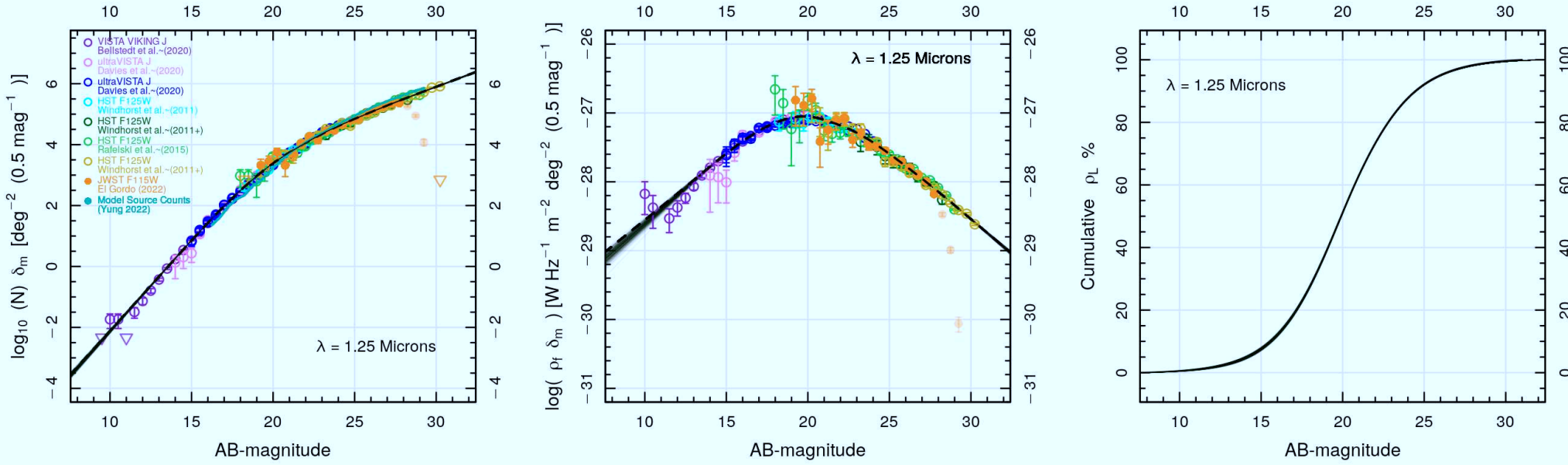
[Left]: Normalized differential galaxy counts.

[Middle]: Galaxy energy counts (after dividing by 0.4 dex/mag slope).

[Right]: Integrated Galaxy Light (IGL) from best fit spline.

$1.02 \mu\text{m}$ Ground-based+HST+JWST galaxy counts ($\text{AB} \simeq 10\text{--}30$ mag).

- Energy counts narrow with increasing λ . Peak amplitude around $2 \mu\text{m}$.



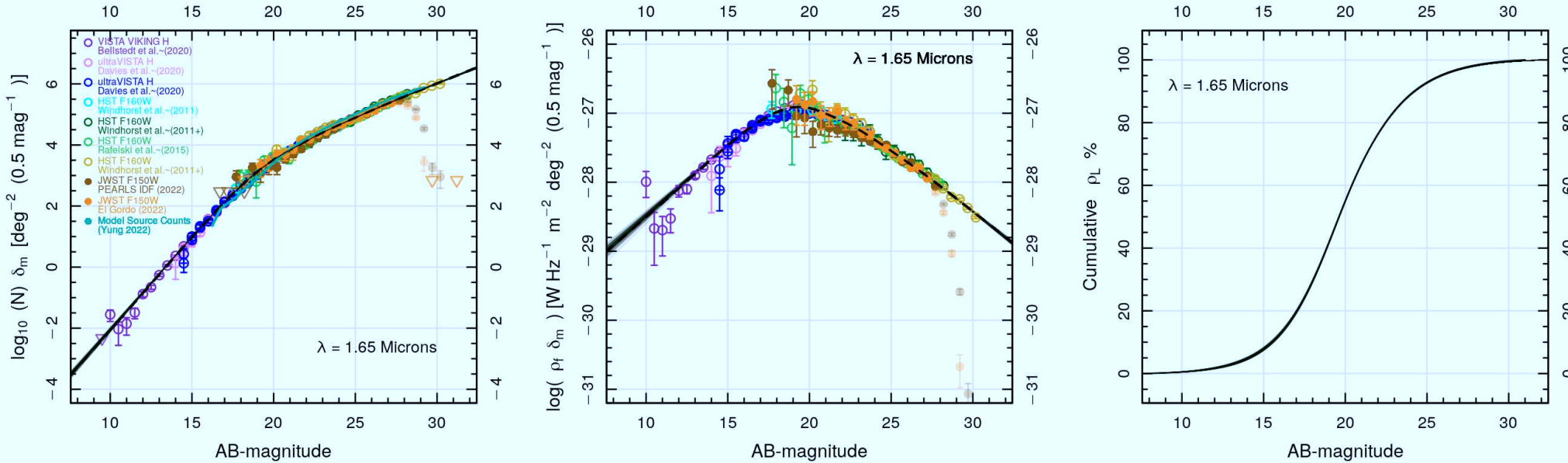
[Left]: Normalized differential galaxy counts.

[Middle]: Galaxy energy counts (after dividing by 0.4 dex/mag slope).

[Right]: Integrated Galaxy Light (IGL) from best fit spline.

1.25 μm Ground-based+HST+JWST galaxy counts (AB \simeq 10–30 mag).

- Energy counts narrow with increasing λ . Peak amplitude around 2 μm .



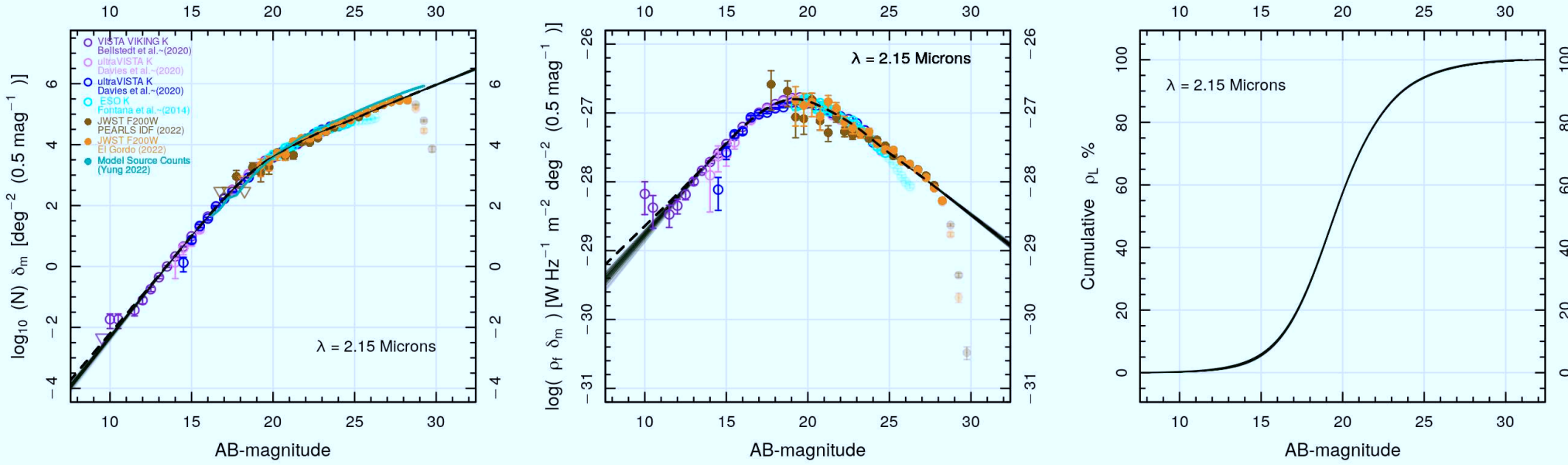
[Left]: Normalized differential galaxy counts.

[Middle]: Galaxy energy counts (after dividing by 0.4 dex/mag slope).

[Right]: Integrated Galaxy Light (IGL) from best fit spline.

$1.65 \mu\text{m}$ Ground-based+HST+JWST galaxy counts ($\text{AB} \simeq 10\text{--}30$ mag).

- Energy counts narrow with increasing λ . Peak amplitude around $2 \mu\text{m}$.



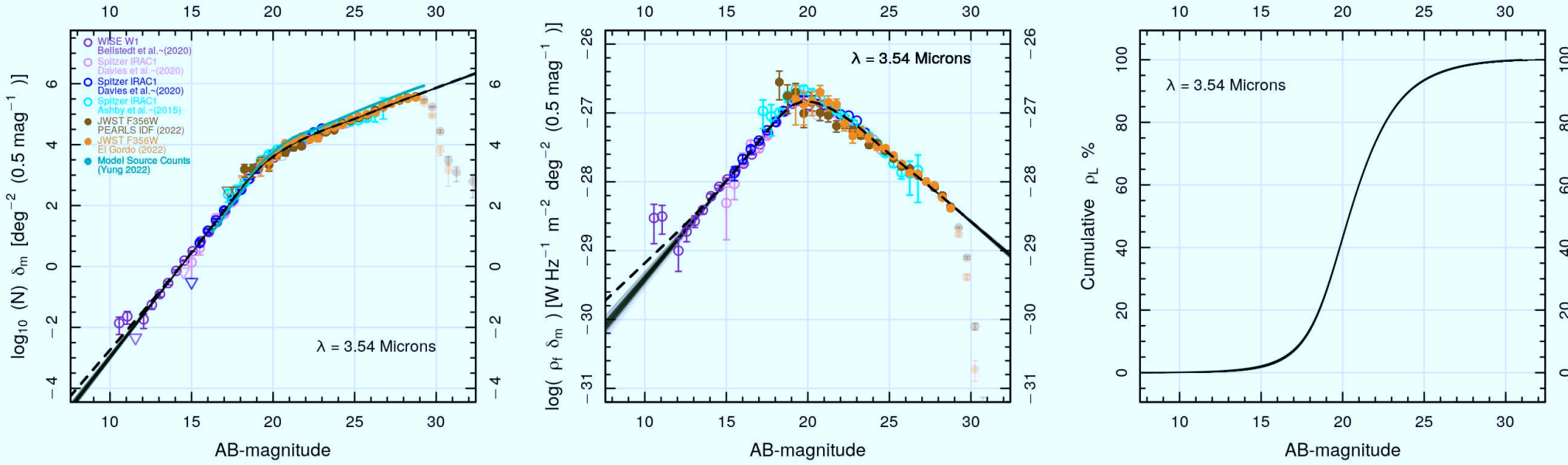
[Left]: Normalized differential galaxy counts.

[Middle]: Galaxy energy counts (after dividing by 0.4 dex/mag slope).

[Right]: Integrated Galaxy Light (IGL) from best fit spline.

2.15 μm Ground-based+JWST galaxy counts (AB \simeq 10–30 mag).

- Energy counts narrow with increasing λ . Peak amplitude around 2 μm .



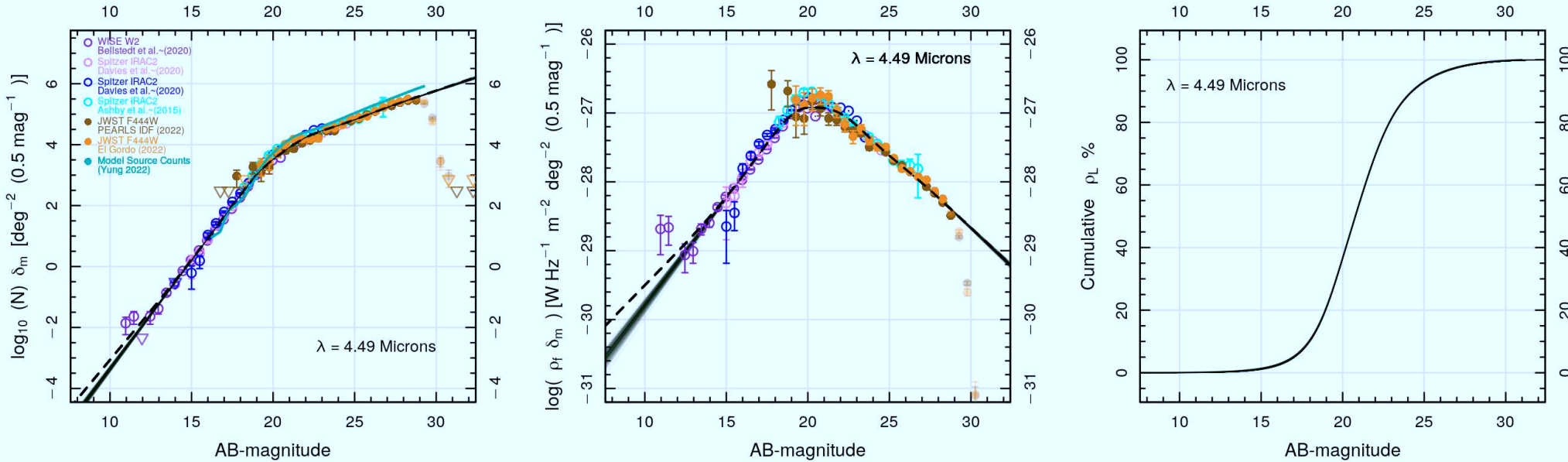
[Left]: Normalized differential galaxy counts.

[Middle]: Galaxy energy counts (after dividing by 0.4 dex/mag slope).

[Right]: Integrated Galaxy Light (IGL) from best fit spline.

3.54 μm WISE+Spitzer+JWST galaxy counts (AB \simeq 10–30 mag).

- Energy counts narrow with increasing λ . Peak amplitude around 2 μm .



[Left]: Normalized differential galaxy counts.

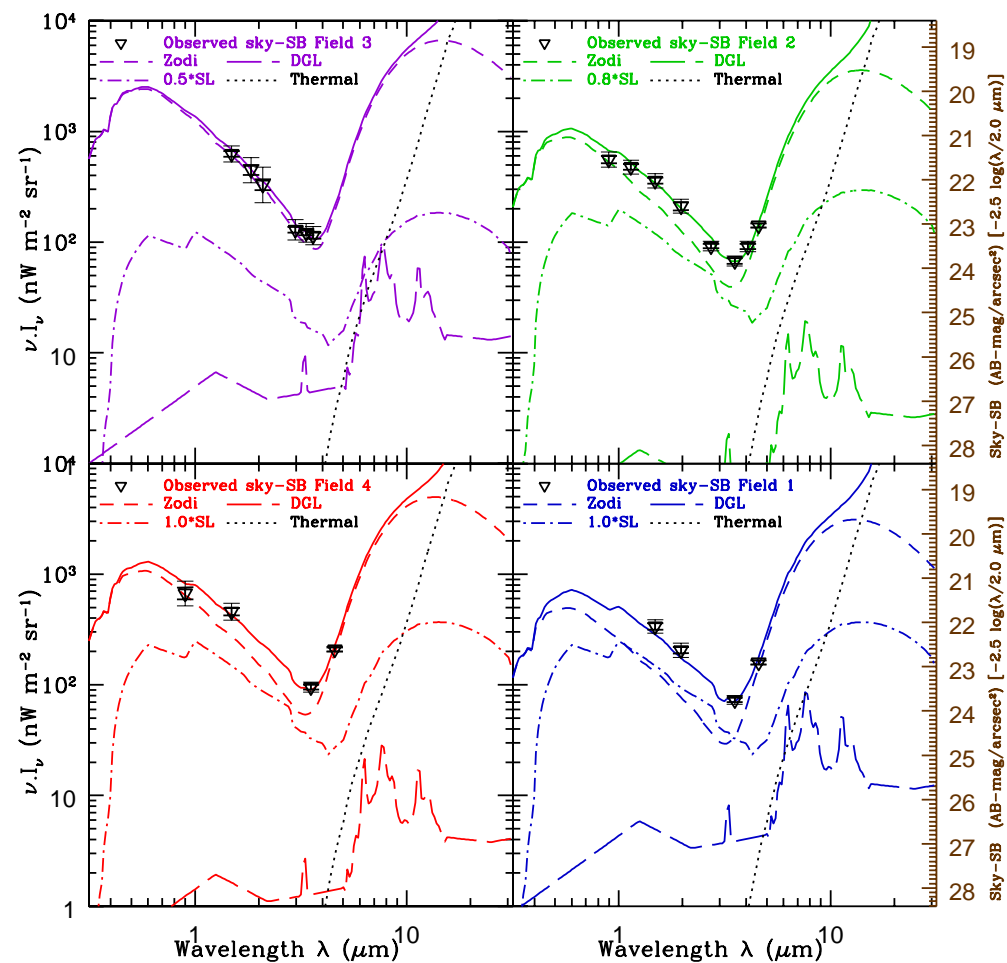
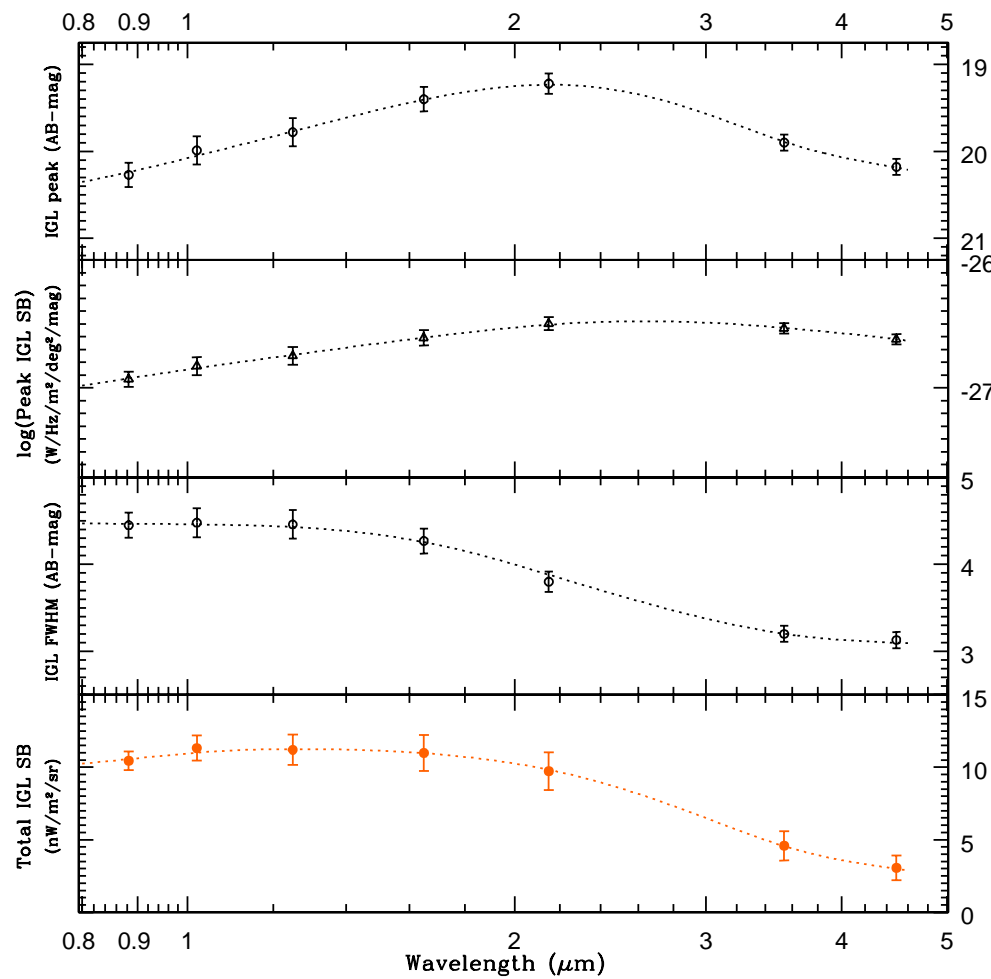
[Middle]: Galaxy energy counts (after dividing by 0.4 dex/mag slope).

[Right]: Integrated Galaxy Light (IGL) from best fit spline.

$4.49 \mu\text{m}$ WISE+Spitzer+JWST galaxy counts ($\text{AB} \simeq 10\text{--}30 \text{ mag}$).

- Energy counts narrow with increasing λ . Peak amplitude around $2 \mu\text{m}$.
- $0.9\text{--}4.5 \mu\text{m}$ Integrated Galaxy Light (IGL) now well determined ($\lesssim 10\%$)!

(Figures by Scott Tompkins; see also Tompkins et al. 2023, MNRAS, 521, 332; astro-ph/2301.03699).

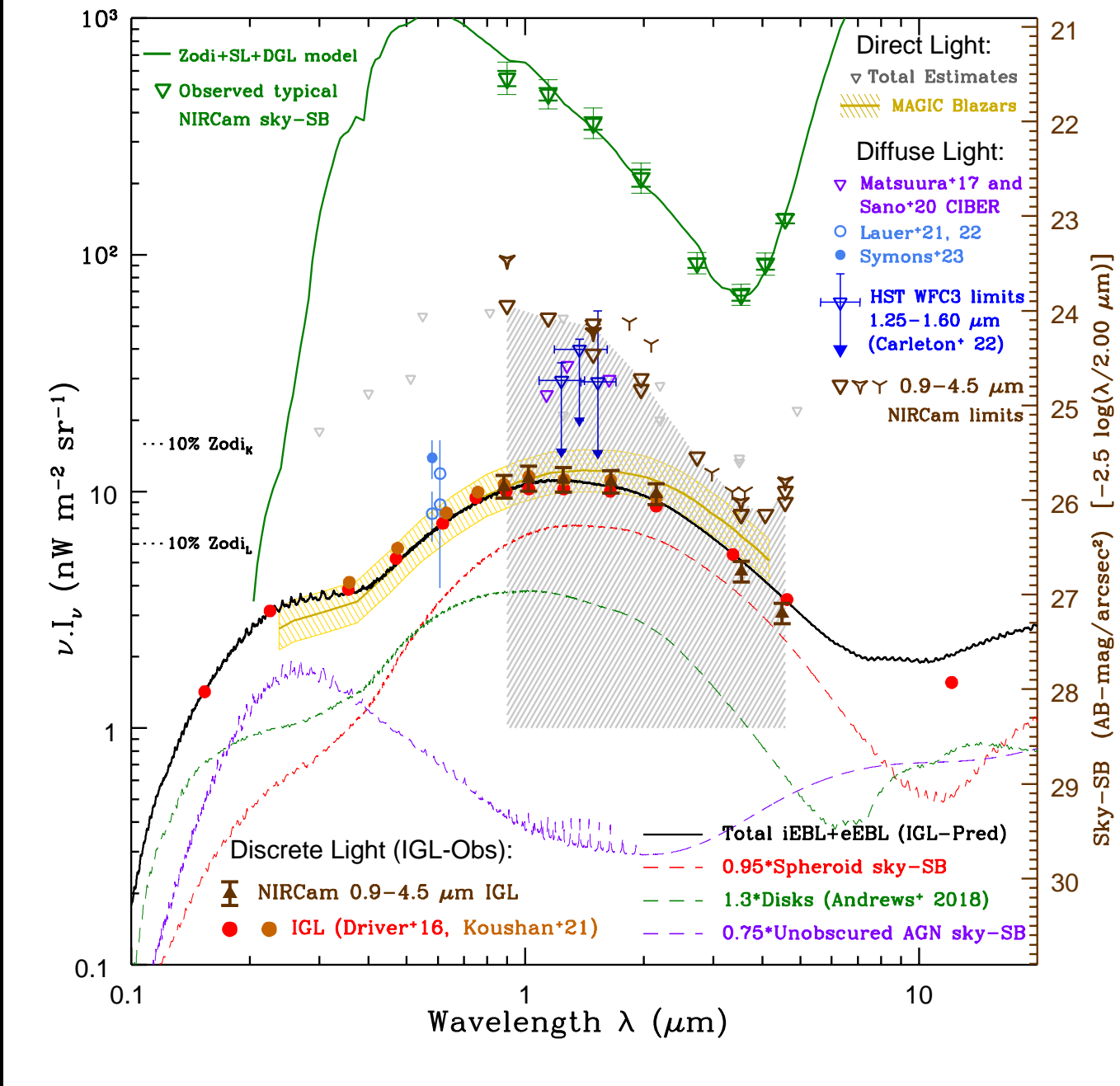


[Left]: IGL vs. λ : Peak (AB & mks units); IGL FWHM (AB); and $\nu \cdot I_\nu$.

- 0.9–4.5 μm Integrated Galaxy Light (IGL) now well determined ($\lesssim 10\%$)!

[Right]: 13-band sky-SB vs. λ : Model-sum = Zodi + JWST-Straylight (SL) + Diffuse Galactic Light (DGL) + JWST Thermal Radiation

- Model-sums match total JWST NIRCam sky-SB within $\sim 10\%$ of Zodi.



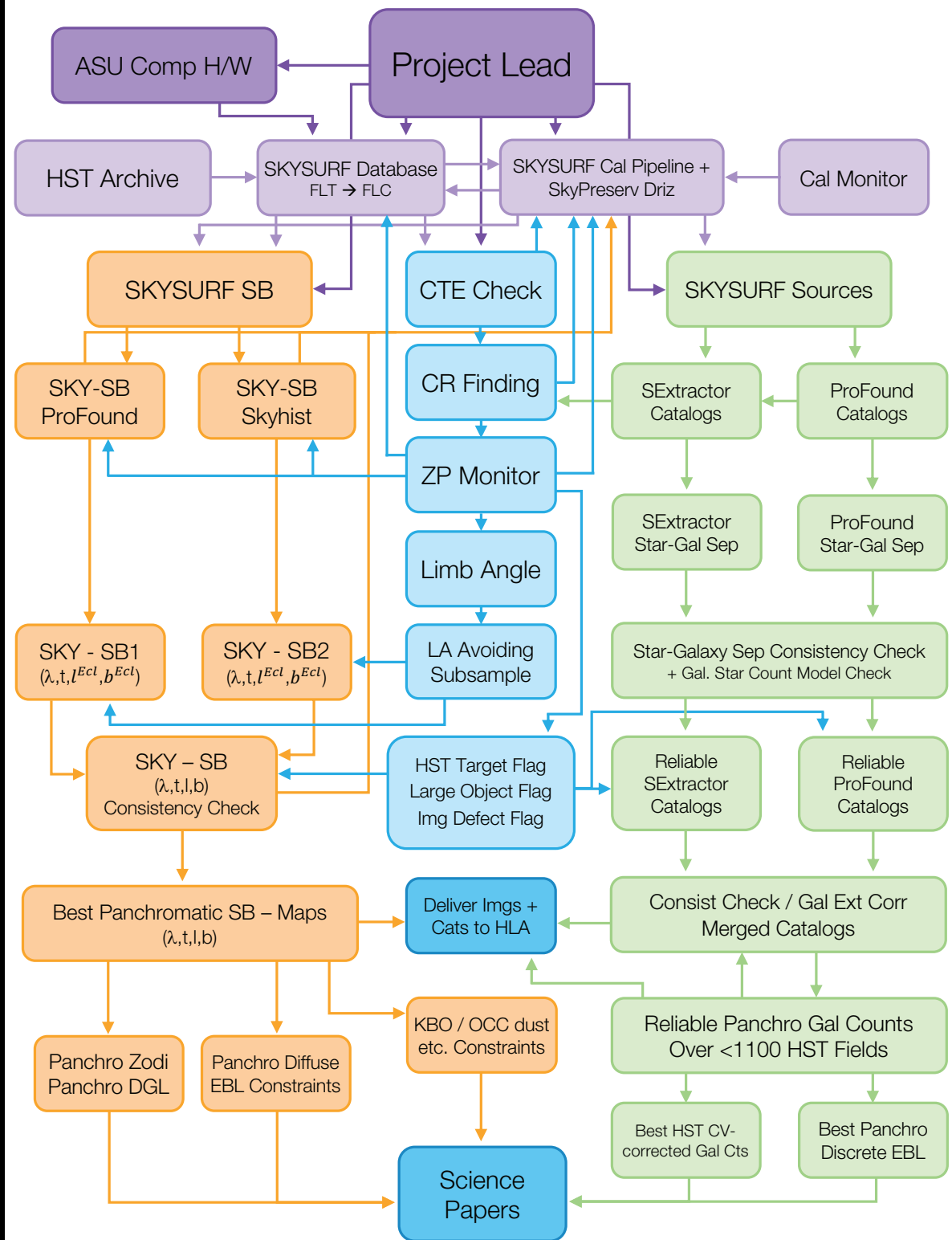
Conclusions: (1) JWST NIRCam accurately determined 0.9–4.5 μm IGL.
(2) 0.9–2 μm diffuse light limits confirm previous work. Firm 2.7–4.5 μm limits.
● 3–5 μm limits ($\lesssim 8$ nW/m²/sr) to improve with many more JWST fields.

(3) Conclusions: combined HST+JWST diffuse light limits

1. HST built to measure faint objects & sky over decades at 0.2–1.6 μm .
2. More than 95% of photons in STScI Archive come from $D \lesssim 3\text{--}5$ AU.
Traditional drizzling techniques ignored sky-foreground for 29 years.
3. SKYSURF can measure sky-SB to $\lesssim 2\text{--}3\%$ & identify orbital straylight.
4. Compared to Kelsall et al.'s (1998) Zodiacal model, SKYSURF finds ~ 20 nW/m²/sr ($\sim 6\%$ of Zodi) of diffuse light at 1.25–1.6 μm .
 - This amounts to the *brightness* of ~ 7 Jupiters over 4π steradian!
 - Compared to Wright's (1998) Zodiacal model, HST finds no significant diffuse light at 1.25–1.6 μm .
5. JWST yields best limits of $\lesssim 8$ nW/m²/sr in its darkest 3–5 μm sky.
6. Zodiacal models need update to include dim spherical diffuse light.
 - Need to include higher-albedo Oort Cloud Comet dust at $D \sim 1\text{--}3$ AU?

SPARE CHARTS

SKYSURF – Project Flowchart



Measuring sky foreground &
making object catalogs:

SKYSURF project flowchart:

Database building and stan-
dard pipeline

Monitor systematics: Cosmic
Ray filter, CTE-correction,
Zeropoints, orbital straylight,
artifact flagging & removal.

sky-SB estimates with two in-
dependent algorithms.

Object finding/catalogs with
two independent algorithms.

Measuring sky foreground & making object catalogs:

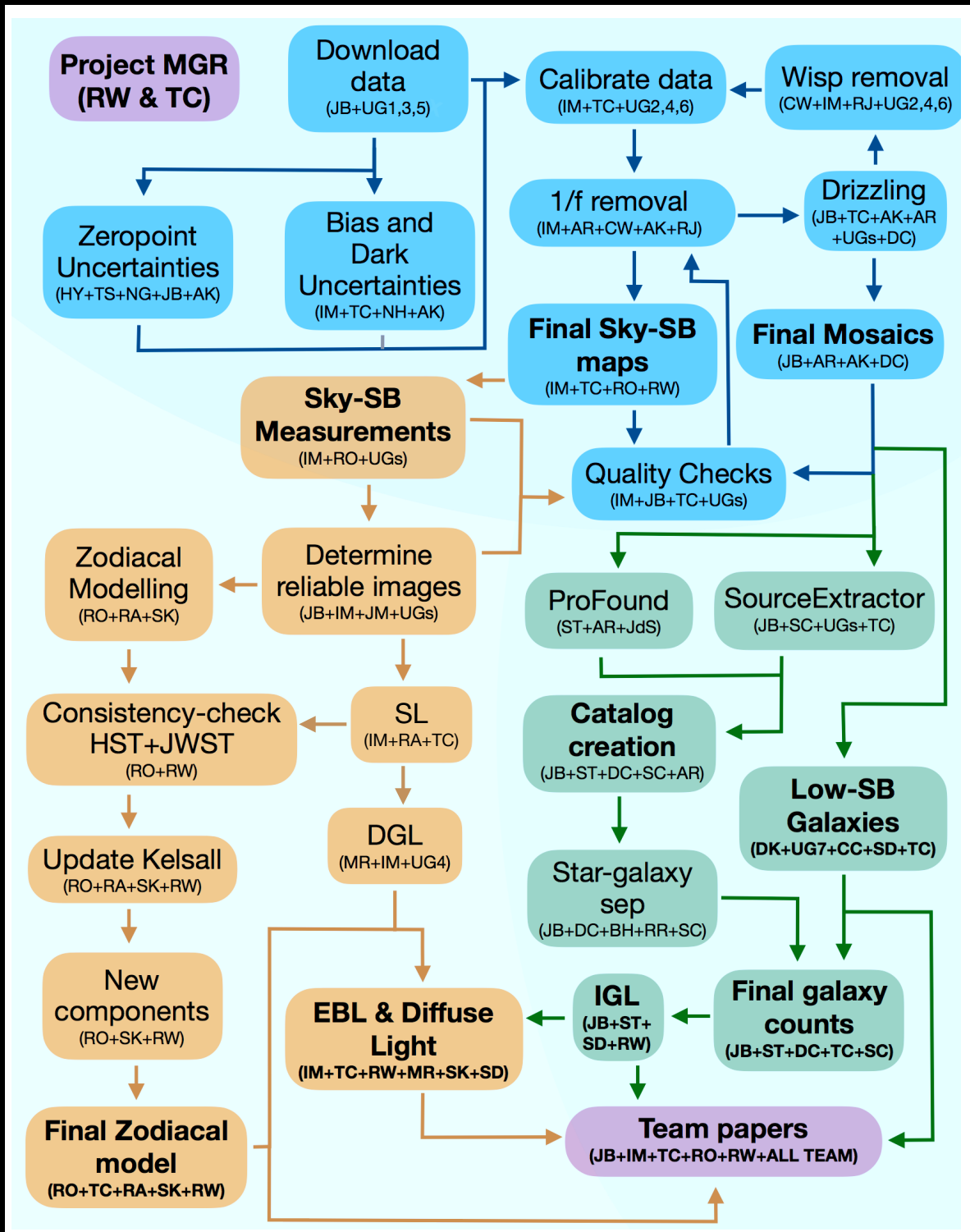
Webb SKYSURFIR project flowchart:

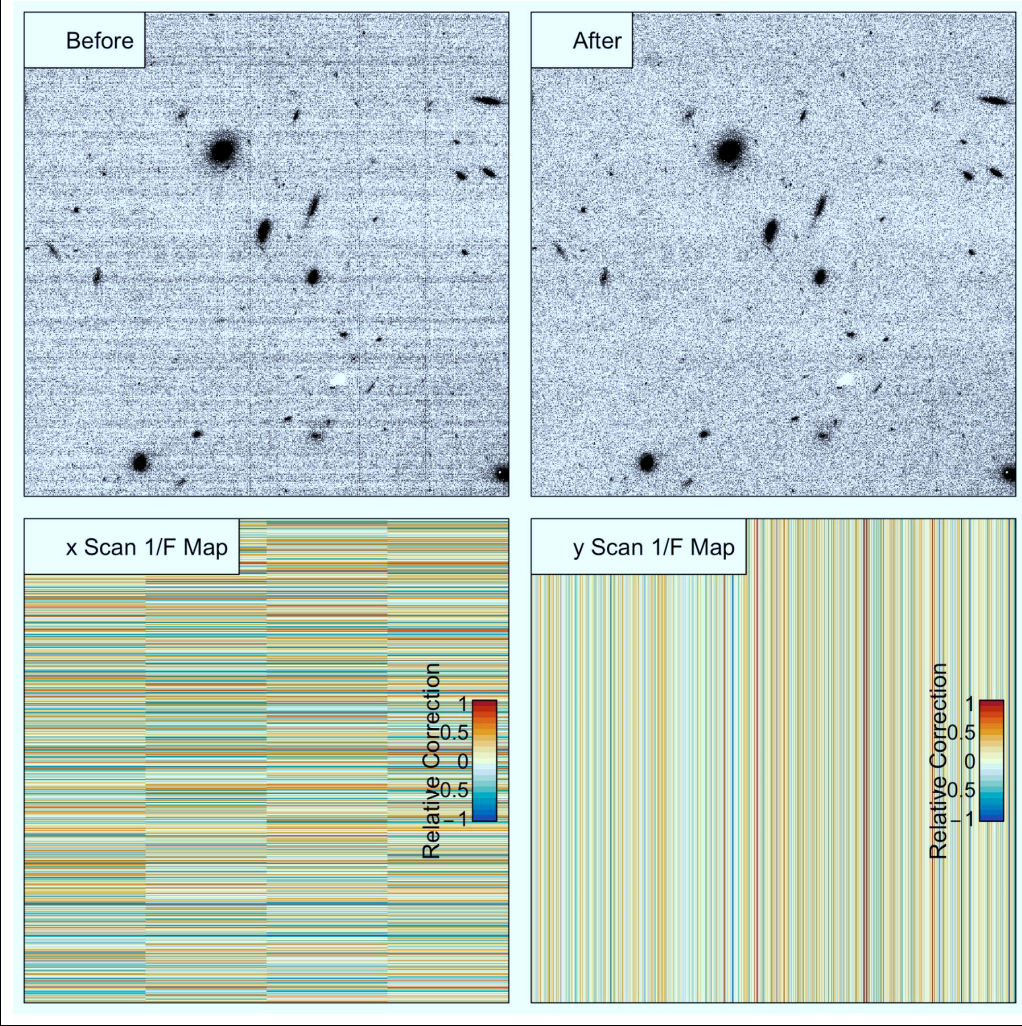
- Database building and standard pipeline

- Monitor NIRCam systematics: stage 1-3 pipeline, 1/f-correction, wisp-mapping and -correction, Cosmic Ray filter, Zeropoints, straylight modeling and correction, artifact flagging & removal.

- Sky-SB estimates with two independent algorithms.

- Object finding/catalogs w/ two independent algorithms.

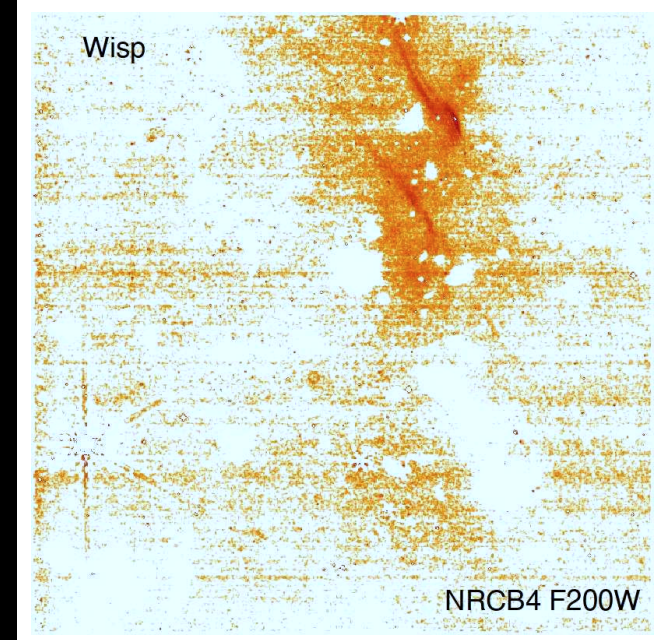
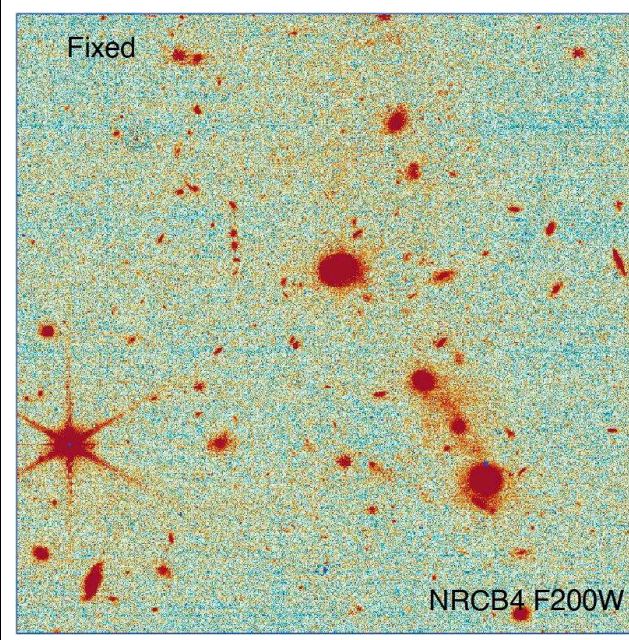
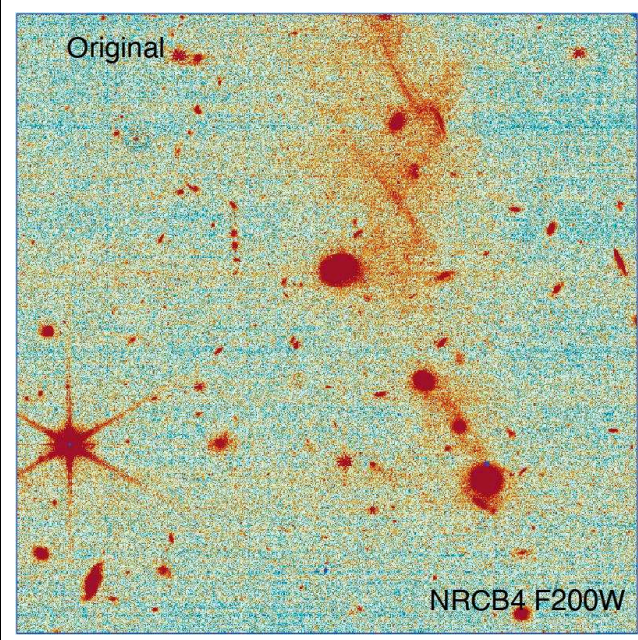




Examples of optimized scene-dependent NIRCam 1/f-removal:

- The NIRCam ASIC 1/f-grounding signal is removed separately horizontally from four vertical A/D converter swaths, and in vertical stripes.
- The NIRCam 1/f-removal is scene-dependent, and less aggressive for crowded fields with larger brighter objects, such as lensing clusters.

(Windhorst, R. et al. 2023, AJ, 165, 13; Robotham, A. S. G., et al. 2023, PASP, 135, 085003).



Examples of optimized scene-dependent NIRCam wisp-removal:

[LEFT]: Example of NIRCam F200W filter image from detector NRCB4 with a clear wisp structure in the foreground (light scattered of OTE struts).

[MIDDLE]: NIRCam F200W image with the best wisp template removed.

[RIGHT]: Wisp template used: white pixels are masked wisp-regions due to real objects outlined in the wisp-free NIRCam LW images (F444W).

- The NIRCam 1/f removal is scene-dependent, and less aggressive for crowded fields with larger brighter objects, such as lensing clusters.

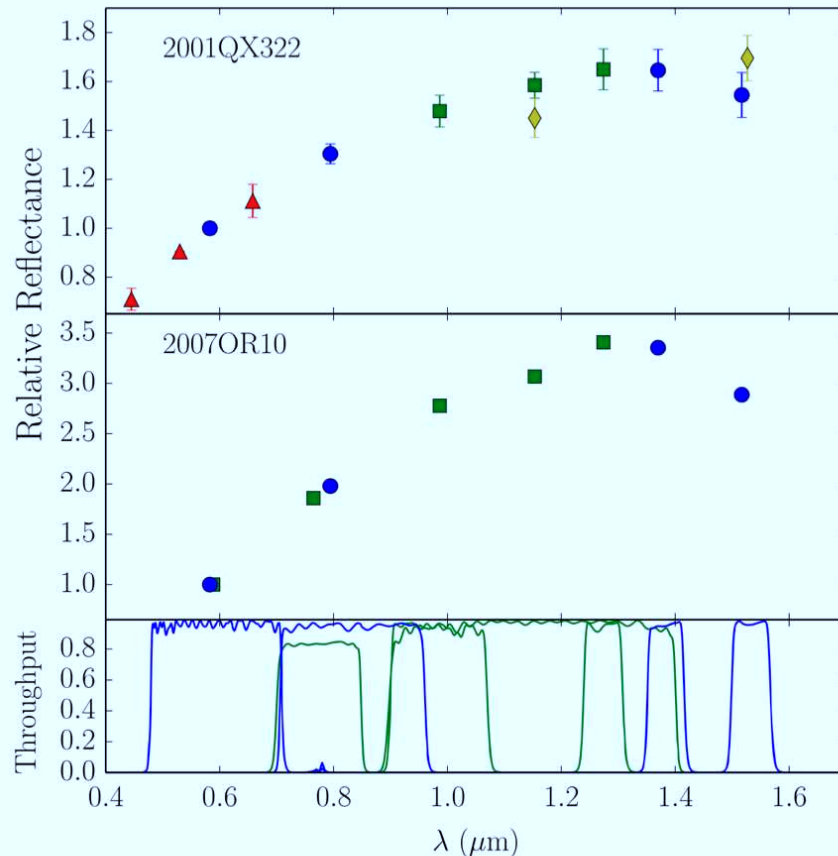


Figure 8. As in Figure 6. The yellow diamonds mark the spectra obtained for 2001 QX322 from the data presented by Benecchi et al. (2011). The F098m, F110w, and F127m photometry of 2001 QX322 have been vertically scaled for visible representation to match the F139m photometry and the photometry of Benecchi.

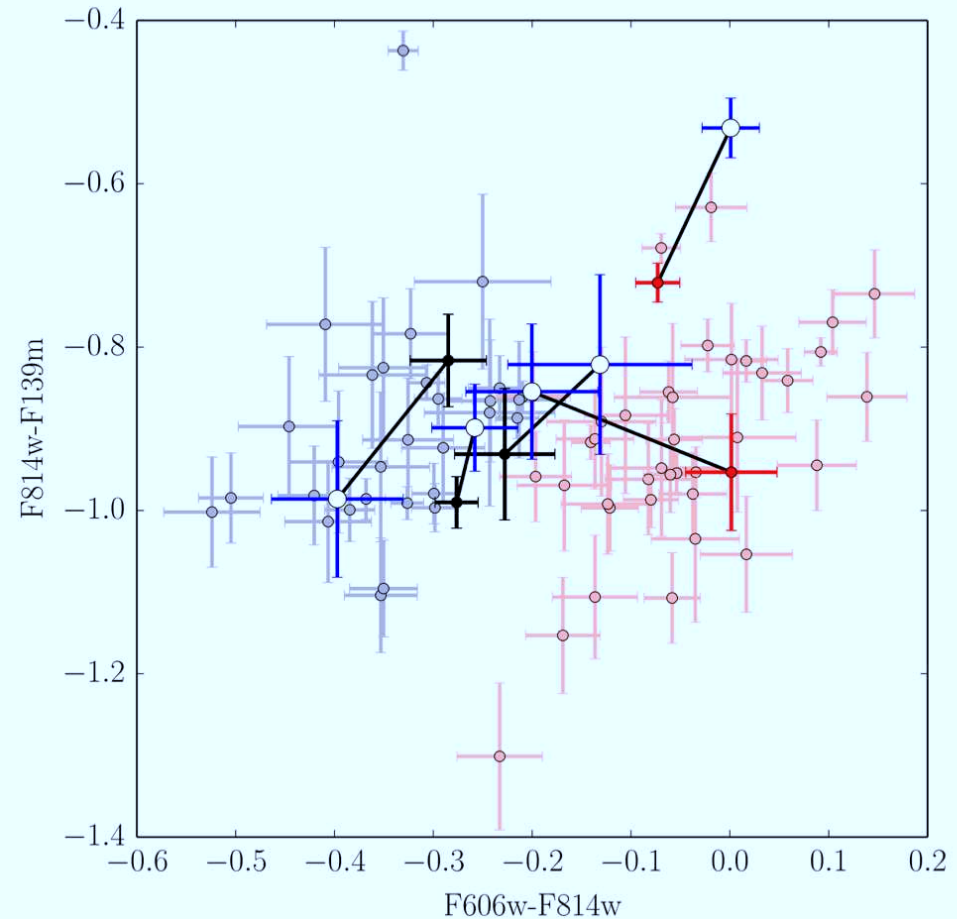


Figure 10. Observed and model optical and infrared colors of the five spectrally variable objects. The model cycle 18 colors are shown in blue points, while the observed cycle 17 colors are shown as solid red or black points according to their cycle 17 classification. Black lines connect the observed and model colors for each source. Gray and light red points show the full cycle 17 colors for comparison.

HST work on KBOs at 10–1000 AU show some remarkably blue IR colors.
Does OCC cometary dust in the inner solar system have similar albedos?

SKYSURF & PEARLS References and other sources of material

Talk: http://www.asu.edu/clas/hst/www/jwst/skysurfir_paris24_windhorst.pdf

Data: <https://sites.google.com/view/jwstpearls> and <http://skysurf.asu.edu/>

- Ashcraft, T. A., Windhorst, R. A., Jansen, R. A., et al. 2018, PASP, 130, 064102 ([astro-ph/1703.09874](#))
- Ashcraft, T. A., McCabe, T., Redshaw, C., et al. 2023, PASP, 135, 024101 ([astro-ph/2208.14572](#))
- Bhatia, P., Carleton, T., Windhorst, R., Jansen, R. & O'Brien, R. 2024, RNAAS, 8, 154 (SKYSURF-6)
- Carleton, T., Windhorst, R. A., O'Brien, R., et al. 2022, AJ, 164, 170 ([astro-ph/2205.06347](#); SKYSURF-2)
- Diego, J. M., Sun, B., Yan, H., et al. 2023, A&A, 679, A31 ([astro-ph/2307.10363](#))
- Kramer, D., Carleton, T., Cohen, S., et al. 2022, ApJL, 940, L15 ([astro-ph/2208.07218v2](#); SKYSURF-3)
- McIntyre, I. A., Carleton, T., O'Brien, R., et al. 2024, AJ, in press ([astro-ph/2407.12290v1](#); SKYSURF-7)
- O'Brien, R., Carleton, T., Windhorst, R. et al. 2023, AJ, 165, 237 ([astro-ph/2210.08010](#); SKYSURF-4).
- Robotham, A. S. G., D'Silva, J. C. J., Windhorst, R. A, et al. 2023, PASP, 135, 085003 ([astro-ph/2305.01175](#))
- Summers, J., Windhorst, R. A., Cohen, S. H., et al. 2023, ApJ, 958, 108 ([astro-ph/2306.13037](#))
- Tompkins, S. A., Driver, S. P., Robotham, A. S. G., et al. 2023, MNRAS, 521, 332 ([astro-ph/2301.03699](#))
- Windhorst, R., Cohen, S. H., Hathi, N. P., et al. 2011, ApJS, 193, 27 ([astro-ph/1005.2776](#))
- Windhorst, R., Timmes, F. X., Wyithe, J. S. B., et al. 2018, ApJS, 234, 41 ([astro-ph/1801.03584](#))
- Windhorst, R. A., Carleton, T., O'Brien, R., et al. 2022, AJ, 164, 141 ([astro-ph/2205.06214](#); SKYSURF-1)
- Windhorst, R. A., Cohen, S. H., Jansen, R. A., et al. 2023, AJ, 165, 13 ([astro-ph/2209.04119](#); PEARLS)
- Windhorst, R. A., et al. 2024, J. BAAS, subm. (White paper for HST SR review; [astro-ph/2410.01187v1](#))

<https://hubblesite.org/contents/news-releases/2022/news-2022-050>

<https://blogs.nasa.gov/webb/2022/10/05/webb-hubble-team-up-to-trace-interstellar-dust-within-a-galactic-pair/>

<https://blogs.nasa.gov/webb/2022/12/14/webb-glimpses-field-of-extragalactic-pearls-studded-with-galactic-diamonds/>

<https://esawebb.org/images/pearls1/zoomable/>